Measurement and Analysis of Piston Inter-Ring Pressures and Oil Film Thickness and their Effects on Engine Oil Consumption

by

L. Bouke Noordzij

B. S., Mechanical Engineering; Northeastern University, 1994

Submitted to the Department Mechanical Engineering in Partial Fulfillment of the Requirements for the Degrees of

MASTER OF SCIENCE IN MECHANICAL ENGINEERING

at the
Massachusetts Institute of Technology; June 1996

Signature of Author_____
Department of Mechanical Engineering, June 1996

Certified by_____
Dr. Victor W. Wong
Lecturer, Department of Mechanical Engineering
Thesis Advisor

Accepted by_____
A. A. Sonin, Chairman
Departmental Committee on Graduate Studies
Department of Mechanical Engineering

(This page intentionally left blank)

Measurement and Analysis of Piston Inter-Ring Pressures and Oil Film Thickness and their Effects on Engine Oil Consumption

by

L. Bouke Noordzij

Submitted to the Department of Mechanical Engineering in Partial Fulfillment of the Requirements for the Degrees of Master of Science in Mechanical Engineering.

ABSTRACT

A four-cylinder spark-ignition engine testing setup was constructed to perform Laser Induced Fluorence (LIF) testing and piston inter-ring pressure measurements during high speed, steady state, operating conditions. The engine setup was constructed in such a manner to allow for high speed motoring and absorbing operating conditions which required the coupling of a low inertia dynamometer and a high speed brush VDC electric motor. The coupling of these two units with a dynamometer controller along with a computer control throttle allowed for complete engine control.

An in-line, four-cylinder, 2.0 liter, spark-ignition engine was modified with eight quartz windows in one of its four cylinders, cylinder 2, such that the laser could access the oil film between the liner and piston. Of the eight windows four were positioned on the anti-thrust line at vertical positions of 50, 73, 87.5 and 102 millimeters down from the top of the cylinder liner (TDC). The remaining four windows were positioned at the same vertical locations with a 30 degree shift off the anti-thrust line away from the flywheel. These shifted window locations were chosen with the interest of observing the effects of bore distortion on the oil film thickness. A pressure transducer port was also machined in the head of cylinder 2 to measure cylinder pressures and indicate the cycle position for corresponding LIF data.

For the initial engine testing four inter-ring pressure ports were machined into cylinder 3 of the four-cylinder engine, along with a pressure port in the cylinder head to measure combustion pressure. The vertical locations of the inter-ring pressure ports were 50, 58, 66 and 74 millimeters from TDC. These four locations were staggered alternately at ±10 degrees off the anti-thrust line to accommodate the 10 millimeter diameter of the pressure transducer adapters. The pressure transducer adapters were required for mounting the transducers and isolating the coolant jacket. After the first two of three different test parameters were completed, two more pressure ports were machined into the engine at the vertical locations of 14 and 22 millimeters.

A test matrix of three different ring pack designs, designated phase 1, 2 and 3, were tested at steady state conditions with an engine speed of 4000 rpm and loads of -15 Nm (closed throttle) and 160 Nm (wide open throttle). LIF data was measured at three window locations, 50 and 87.5 millimeters from TDC on the anti-thrust line and 50 millimeters from TDC at 30 degrees off the anti-thrust line. The inter-ring pressures were also measured, along with cylinder pressures. Phase 1 ring pack was the standard design for the test engine. Phase 2 replaced the original hooked second ring using a ring gap of 0.56 millimeters with a negative twist second ring using a reduced ring gap of 0.11 millimeters. Phase 3 replaced the original top ring using a gap of 0.35 millimeters, with a similar ring using an increased gap of 0.60 mm, and the remaining rings were from phase 1.

From the results of the inter-ring pressures measured at -15 Nm operating condition for phases 1 and 2, top ring flutter was predicted and was later verified in phase 3 testing with the addition of two pressure ports. The LIF data comparison for the three phases clearly shows that the oil film thickness on the second land was smallest for the phase 1 ring pack at the -15 Nm condition, which was related to the manufacturer's oil consumption data which also shows the least amount of oil consumption at -15 Nm condition using the phase 1 ring pack.

Thesis Supervisor:	Victor W. Wong
Title:	Lecturer, Department of Mechanical Engineering

(This page intentionally left blank)

ACKNOWLEDGEMENTS

I would like to thank the faculty at the MIT Sloan Automotive Lab who have made my two years as a graduate student pleasant and challenging. In particular I'd like to thank my advisor, Dr. Victor Wong, who granted me the freedom and space to excel, while always offering his support and guidance. I would also like to thank Prof. John Heywood, Prof Wai Cheng, Prof Simone Hochgreb, Prof. Doug Hart and Dr. David Hoult .

I am fortunate to have the opportunity to thank two fine engineers working at Renault, Paris, Mokhtar Maamouri and Gerard Desplanches. Working closely with these two individuals throughout this project has given me valuable industry experience. Without their support this project would not have been accomplished.

During the five months it took me to build the engine test facility, I need to pay special thanks to Brian Corkum, the lab's technician. His advise and guidance were most valuable, and his friendship made the experience extremely pleasant. I would also like to thank Nancy Cook, the lab's administrative support, whose patience and help with all my purchases was appreciated.

Of all the people I would like to thank at MIT one individual stands alone, my office mate, Tian Tian. Tian is a true scholar and the finest friend I could have gained at MIT. Our many and extensive conversations discussing research topics was a major source in my masters education.

I would also like to thank two more office mates, a former, Goro Tamai and a present, Steve Casey. Goro passed along the LIF system to me fully operational and well documented, and his advise during the engine modification was most valuable. To Steve, who had big shoes to fill, his friendship and pleasantness were much appreciated.

At far as the general environment at the Sloan lab, I found it to be very supportive and quite fun. I would like to thank the following list of fellow graduate students: Gatis Bazbauers, Mark Lusted, Richard Versteegh, Janice Dearlove, Doug Schofield, Eric Ford, Vincent Frottier, Denis Artzner, Kelly Baker, Wolf Bauer, Jon Fox, Kent Frolund, Stefan Groenniger, Haissam Haider, Peter Hinze, Mark Jackson, Robert Meyers, Tom Miller, Pierre Mulgrave, Chris O'Brien, Norman Peralta, Mike Shelby, Alan Shihadeh, Younggy Shin, Marcus Stewart, Tung-Ching Tseng, Brad VanDerWege, Kuo-Chun Wu, Christian Ziegler, and Josmar Pagliuso. I'd also like to thank a fine visiting engineer from Caterpillar, Mark Kiesel. Lastly I would like to thank two excellent undergraduate student who helped me with my work: Andrew Carnell and Luis Palacious.

Outside of MIT I would like to thank all my friends for their support over the last two years. I would like to give special thanks to one group in particular, Terri and her two children, Kurt and Liza. I thank them dearly for their love and comfort during my first year and half at MIT.

The last group of people I would like to acknowledge and thank are the most important, my family. To my brothers, Pieter and Duco and to my sister, Margot, a special thanks. To my mother and father, without their support and advise I would not have achieved this degree, thank you.

Bouke Noordzij
May 1996

(This page intentionally left blank)

TABLE OF CONTENTS

LIST OF FIGURES

LIST OF TABLES

LIST OF ABBREVIATIONS

LIF _____ Laser Induced Fluorescence

PT _____ Pressure Transducer

TDC _____ Top Dead Center

BDC _____ Bottom Dead Center

CHAPTER 1 MOTIVATION

1.1 INTRODUCTION

The engine and automotive industry is constantly trying to better their understanding of the mechanisms behind engine oil consumption with the goal of minimizing this negative operation. The effects of lowering engine oil consumption are as simple as improving customer satisfaction to as crucial as lowering hydrocarbon emission. Low oil consumption is not only seen as good quality control but is also essential for meeting ever more stringent vehicle emissions limits.

To gain a better understanding of the engine's oil consumption mechanisms the piston ring pack system must be studied or even possibly modeled. It has always been extremely difficult to experimentally study the oil flow and accumulation in the piston ring pack during operation and this difficulty has limited the forward progress of improving the piston ring pack to fully minimize oil consumption [1]. There has also been aggressive studies in attempting to measure the inter ring pressures and relative ring positions to determine the driving forces and passage ways for which the oil is forced to travel.

In recent years production engines have become smaller in size requiring higher power outputs thereby minimizing costs, increase fuel economy while maintaining driver needs. With these smaller high output engines the normal operating engine speeds have increased and the demand for high speed engine studies has risen. These high speed engine studies are of particular interest because the engine ring pack is subject to extreme conditions.

In an attempt to gain a thorough understanding of the behavior of a piston ring pack under all operating conditions including high speed testing a wide array of tests can be performed on an engine. These tests include measuring oil consumption, oil film thickness on the piston, cylinder and inter-ring pressures and relative ring positions. For this project the primary goal was to measure these values and correlate them to characterize the behavior of the piston ring pack system. To aid in this understanding certain ring geometry's were altered in hopes of revealing the significance of such changes.

1.2 APPROACH

To achieve a solid understanding of the piston ring pack system three major areas were studied, the oil consumption rate, oil film thickness on the piston, and the pressures within the engine. These areas of interest were directly measured at high speed engine operation conditions and the data was processed along with computer modeling to achieve a complete view of the ring pack performance.

Oil consumption rate measurements at steady state engine operation can be obtained from measuring the amount of oil lost from the engine over prolonged operation. This method, commonly referred to as drain and weight, was used to measure the oil consumption rate for different load conditions and various ring pack designs.

To measure the oil film thickness on the piston during engine operation, a laser induced fluorence (LIF) system has been developed. This system utilizes a small quartz window that is modified into the cylinder liner exposing the reciprocating piston to the LIF system. This type of measurement is confined to one point measurements and for this project several windows were installed at various locations in the liner. The LIF system records the oil film thickness on the piston as it travels past the window revealing the amount of oil that has accumulated on the piston lands. This type of information reveals the potential for oil to enter the combustion chamber with hopes of minimizing the amount of oil on the piston crown land in order to reduce oil consumption.

The cylinder pressure was measured by means of a dynamic pressure transducer mounted in the combustion chamber. The more difficult task was to record the pressures between the piston rings during engine operation. Ideally, transducers mounted to the piston and channeled to the second and third lands would allow for a complete cycle measurement, but this method was avoided due to the relatively small size of the pistons for the test engine used and the extreme environment the transducer would be subject to, mounted to the piston during high speed testing. An alternative method was to mount pressure transducers to the back side of the cylinder liner and machine tiny port holes to the cylinder. These tiny ports would connect the transducers to the pressures between rings as the lands are exposed to the port hole during operation. Only a short duration of the full cycle land pressures could be measured but if the number of ports and their locations were chosen properly the information acquired could reveal the basic trend that the land pressures follow.

A computer model was also used to predict full cycle land pressures, relative ring positions and mass flow rates through the ring gaps. This model was calibrated using the segments of the land pressures measured from the inter-ring pressure ports. The model was proven to be useful in predicting the relative positions of the rings, especially ring fluttering, which may effect the performance of the ring pack on oil consumption.

1.3 PREVIOUS WORK

There has been extensive oil film thickness work done at MIT using a LIF system over the past ten years. The latest contributions to the system performed by Goro Tamai [2] during his graduate work have contributed in such a manner that the system was fully operational and well documented such that few modifications were needed to implement the system for this project. The design criteria for modifying an engine cylinder liner with quartz windows was closely followed for this project such that the same productive results could be achieved. The analysis procedures for converting raw LIF data to actual oil film thickness values were also well documented. Therefore this project consisted of modifying a production engine to utilize the existing LIF system at MIT.

There has been little documented work on recording inter-ring pressures from accessing port holes in the cylinder liner. Usually pressure transducers were mounted to the piston of direct injection engines for low speed operation [3]. For this project the port hole design was created such that the port holes were as small as possible as not to alter the liner surface and to mount the transducers as close as possible to the liner surface to minimize delay time.

1.4 PROJECT OBJECTIVES

The objectives for this project were:

1) The objective for the first half of this project was to set up the test engine facility for high speed steady state and transient operations. The load conditions that the engine facility were to handle included both firing (positive) and motoring (negative) load conditions.

2) Eight quartz windows were modified into one of the engines cylinder wall so that various location could be tested for oil film thickness, which included different vertical locations and different circumferential locations.

3) The inter-ring pressures were measured at strategic points to understand the effects of ring gap sizes. These recorded pressures would also reveal the pressure driving force on the oil on the piston lands. Lastly by measuring the inter-ring pressures indirect ring fluttering could be revealed by fluctuating pressure measurements or possibility by recording excessively high land pressures.

4) To understand the affects of the ring gap area three different ring pack designs were studied with each ring pack altering the gap area of one of the top two rings.

5) The ultimate object was to correlate the oil film thickness and inter-ring measurements with the oil consumption measurements for the three test cases to achieve a better understanding of the oil transport mechanisms within the piston ring pack.

CHAPTER 2 EXPERIMENTAL APPARATUS

2.1 LASER INDUCED FLUORESCENCE (LIF) SYSTEM

The LIF system at MIT has been used over the years to measure the oil film thickness on the free cylinder liner, on the piston lands and under the piston rings. The system has been well documented and was fully operational for this project [2]. A simple schematic of the LIF system is shown in Figure 2.1.

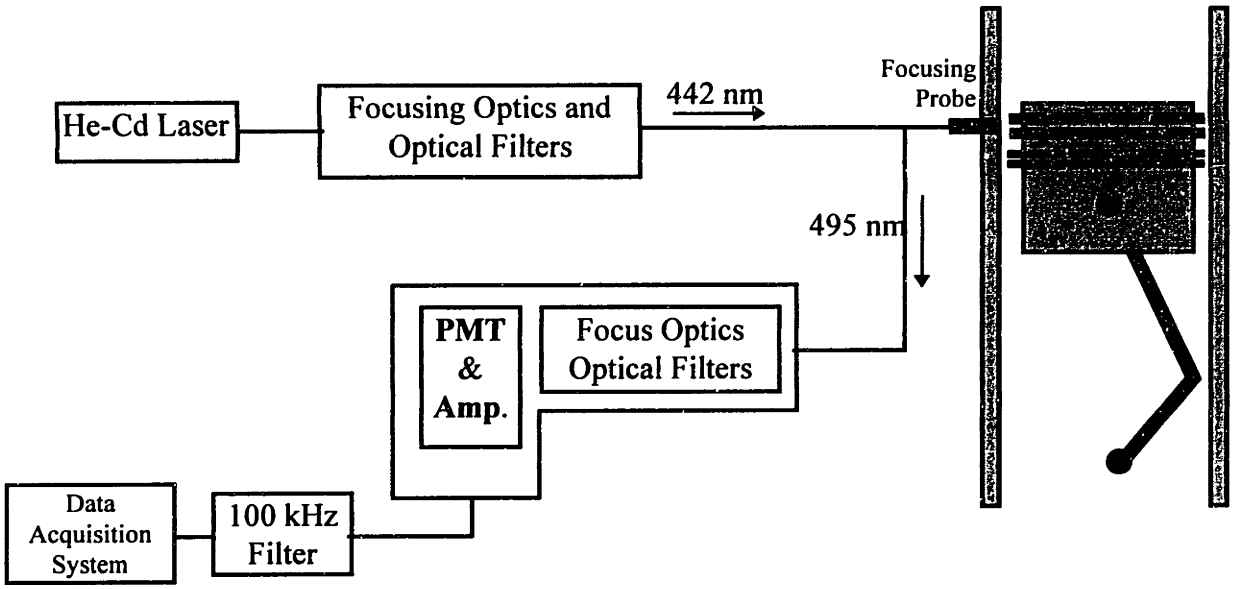

Figure 2.1 Schematic of Laser Induced Fluorescence System.

There were several changes made to enhance the LIF system. The first two changes were made to the fiber optics system which channels the laser light (442 nm) and the return (495 nm) signals with in the LIF system. The laser signal is directed into the fiber optics cable via an eccentric coupler which was upgraded from General Fiber-Optic model 85-22 to a model 8612-12501. The major difference between these two models was a built in focusing lense which would increase the amount of laser light directed into the fiber optic cable. The bifurcated fiber optic cables were replaced for the LIF system with higher quality cables to enhance the light carrying capability. These two changes significantly increased the LIF signal strength.

The LIF focusing probe assembly mounted to the engine was slightly altered. The past engine set-ups have used high purity UV fused silica lenses in the focusing probe assembly, which are costly and can be in limited supply. For this project, glass lenses were used in the probe housings with no noticeable negative effects on the LIF signal intensity. The inner dimensions of the probe housing were changed to allow for the newer type lenses, refer to Figure 2.2.

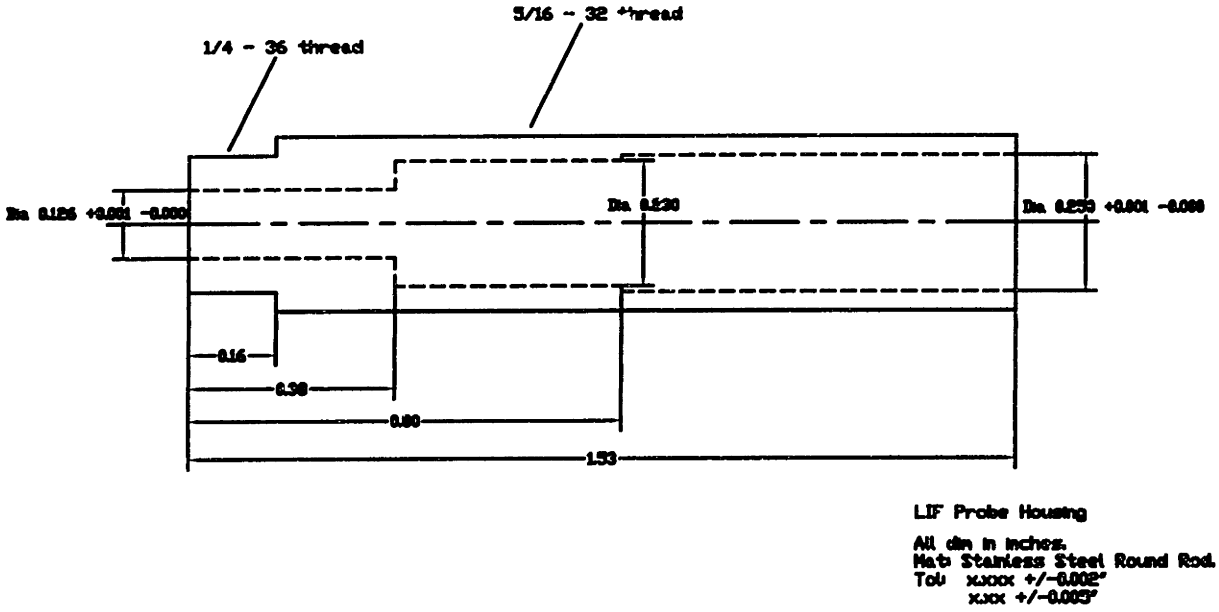

Figure 2.2 LIF Probe Housing.

The two optic lenses, of diameter 6.35 mm (0.25 in.), slide into the probe housing and are separated by a spacer ring of length 11.99 mm (0.472 in.).

A full description of all the LIF system parts is listed in Table 2.1

Component	Manufacturer	Part Number
14 mW He-Cad laser, 442 nm and Power Supply	Liconix	4214 N
442 nm optical filter (2)	Oriel	52086, 1 inch OD
Filter Holder	Oriel	51594
Laser to Fiber Optic Cable Coupler (eccentric coupler)	General Fiber-Optic	8612-12501
Bifurcated Fiber Optic Cables	General Fiber-Optic	B16-0200-HAS-C22-G-0066-2.5-SMA/3
LIF Focusing Probe	F. H. Peterson Machine Corp.	custom made for application (see figure 2.2)
Laser-to-Engine LIF Focusing	Melles Griot	01LPX007

Probe Lenses (2 per probe)		
LIF Windows (fused quartz/silica)	Gould Precision Optics	custom made for application
- Start of PMT Focusing Assembly. -		
Oriel Fiber Input Flange	Oriel	77850
Flange Collar	Oriel	77829
Collar Coupler (male/male)	Oriel	78122
Optic Holder w/ lens holding collar. (1 of 3)	Oriel	7123
Lens (laser to PMT #1, focal length = 38mm, convex toward PMT.)	Oriel	41330
Optic Holder w/ lens holding collar. (2 of 3)	Oriel	7123
495 nm Optical Filter (2)	Omega Optical	495DF20
Optic Holder w/ lens holding collar. (3 of 3)	Oriel	7123
Lens (laser to PMT #2, focal length = 150mm, convex away from PMT.)	Oriel	41370
4 inch Spacer	Oriel	7132
Collar Coupler (female/female)	Oriel	77829
PMT Housing	Products for Research	custom made for application
- End of PMT focusing assembly.		
Photo Multiplier Tube (PMT)	Hamamatsu	R4220
PMT Socket and Amplifier	Hamamatsu	C1053-01
High Voltage Power Supply for PMT	Bertan	230-03R

+/- 15 Volt Power Supply for PMT Amplifier	Newark Electronics	SLD-12-1010-12
100 kHz Low Pass Filter with BNC input and output	Sloan Electronics	custom made for application
Fluorescent Oil Coumarin Dye (5g)	Exciton	Coumarin 523
Data Acquisition System	Keithley Metrabyte	DAS-55 & SSH-58

Table 2.1 Components of the LIF System.

2.2 THE ENGINE: FOUR CYLINDER SPARK IGNITION PRODUCTION ENGINE

The engine used for the LIF and inter-ring pressures was a 2 liter, four cylinder, spark ignition production engine. This particular engine was chosen due to extensive documentation collected by the manufacturer and the many alternative piston ring configurations manufactured for this engine. The test engine is a spark ignition, four stroke engine with the general specifications listed in Table 2.2.

Engine	Four cylinder spark ignition
Engine Head	Cast aluminum, two valves per cylinder
Engine Block	Cast iron and liners
Displacement	1.998 liters
Bore	82.7 mm
Stroke	93 mm
Crank Radius	46.5 mm
Connecting Rod Length	149.5 mm

Table 2.2 Test Engine Specifications.

There were three major modifications performed to the test engine; the installation of LIF windows, pressure transducers and thermocouples. The engine was conveniently accessible on the anti-thrust side of the two middle cylinders, cylinders 2 and 3, due to both the attachments of the intake and exhaust manifolds on the thrust side. These manifold configurations, along with the absence of engine accessories allowed for unlimited access for LIF and pressure transducer locations along the anti-thrust line and approximately 30 degrees to each side of the anti-thrust line. The only point of concern for the modifications to the engine block was the water jacket which surrounds the cylinder liner, this issue will be addressed further in Section 2.2 and 2.3.

The base engine block casting, before engine honing and assembly, was first modified at MIT to incorporate the LIF windows, inter-ring pressure transducers (PT) and thermocouples. After modifications, the engine was shipped back to the manufacturer where engine honing and

assembly was performed. While at the engine manufacturer test facility a full engine oil consumption and blow-by mapping was performed to ensure that the engine modifications did not disturb the integrity of the engine. The engine manufacturer engineers were satisfied with the modified engine's performance as being standard for all similar production engines and it was returned to MIT for engine setup.

2.3 LIF WINDOW LOCATIONS

Due to the engine configuration of the intake and exhaust manifold, plus engine accessories, the cylinder chosen to hold the LIF windows was cylinder 2 on the anti-thrust side away from the exhaust manifold. Four vertical locations were chosen on the anti-thrust line and an additional four windows were placed 30 degrees off the anti-thrust line (away from the flywheel) at the same corresponding vertical locations as the anti-trust windows, refer to Figure 2.3.

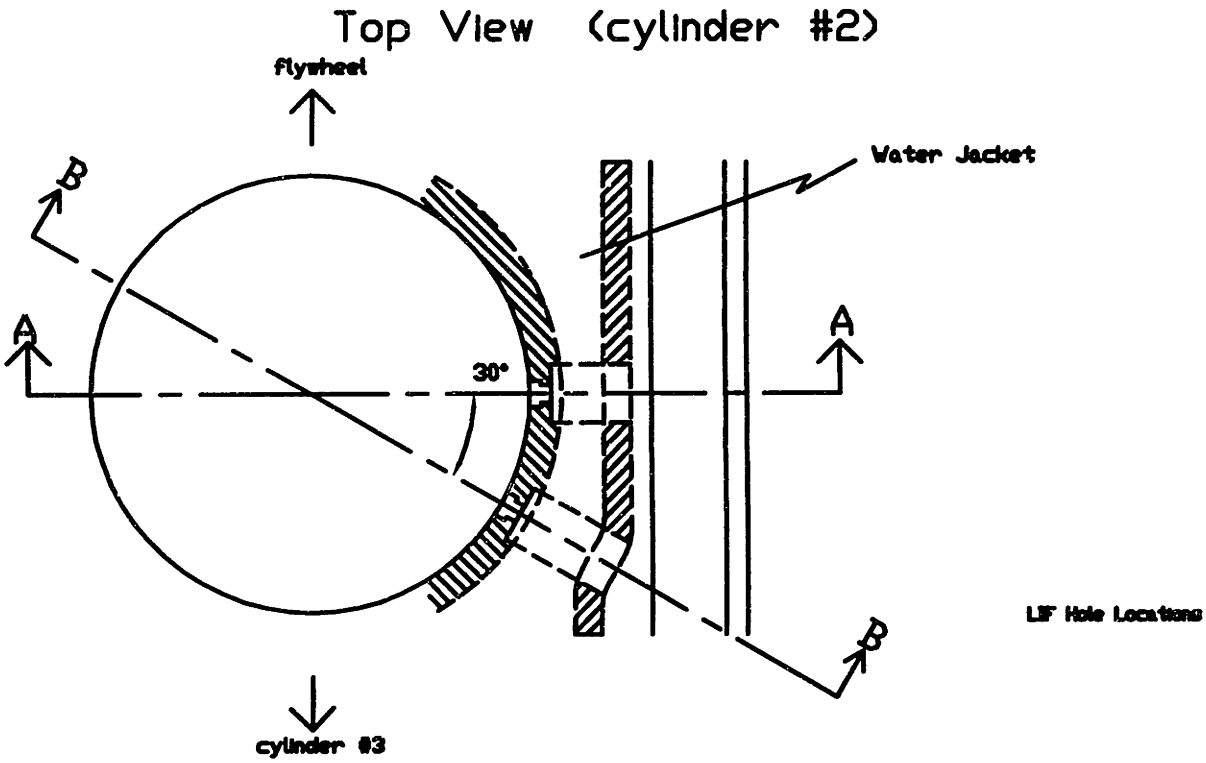

Figure 2.3 Top View of Cylinder 2 LIF Window Locations.

The locations of 30 degrees off the anti-thrust line was chosen as a point of measuring the effects of bore distortion to the oil film thickness where 30 degrees was a point of 30 micron bore distortion at 50 mm down from TDC with a running condition of 4000 rpm, wide open throttle, refer to Figure 2.4 [4].

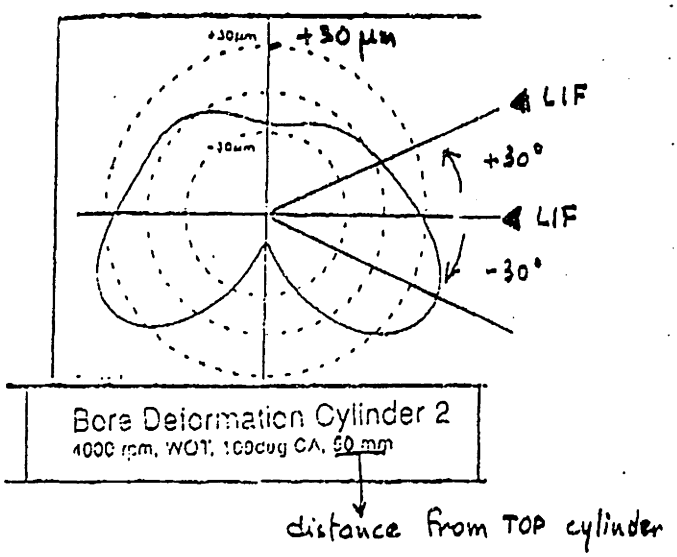

Figure 2.4 Measured Bore Distortion at 4000 rpm, Wide Open Throttle, 50 mm from TDC.

The vertical positions were chosen from the geometric limitations and points of interest. The upper most window is located directly below the oil return jacket, at 50.0 millimeters below the top of the cylinder, so that the possibility of coolant contamination into the oil was eliminated. The lowest window, located at 102.0 millimeters from TDC, is below the water jacket and directly above an oil passage. The middle two window locations, at 73.0 and 87.5 mm, were chosen at point were ring flutter was predicted, and were also limited by the required spacing between each quartz window.

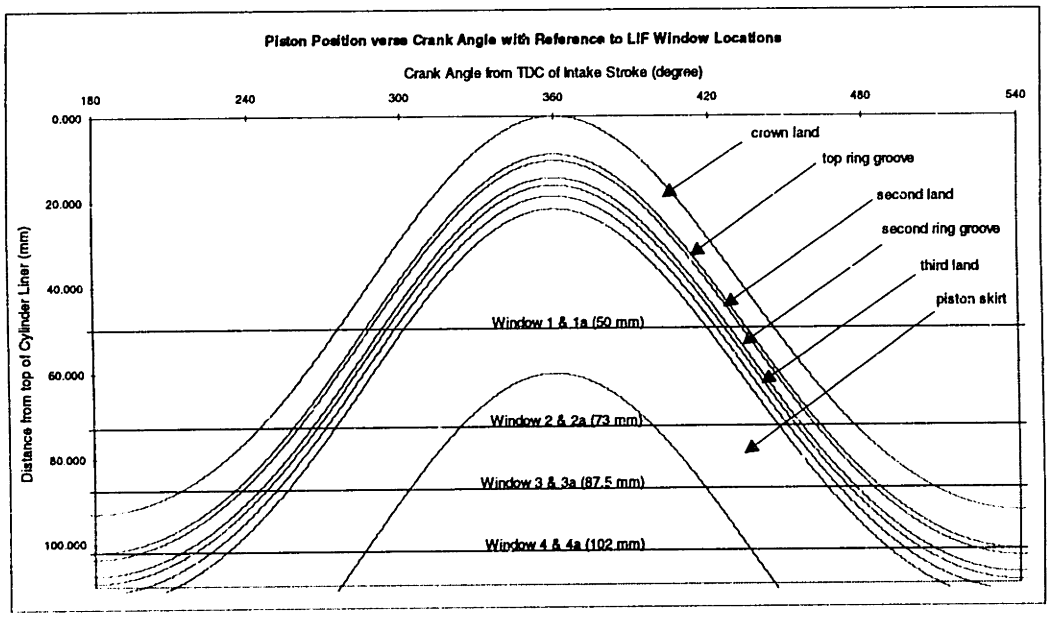

Figure 2.5 Piston Profile verse Crank Angle with Reference to LIF Window Locations.

To clarify where each vertical window locations scan the piston profile, Figure 2.5 plots each region of the piston as a function of the crank angle degrees. The piston's speed and acceleration varies with crank angle such that the piston motion is close to sinusoidal. Each vertical window location is plotted as a dark line and the points where each line crosses the lines of the piston profile determine the time period for recording land oil film thickness. Note that window 4 and 4a can not record crown land oil film thickness or free liner film thickness.

Refer to Figure 2.6 for the anti-thrust line vertical locations and Figure 2.7 for the 30° off the anti-thrust line.

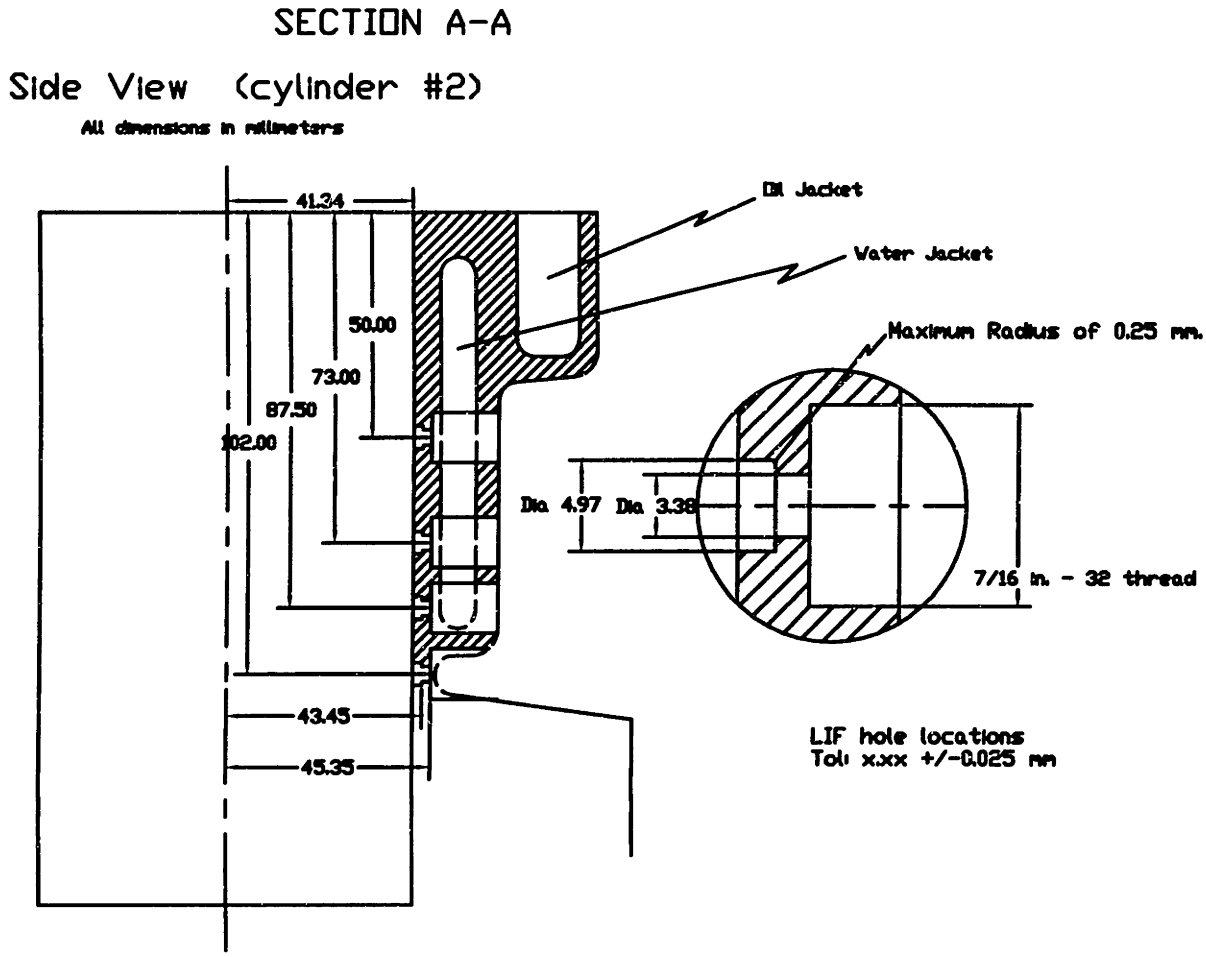

Figure 2.6 Side View of Cylinder 2 LIF Window Locations on the Anti-Thrust Line.

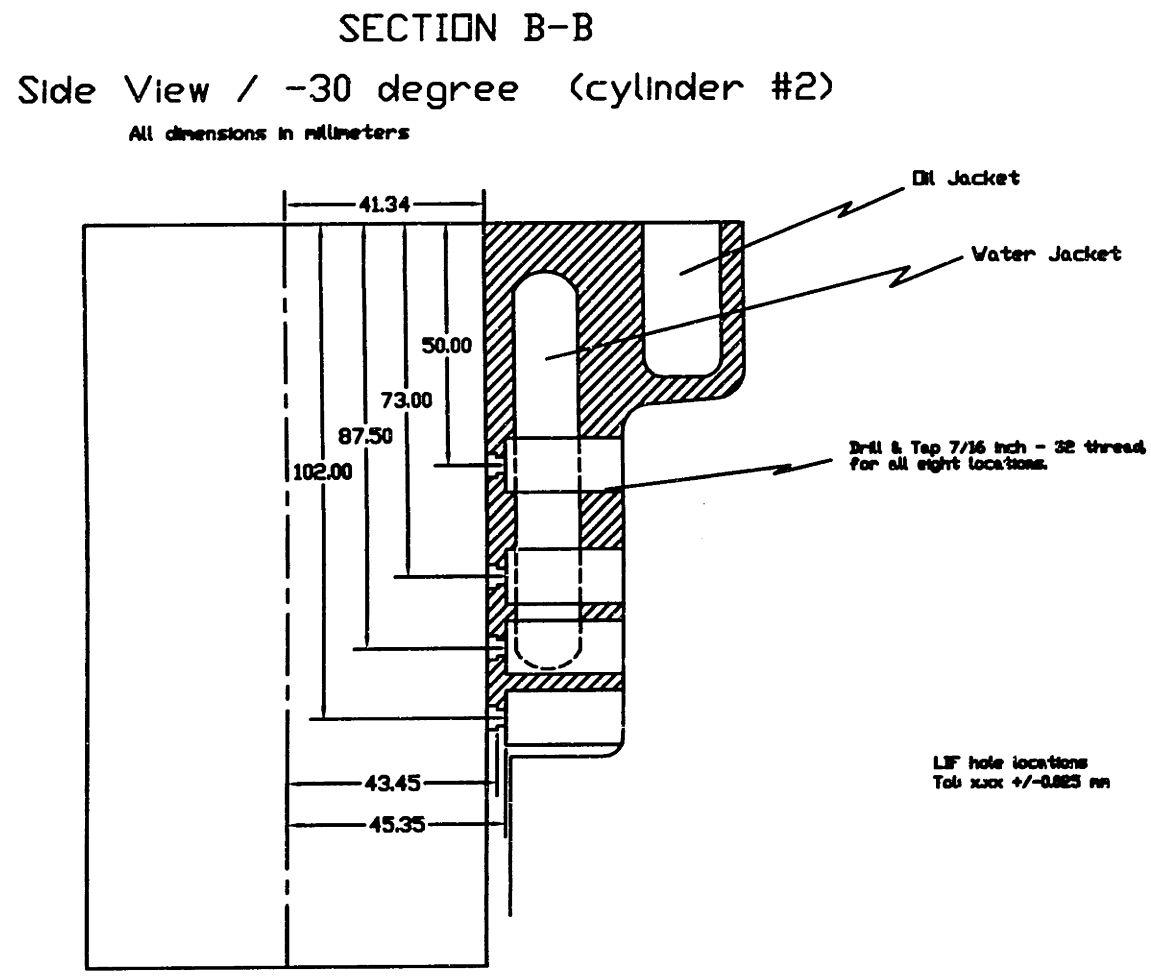

Figure 2.7 Side View of Cylinder 2 LIF Window Locations 30° off the Anti-Thrust Line.

The eight windows modified into the cylinder liner were designated for simple refer through out this project. Table 2.3 lists the reference names for each window location.

Distance From Top of Cylinder Liner (mm)	Anti-Thrust Line	30° off the Anti-Thrust Line
50.0	Window 1	Window 1a
73.0	Window 2	Window 2a
87.5	Window 3	Window 3a
102.0	Window 4	Window 4a

Table 2.3 LIF Window Location Reference Names.

The LIF windows were manufactured of fused quartz silica with a head radius of 41.3 mm (half the bore). This head radius is of utmost importance to ensure undisturbed continuity with the cylinder liner and window alignment became the primary focus when gluing the windows in place. The machining of the window ports was performed with a tolerance to allow for a 50 to

75 micron recess of the glued window, such that the honing process performed at engine manufacture would bring the two surfaces flush. The results after honing were acceptable for the purposes of the experimentation with an average window recess of 1.5 microns. See Appendix A for the surface profile of each window [4].
The windows were glued in place using Eccobond® 285 with a catalyst 9, manufactured by Emerson & Cumming™. This epoxy was chosen for the features of high strength, good thermal cycling, and low thermal expansion. The upper limit service temperature of the Eccobond® 285 with catalyst 9 is 120° C and this upper limit put a limitation on the allowable engine operating temperature.

2.4 CYLINDER AND INTER-RING PRESSURE TRANSDUCER LOCATIONS

The two cylinder PT locations were machined into the aluminum head for cylinders 2 and 3 to obtain combustion chamber pressures. The PTs are water cooled AVL 8QP500c quartz transducers with the following specifications:

AVL 8QP500c	Cylinder 2	Cylinder 3
Measurement Range	150 bar	150 bar
Sensitivity	11.17 pC/bar	11.54 pC/bar
Linearity	<± 0.6%	<± 0.6%
Natural Frequency	100 kHz	100 kHz
Tightening Torque	15 Nm	15 Nm
Serial Number	3600	3599
Sealing Gasket	Z 130	Z 130

Table 2.4 Cylinder Pressure Transducer Specifications.

At the start of the project four locations were chosen for the placement of the PT to pick up inter-ring pressures. These locations were directly related to the LIF window locations which were chosen to record erratic inter-ring pressures that would reveal ring fluttering. After observing the pressure data for the first two thirds of the project it became evident that the PT locations were too low to record top ring fluttering and two more PT ports were machined into the engine block at points where ring flutter would more likely be observed.

The PTs chosen for measuring inter-ring pressures were the smallest transducers available such that close staggering could be accomplished such that a interpolation of the four pressure recording would be possible. Special transducer adapters were fabricated to isolate the coolant jacket and mount the transducers with proper sealing of the combustion chamber, refer to Figure 2.8.

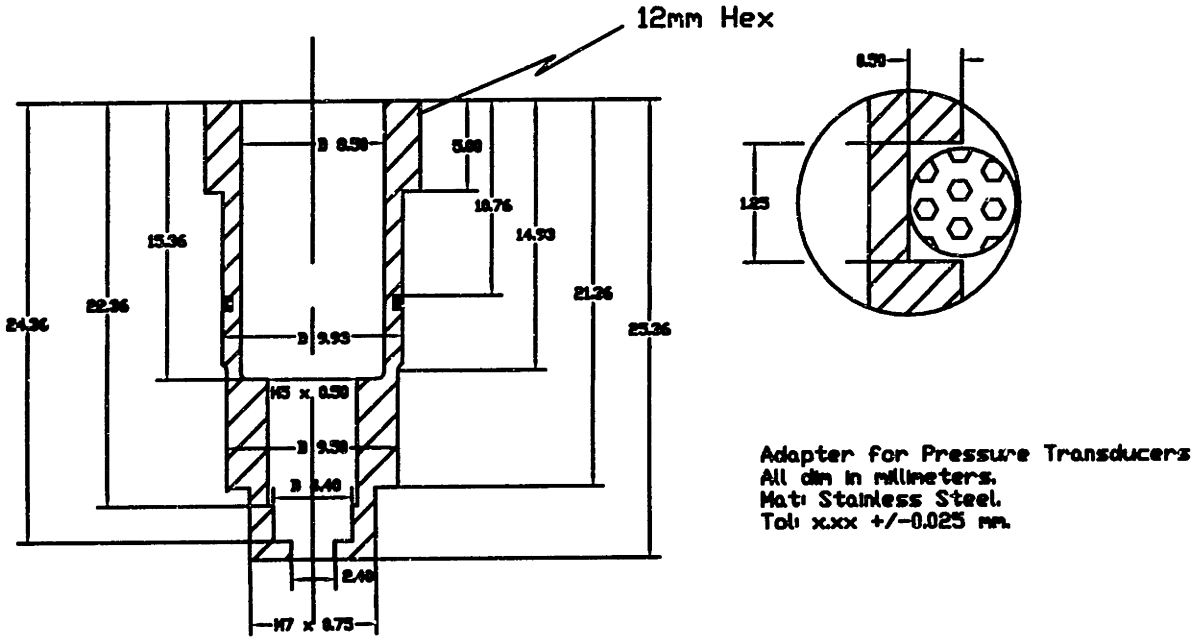

Figure 2.8 Pressure Transducer Adapter for Ports 1, 2, 3 and 4.

A one millimeter diameter hole of length three millimeters was drilled into the combustion chamber to pick up the inter-ring pressures as the piston and rings passes by the ports. This one millimeter channel then opened into the face of the transducer. Then vertical locations of the transducers were 50.0, 58.0, 66.0 and 74.0 millimeter down from the top of the cylinder liner, designated ports 1, 2, 3 and 4, respectively. The equally spaced distance between pressure ports of eight millimeters was chosen to be twice the length of the second land.

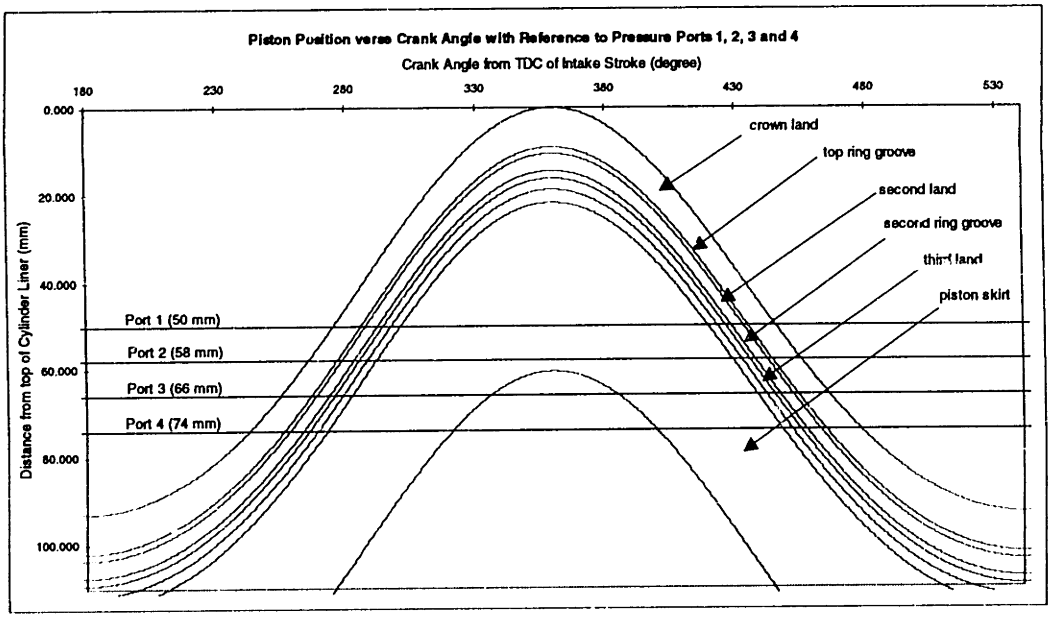

Figure 2.9 Piston Profile verse Crank Angle with Reference to Pressure Port 1, 2, 3 and 4.

The piston profile was plotted as a function of crank angle with the locations of the four pressure ports included to clarify the regions of inter-ring pressure measurements, as shown in Figure 2.9.

Due to the ten millimeter diameters of the PT adapters, the ports were staggered 10 degrees off the anti-thrust line. Refer to Figure 2.10 for a top view of cylinder 3, and Figures 2.11 and 2.12 for the side views at +10° and -10°, respectively.

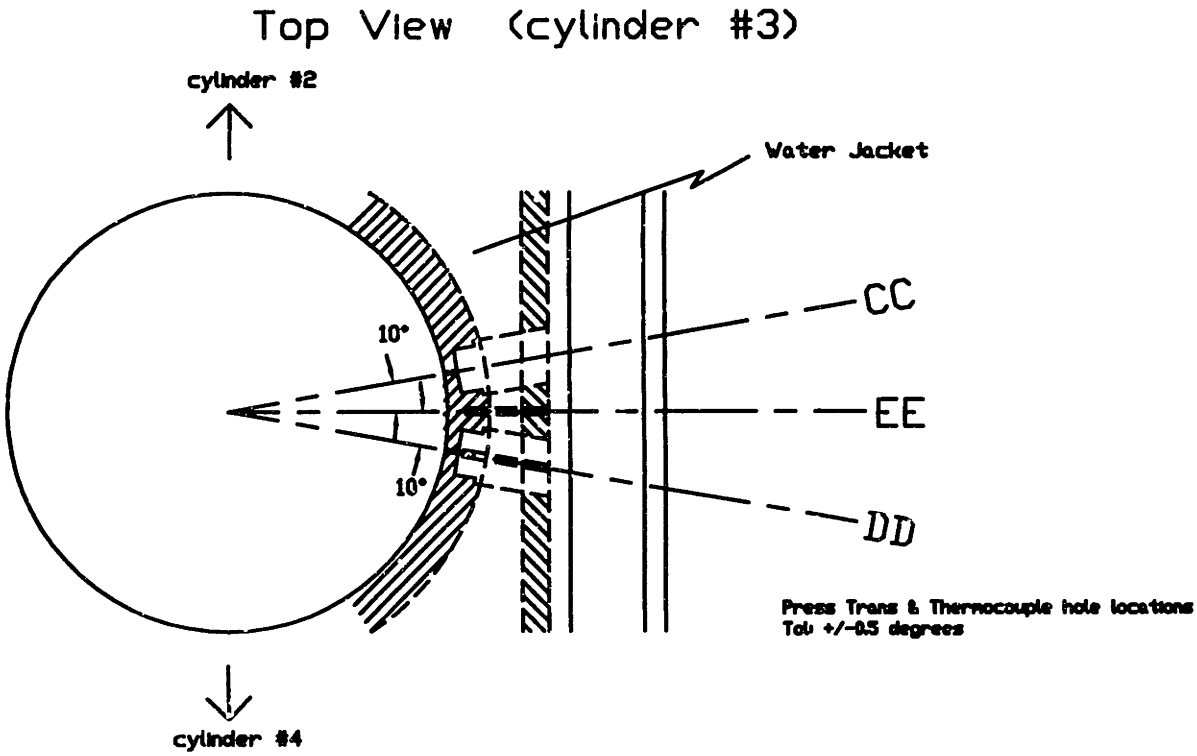

Figure 2.10 Top View of Cylinder 3, Pressure Transducer Locations.

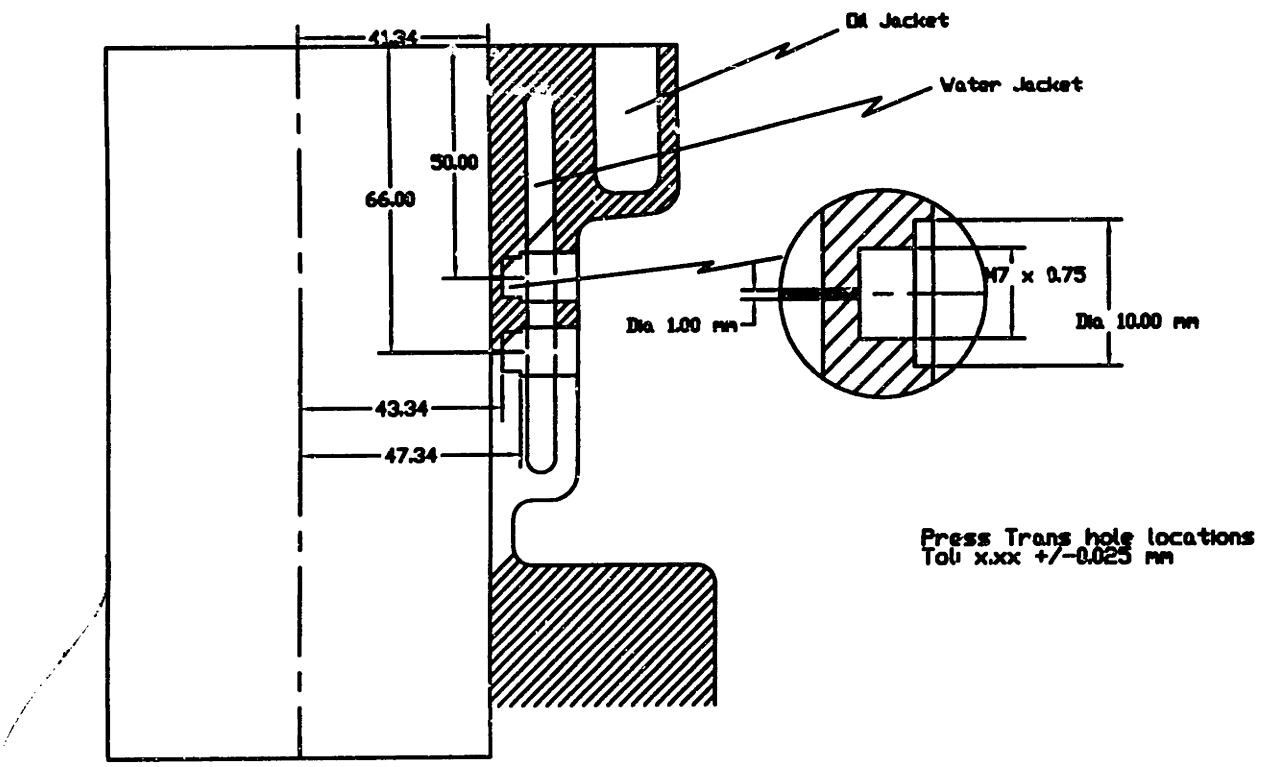

Figure 2.11 Side View +10° of Cylinder 3, Pressure Transducer Ports 1 and 3.

Table 2.5 lists all the specifications of the four inter-ring PT used. The sensitivity values for the range 0 to 50 bar were the values entered into the PT amplifiers for this project.

Kistler 6051B	**SN 554915**	**SN 554916**	**SN 557991**	**SN 557992**
Calibrated Range	0...250 bar	0...250 bar	0...250 bar	0...250 bar
Sensitivity	7.47 pC/bar	6.86 pC/bar	7.26 pC/bar	7.13 pC/bar
Linearity	<± 0.2%	<± 0.3%	<± 0.3%	<± 0.2%
Calibrated Range	0...50 bar	0...50 bar	0...50 bar	0...50 bar
Sensitivity	7.49 pC/bar	6.76 pC/bar	7.28 pC/bar	7.16 pC/bar
Linearity	<± 0.1%	<± 0.3%	<± 0.1%	<± 0.1%
Tightening Torque	2 Nm	2 Nm	2 Nm	2 Nm
Sealing	Front Sealing	Front Sealing	Front Sealing	Front Sealing

Table 2.5 Inter-Ring Pressure Transducer Specifications.

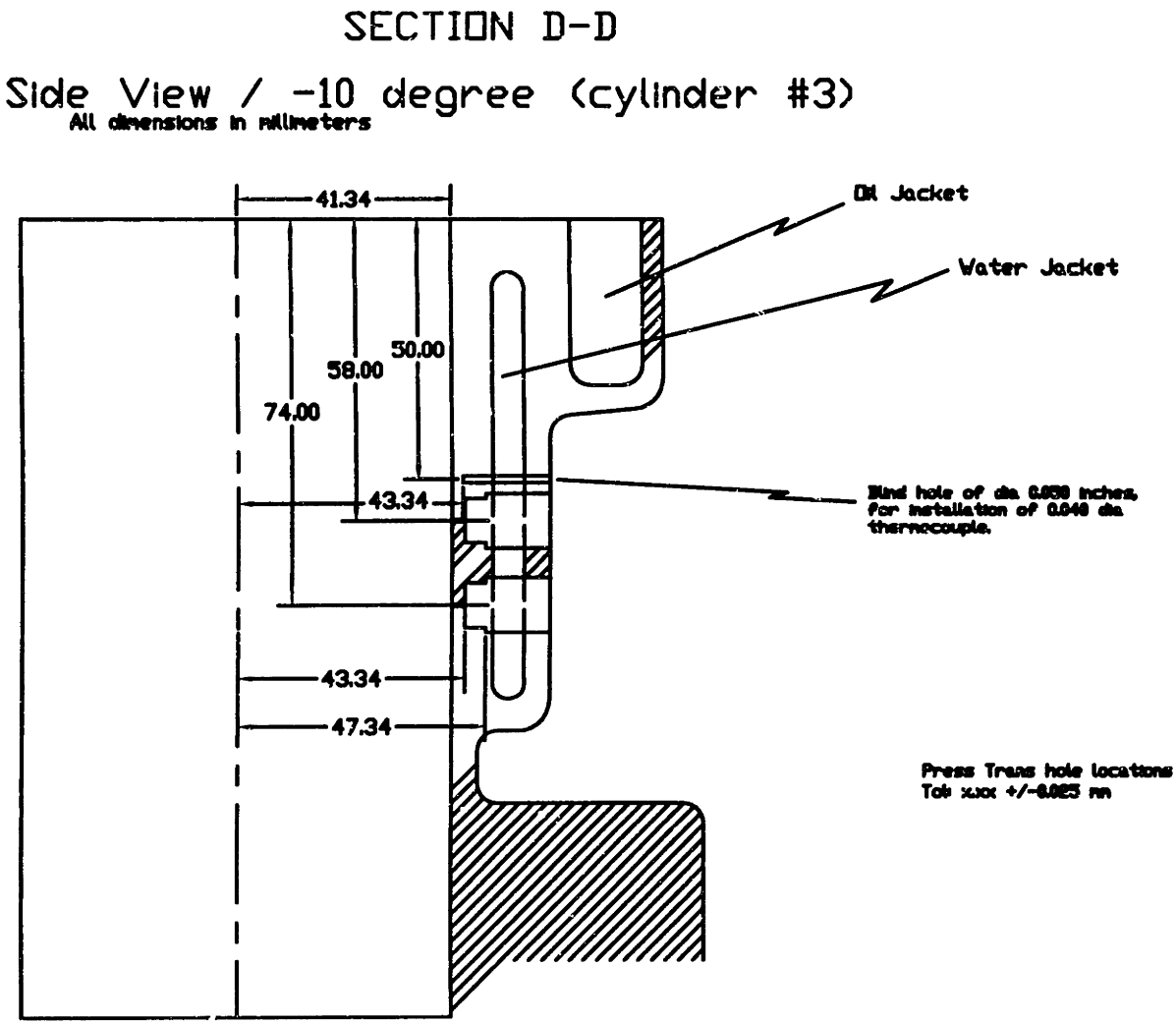

Figure 2.12 Side View -10° of Cylinder 3, Pressure Transducer Ports 2 and 4.

The first of the two additional pressure ports, port A, that were machined into the engine block after the first two thirds of the test matrix was completed, was placed slightly higher then the highest point that the second ring would reach on the cylinder liner, 14 mm from TDC. At this point the piston and rings come to a stop and the duration of second land exposure is longest, allowing for approximately 40 crank angle degrees of measuring time, refer to Figure 2.13.

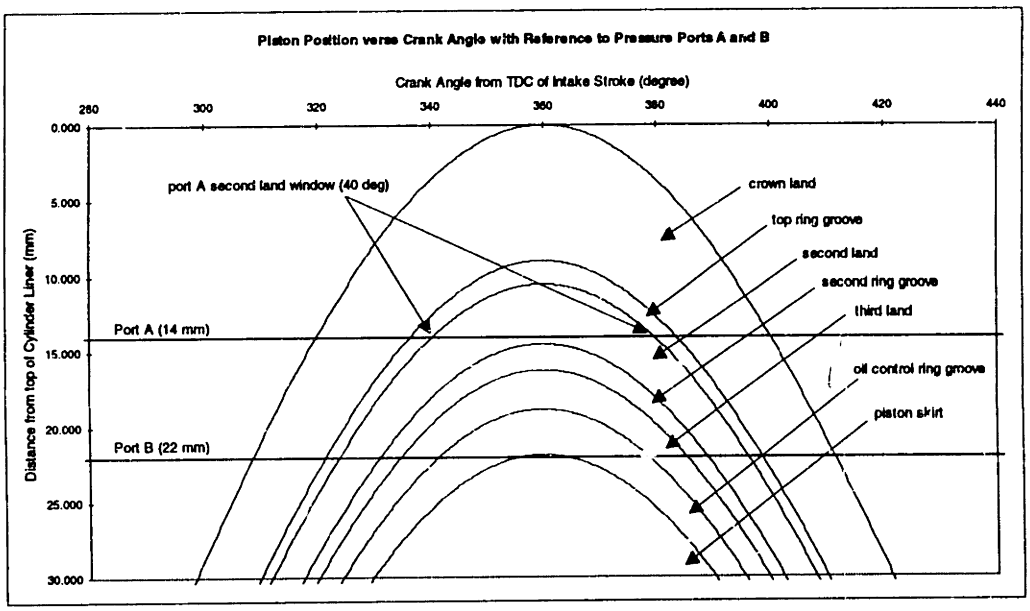

Figure 2.13 Piston Profile verse Crank Angle with Reference to Pressure Port A and B.

See Figure 2.14 for the machine drawing for the port A.

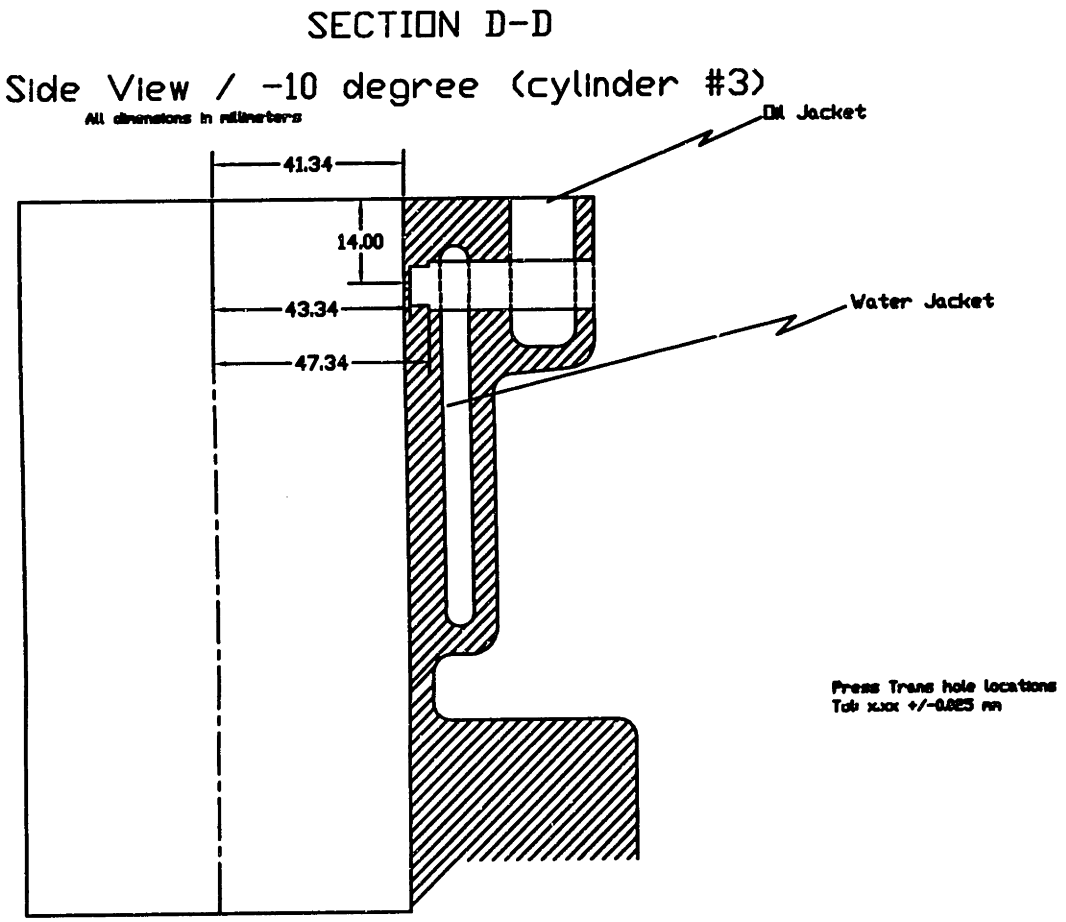

Figure 2.14 Side View +10° of Cylinder 3, Pressure Transducer Port A.

The second of the two additional pressure ports was placed 22 mm below TDC, 8 mm below the top most transducer, as shown in Figure 2.15.

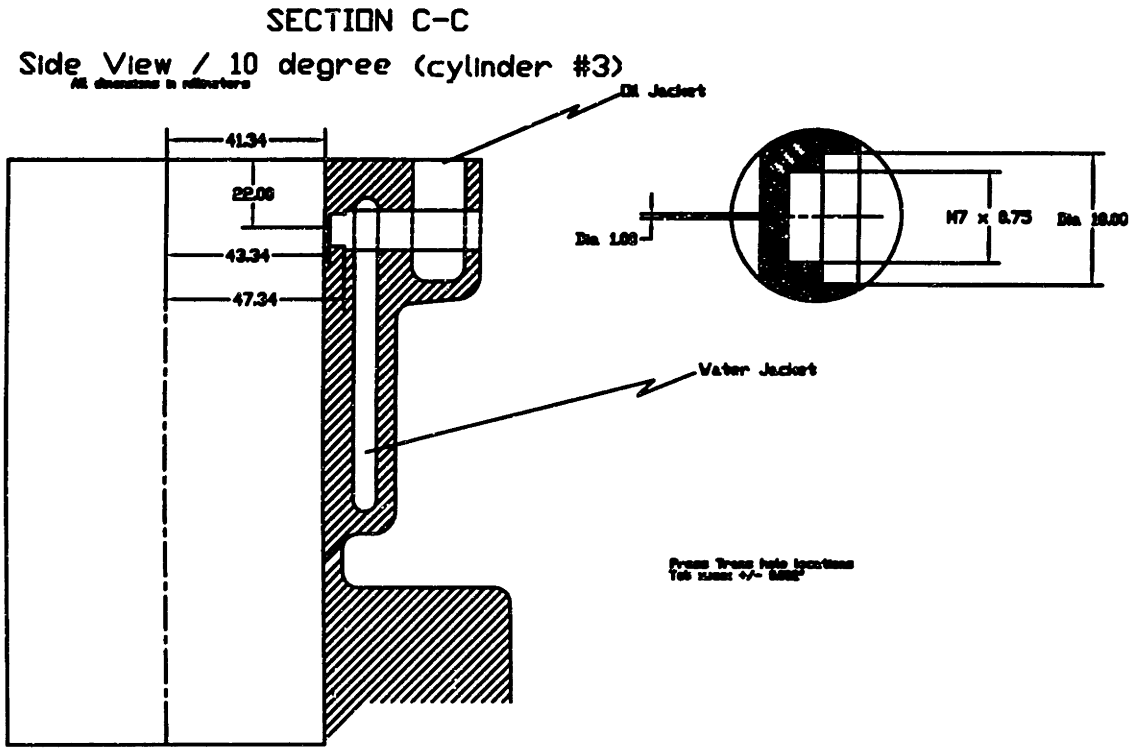

Figure 2.15 Side View -10° of Cylinder 3, Pressure Transducer Port B.

The two transducers were staggered 10 degrees off the anti-thrust line, for the same reasons as the initial four transducers.

As seen in Figures 2.14 and 2.15, the pressure ports must penetrate the water jacket and an oil jacket therefore the PT adapter were modified to accommodate this change, as soon in Figure 2.16.

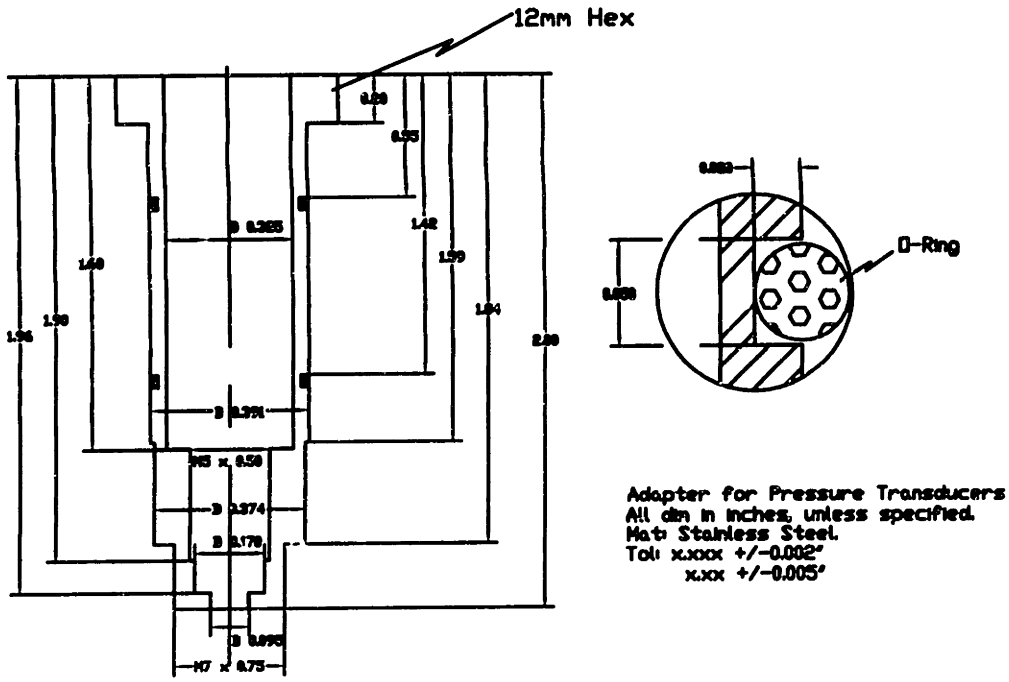

Figure 2.16 Pressure Transducer Adapter for Ports A and B.

Due to the limitations of the number of channels into the data acquisition system only four PT were used for the six PT ports, these ports being 14, 22, 50 and 74 mm from TDC. The remaining two ports were isolated using dummy plugs.

2.5 THERMOCOUPLE LOCATIONS

Two thermocouple ports were machined into the engine at 50.0 and 102.0 mm down from the top of cylinder 3. These locations were chosen at the upper and lower limits of the LIF window locations such that engine operating conditions could be monitored as not to exceed the maximum allowable temperature limit of the epoxy used to glue the windows, causing oil leakage. The ports consisted of 1.27 mm (0.050 in.) blind holes, drilled to 3 mm behind the cylinder liner. The upper port went through the water jacket and thermocouple was glued in place to isolate the coolant. The lower thermocouple was located below the water jacket and simply glued in place.

Omega GKMQSS-040(G)-6	
Type	K (Chromega™ - Alomega™)
Junction Type	Grounded
Sheath Type	304 Stainless Steal
Sheath Diameter	1.016 mm (0.040 in.)
Length	152.4 mm (6 in.)

Table 2.6 Thermocouple Specifications.

2.6 DATA ACQUISITION SYSTEM

The data acquisition system used for the testing of this project was Keithley Metrabyte DAS-58 and SSH-58 system which was operated by a personal computer. This data acquisition system was ideal for the simultaneous sampling of data at high resolution which the LIF system requires. The addition of the external SSH-58 allows the DAS-58 to operate in a simultaneous sample and hold mode. In this mode, up to eight single-ended inputs are sampled within ±20 nanoseconds of each other. This allows accurate comparisons of the two LIF systems along with proper analysis of the four inter-ring pressures in conjunction with the combustion chamber pressure.

Keithley Metrabyte DAS-58 & SSH-58	
Number of Channels	8
Maximum Acquisition Rate	1,000,000 samples/sec
On-Board Memory	1 M Word
Burst Support Mode	Yes
External Clock	Low Input <0.8 V High Input >2.0 V
Digital Trigger	Low Input <1.1 V High Input >4.0 V

Table 2.7 Data Acquisition Specifications.

The eight channels of the DAS-58 were used by two LIF signals, two cylinder PTs for cylinders 2 and 3, and by four inter-ring PTs.

2.6.1 Crank Angle Reference Encoder

The DAS-58 incorporates an external clock and a digital trigger which were obtained from an optical encoder mounted to the engine's crankshaft. The encoder used for this project was a BEI optical encoder with 2000 pts/rev resolution. This high resolution was required for LIF calibration, but was too fast a sampling rate for the data acquisition system when acquiring more then four channels of data. Since there were five pressure transducer signals the 2000 pts/rev signal was reduced to 1000 pts/rev when acquiring pressure data.

The digital trigger was connected to the 5 volt pulse per revolution channel from the encoder. This pulse was aligned with start of the intake and expansion strokes. The alignment of the shaft encoder is performed while the engine is being motored with the throttle wide open, producing a symmetric cylinder pressure peak. The one pulse per revolution mark is aligned with the cylinder pressure peak to reference TDC.

For consistent analysis of the data it is desirable to start the acquisition system at same stroke for all testing, which has commonly been the intake stroke for previous LIF sampling. For simplicity the system would randomly start acquiring at either the intake or expansion stroke so an extra half cycle was acquired and the data could be shifted accordingly.

Table 2.8 listed the shaft encoder's pin connects.

Pin	Output Name	Output Function
A	Channel A	2000 pulses/rev
B	Channel B	2000 pulses/rev shifted half a pulse
C	Channel Z	one pulse/rev
D	+ VDC	power source
E		(not used)
F	0 V	ground
G	Case Ground	ground for wire shielding
H	Channel $\overline{A}$	inverse signal A
I	Channel $\overline{B}$	inverse signal B
J	Channel $\overline{Z}$	inverse signal Z

Table 2.8 BEI Encoder Pin Specifications.

The BEI encoder incorporates a line driver for each of the three pulses it transmits, i.e. channel A and $\overline{A}$. To obtain strong clear signals from the encoder it was necessary to include a line receiver for the external clock signal, A and $\overline{A}$ channels, and the digital trigger, Z and $\overline{Z}$ channels. The line receiver used was National DS8820 dual line receiver.

2.6.2 Transient Triggering

During the desired one second transient testing it was essential to trigger the data acquisition system at the start of the throttle travel so that the optimal number of cycles could be recorded during the transient. The digital trigger must come from the encoder, therefore an electronic switch was needed to turn on the one pulse per revolution and send it to the DAS-58 system. A stepper motor controller, used for the throttle positioning, contained an external port that could deliver a 5 volt signal when activated. Therefore before the controller engaged the stepper motor in throttle travel, the 5 volt signal closed the switch for the one pulse per revolution, from the encoder, sending it to the data acquisition system and triggered the data sampling. A sample program for the stepper motor controller explains the procedure.

E0	V 730	(speed of the motor)
E3	Y 0	(open 5 volt signal for one pulse/rev switch)
E6	W 5	(wait 0.005 second)
E9	+365	(engage stepper motor 365 steps, full throttle travel)
E12	Y 1	(close 5 volt signal, for next transient)
E15	W 2000	(wait 2 seconds)
E18	V 40	(set slower motor speed)
E21	-365	(return stepper motor to original position)

Table 2.9 Sample Program for Throttle Stepper Motor Controller.

2.7 ENGINE CONTROL SYSTEM

The engine control system was primarily designed to perform high speed transients and by this requirement all other test conditions would be possible. The highest test speed was 4000 rpm and the transient operation was from a fully closed throttle position to wide open throttle position, and the reverse, in time span of one second. To accomplish such a running condition a high speed DC brush motor was directly coupled inline with a high speed eddy-current dynamometer which were coupled directly to the engine via a drive shaft. The DC brush motor had a speed controller as well as a 120 VDC power source capable of delivering 400 amps. The dynamometer incorporated a controller capable of controlling speed and load.

Component	Description
Motor	FB1-4001A Advanced DC Brush Motor
Motor Controller	1221B-7401 Curtis Controller
Motor Power Source	(20) 6 VDC Trojan T-145 Batteries
Dynamometer	AG 80 Froude Consine Limited Eddy-Current Dynamometer
Dynamometer Controller	1022A Digalog Controller
Throttle Stepper Motor	E22NRFC-LNN-NS-00 Pacific Scientific Stepper Motor
Throttle Controller	5240 Pacific Scientific Stepper Motor Indexer Driver

Table 2.10 Engine Control System Component Specifications.

During transient operation the motor speed controller was set to a speed slightly higher than desired and the dynamometer controller was set to absorb the actual desired speed, therefore controlling the speed of both the electric motor and the engine. With the speed control engaged on the dyno controller, the transient was performed by throttle operation. The test engine throttle body was modified with a 60 tooth gear such that a Pacific Scientific stepper motor and index driver could control the movements and position of the throttle.

As an example of a common transient test for a engine speed condition of 4000 rpm, with closed throttle (-15 Nm) to wide open throttle (160 Nm) travel, and with throttle travel lasting one

second, the following procedure was used. First the dyno controller was set at constant speed of 4000 rpm. Second, the engine was operating at a closed throttle position, commonly referred to as idle condition. Third, the electric motor was set at a speed slightly higher then 4000 rpm with the dyno controller maintaining a system speed of 4000 rpm with the engine operating. After a significant time period, to allow for steady state conditions, the fourth procedure was to engage the throttle in its travel using the Pacific controller and a supporting program, refer to Table 2.6. The program would trigger the data acquisition before opening the throttle such that data sampling would occur through out the throttle ramp.

2.8 ENGINE COOLANT TEMPERATURE CONTROL

To have full control of the coolant temperature, thereby controlling the cylinder liner temperature, the stock engine's thermostat was removed. The coolant could then circulate unrestricted through the engine block. The coolant was cooled by a heat exchanger with used city water as the cooling agent. The flow rate of the city water through the heat exchanger was the means of controlling the coolant temperature. The flow rate of the city water was controlled using a regulating valve with a Borden capillary tube. The Borden tube was submersed in the coolant reservoir tank and depending on the coolant temperature would regulate the flow of city water through the heat exchanger. The regulating valve could be adjusted for different operating conditions, when the desired coolant temperature would vary to maintain a safe operating liner temperature.

2.9 ENGINE OIL TEMPERATURE CONTROL

To eliminate the effects of varying oil temperatures with various load conditions, a system for controlling the oil temperature was incorporated into the engine setup. This system included an external pump, heat exchanger, thermocouple and temperature control unit. The thermocouple, placed in the oil passage after the engine oil pump, was connected to the temperature controller. The controller could be set to a specific temperature and when the oil exceeded this value the controller would power the external oil pump. The external oil pump drew oil from the engine sump, through a heat exchange, cooled by city water, and returned the cooled oil to the engine sump. This system allowed for near constant temperature oil to be delivered to the cylinder liners.

CHAPTER 3 TEST MATRIX

The experimental test matrix for this project was designed to study the effects of inter-ring pressures and piston land oil film thickness by varying the ring gaps of the top and second ring. Three test cases, designated phase 1, 2 and 3, were investigated by three of the eight LIF windows and all four of the inter-ring pressure ports. The LIF windows used were windows 1, 3 and 1a, located at 50 and 87.5 millimeters on the anti-thrust line and 50 millimeters 30° off the anti-thrust line, respectively. For the first two phases pressure transducers at the ports located at 50, 58, 66 and 74 millimeters, designated port 1, 2, 3 and 4, respectively, were simultaneously recorded. For phase 3 the transducers were placed at 14, 22, 50 and 74 millimeters from TDC, designated port A, B, 1 and 4 respectively.

The ring pack for phase 1 was the standard design for the test engine. The top ring for phase 1 had a ring gap of 0.35 mm and the second ring gap was 0.56 mm. For phase 2 the second ring gap was reduced to 0.11 mm, and the top ring gap remained at .35 mm. The second ring used in phase two was also of a different type design then phase 1, which must be noted for the analysis of the recorded data. The phase 1 second ring was a hooked ring design, whereas for phase 2 the second ring was a negative twist ring design, as shown in Figure 3.1.

For phase 3, the top ring gap was increased from 0.35 mm to 0.60 mm using the same type ring and the phase 1 second ring. Refer to Table 3.1 for the ring gap test matrix performed.

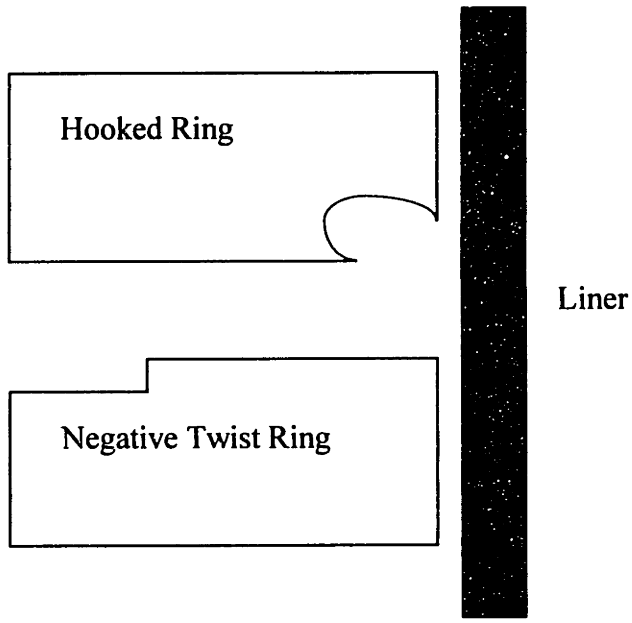

Figure 3.1 Hooked and Negative Twist Second Rings.

	Top Ring Gap	Second Ring Gap
Phase 1	0.35 mm	0.56 mm
Phase 2	0.35 mm	0.11 mm *
Phase 3	0.60 mm	0.56 mm

Table 3.1 Ring Gap Test Matrix.
*using a negative twist ring

The running conditions for each phase were the steady state conditions at 4000 rpm of loads at -15 Nm (closed throttle) and 160 Nm (wide open throttle). These two load conditions were chosen to study the effect of intake manifold pressure on oil film thickness and inter-ring pressures. The load condition of -15 Nm provides the lowest possible intake pressure and 160 Nm the highest possible pressure, atmospheric.

The only two temperatures that were closely monitored and controlled were the pressurized oil temperature and the cylinder liner temperature. The oil temperature was held constant for both running conditions at 95° C, this temperature was measured at a point after the oil pump and before the oil filter. This thermocouple was at the closest possible location before the pressurized oil reaches the cylinders. The cylinder liner temperature was monitored and controlled as not to exceed 110° C, which is 10° C lower then the upper limit of the service temperature for the LIF window glue.

CHAPTER 4 DATA PROCESSING

4.1 LIF PROCESSING

There are several steps to processing a raw LIF data set consisting of a simple bit to volts conversion, crank angle to piston distance conversion and voltage to micron calibration. The most difficult and time consuming is the latter, LIF calibration.

The LIF data was recorded for ten and half cycles for each tested running condition. This data file was processed twice using two different FORTRAN programs. One program, called SINGLE.FOR, took the raw data file of ten and half cycles and split into ten files of each consecutive single cycle starting at the intake stroke. The other program, called AVERAGE.FOR, averaged ten cycles, starting at the intake stroke, into one averaged cycle. The single cycles were used to obtain the calibration coefficient, which was then applied to the averaged cycle. Refer to Appendix B for a listing of these two programs.

4.1.1 Raw Data LIF Trace

The raw LIF trace for a full engine cycle is shown in Figure 4.1. The trace is plotted with the cylinder 2 pressure transducer data which was simultaneously recorded such that reference to the four strokes of the cycle can be verified. From the pressure data it is determined that the LIF trace begins at the start of the intake stroke.

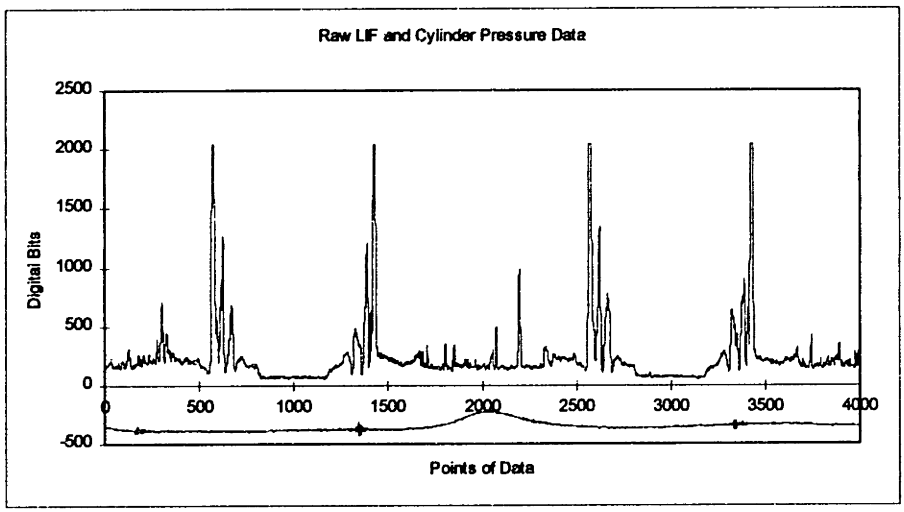

Figure 4.1 Raw LIF and Cylinder Pressure Data from Window 3.

Examining the LIF trace during the intake stroke, the first 1000 data points, the LIF system records the oil thickness below the piston. This period when the piston is above the quartz window is a stationary time measurement of the oil located in front of the window. After approximately 300 data points, the bottom of the piston skirt moves down into direct view of the

LIF window, at which point the LIF system "scans" the piston as it travel past the window. The first half of the piston trace consists of the skirt oil film thickness. Next, the region of the oil control ring comes into view, seen as large spikes of oil film thickness. The three piston lands follow the control ring and are separated by the low oil lines caused by the rings passing the window. After the crown land, approximately 800 data points into the trace, the LIF records the free liner oil film thickness above the piston as a function of time. This period when the piston is below the LIF window lasts until the piston returns to the window in the compression stroke and the oil film thickness on the piston is recorded in the reverse order as seen in the intake stroke. The expansion and exhaust strokes are identical to the intake and compression strokes in the viewing of the piston.

4.1.2 LIF Signal Orientation

The LIF data is obtained in crank angle degree increments of 0.18° when using a 2000 pts/rev encoder. Because the primary interest of the LIF is to observe oil films on the piston it is necessary to convert the increments of rotation, crank angles, to a linear unit, which is chosen as distance from the top of the piston. The distance from the top of the piston for each window location is given by

$$DP = WL - (a+l) + a\cos\theta + (l^2 - a^2\sin^2\theta)^{1/2} \qquad (4.1)$$

where:
DP = distance from the top of the piston
WL = window location from TDC
a = crank radius
l = connecting rod length
θ = crank angle

It is also convenient to plot a simple piston profile along the x axis for clarity, as seen in Figure 4.2, an example figure of the intake stroke for single un-calibrated LIF trace.

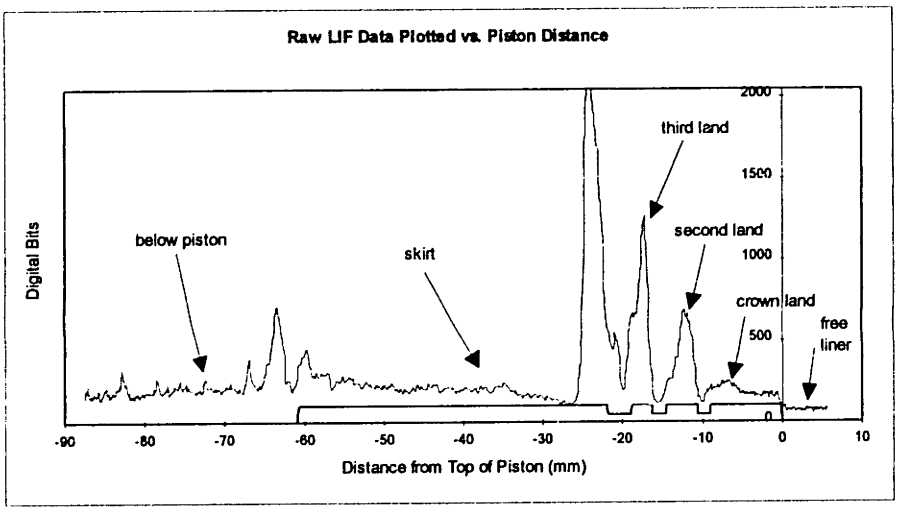

Figure 4.2 Raw LIF Data for the Intake Stroke Plotted verse Piston Distance.

4.1.3 LIF Calibration

4.1.3.1 Piston Skirt Machining Marks

There are several methods that can be used to calibrate an LIF trace, as described by Tamai [2]. The method chosen for this project was the piston skirt machining tool mark calibration method which uses the upper portion of the piston skirt as a calibration reference. These tool marks are often flooded on the compression and exhaust strokes allowing for relatively accurate calibration; different oil temperatures affect the signal intensity of the LIF. Figure 4.3 is a surface profile trace of the entire piston skirt with actual incremental measuring points of approximately 0.14 mm increments.

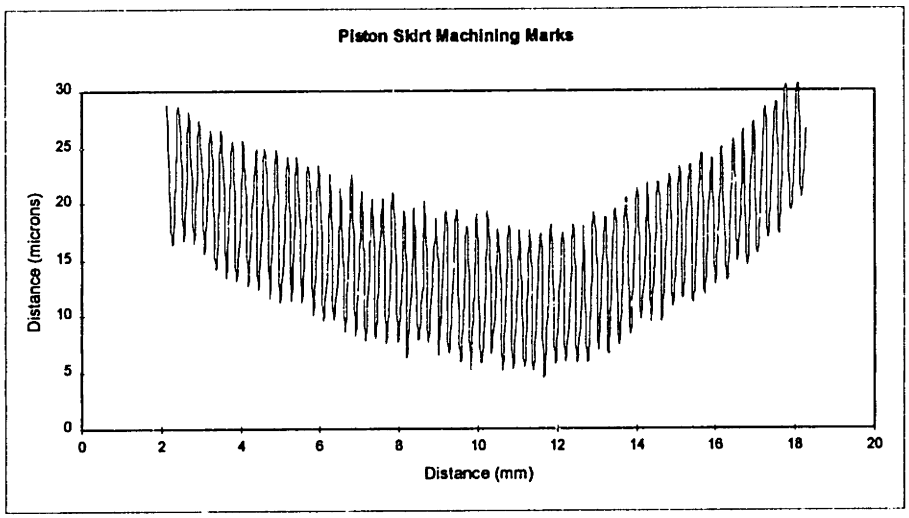

Figure 4.3 Piston Skirt Machining Marks at Measured Increments.

Using a shaft encoder with 2000 pts/rev resolution the increments between measuring points of the LIF system is not as fine as the piston skirt trace. Also due to the fact that at each vertical window location the piston speed varies, the measured piston skirt profile was interpolated to the points that each window would observe the skirt profile. The skirt trace was converted to distance increments for each vertical window such that the profile would match the actual profile that the LIF system would scan, refer to Appendix B.3 for the FORTRAN program used for this conversion. This increment conversion proved to aid in matching oil film thickness data with the skirt profile to obtain a calibration coefficient. Figure 4.4 shows the skirt profile as converted to increments of distance as seen from window 3, located 87.5 mm below TDC.

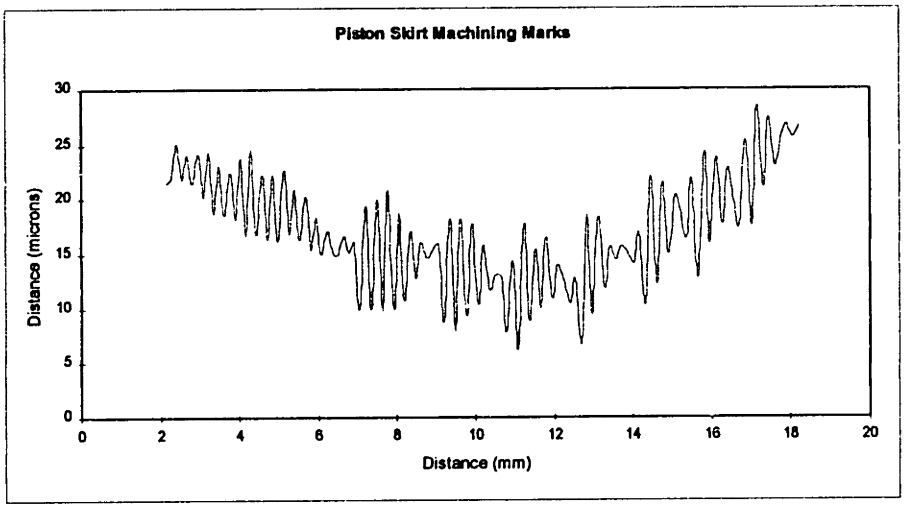

Figure 4.4 Piston Skirt Machining Marks at LIF Point Increments for Window 3.

4.1.3.2 Zero Offset and Window Recess

The LIF system was routinely checked for any offset that the system might incur on the recorded data. While the engine was running at the testing speed, a data set was recorded with a black rubber plug capping the LIF system optical input. The offset recorded was minimal and constant throughout the testing. Typical the offset was approximately 10 millivolts out of 10 volts, which could correspond to anywhere from .20 to .50 microns of oil depending on the calibration coefficient. These values were included into the calibration files of the test cases.
After the quartz windows were glued into place, the engine's cylinder liners were bored and honed to the proper diameter and surface roughness by the engine manufacturer. A surface profile was then performed on each LIF windows. For each window a slight recess of 1 to 2 microns was measured and these values were included into the calibration of the LIF oil film trace. Table 4.1 lists each windows average recess and Appendix A contains the actual surface profiles [4].

Window Location from TDC	**Window Recess (microns)**
Window 1 (50 mm)	1.5
Window 2 (73 mm)	1.5
Window 3 (87.5 mm)	1.5
Window 4 (102 mm)	1.5
Window 1a (50 mm, 30° off)	1.0
Window 2a (73 mm, 30° off)	2.0
Window 3a (87.5 mm, 30° off)	1.0
Window 4a (102 mm, 30° off)	1.5

Table 4.1 LIF Window Recess.

4.1.3.3 LIF Oil Film Calibration

For each test condition a LIF data measurement would include ten consecutive cycles, which would be averaged to determine the oil film thickness for each running condition. The average of ten cycles was deemed necessary and acceptable for characterizing a steady state condition. To calibrate the LIF signal off the machining marks on the piston skirt only a single trace will reveal these flooded marks. Of the ten cycles recorded there were usually several cycles where a number of flooded machining marks could be seen and this repeatability allowed for accurate calibration. In general when two or three consecutive machining marks were observed the calibration coefficient was determined. The compression and exhaust strokes, the up strokes of the piston, were the strokes that fully flooded machining marks were observed. A sample calibration overlay is shown in Figure 4.5.

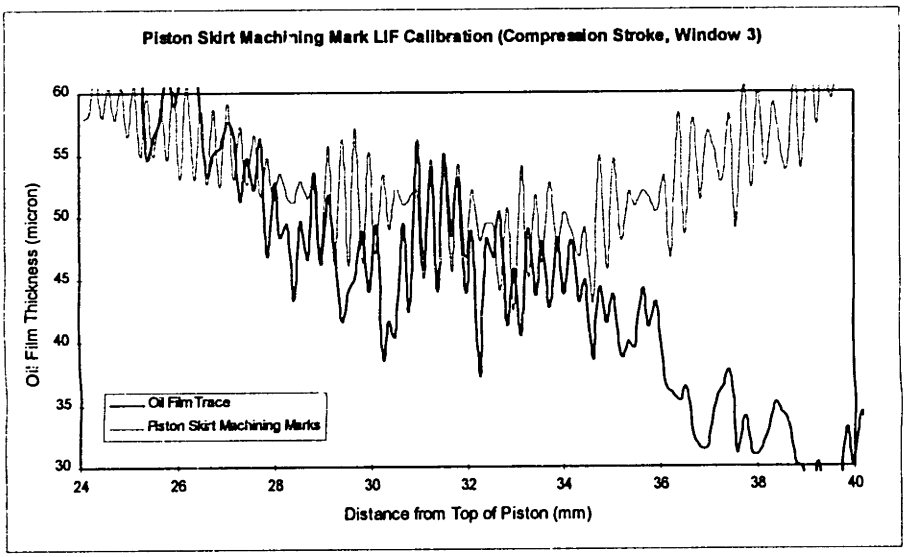

Figure 4.5 Piston Skirt Machining Marks LIF Calibration Method.

After the calibration coefficient is determined from the single cycle trace files, it could then be applied to the ten cycle averaged LIF data file using the following equation applied to each data point

$$h = (Raw * \frac{10volts}{1024bits} - offset) * Coef - recess \qquad (4.2)$$

where h = oil film thickness (microns)
Raw = raw LIF data point (bits)
$offset$ = LIF system offset
$Coef$ = Calibration Coefficient (microns / volts)
$recess$ = window recess from cylinder liner

4.2 INTER-RING PRESSURE TRANSDUCER PROCESSING

The processing of the inter-ring pressure transducers for cylinder 3 is a two part process. The first aspect is to convert the ACSII file in bit form to a pressure unit of bar. The second part of the data processing is to align all four transducers with the combustion pressure for cylinder 3. The combustion pressure is also processed into pressure units of bar and could be aligned with a static transducer that is mounted in the intake manifold.

4.2.1 Signal Processing

The pressure signals, as recorded by the data acquisition system, are shown in Figure 4.6. These pressure signals must be converted to pressure units and shifted to the proper heights.

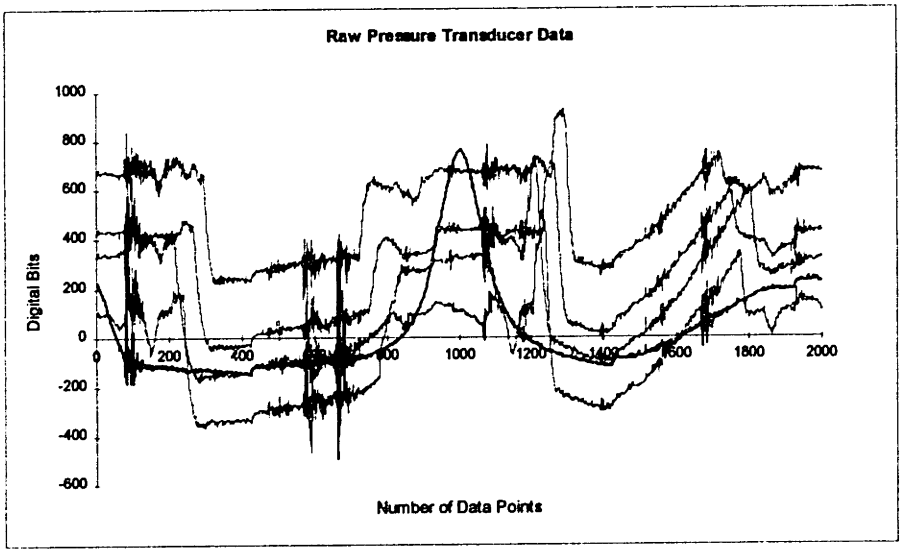

Figure 4.6 Typical Raw Pressure Transducer Data.

The signal recorded by the data acquisition system is in the form of bits and must be converted to the pressure unit of bar. Equation (4.3) is used in the conversion process

$$x_{bar} = x_{bit} \cdot \frac{10volt}{1024bit} \cdot scale\left\{\frac{bar}{volt}\right\} \tag{4.3}$$

where *scale* is the value set in the pressure transducer amplifier. This scale value must be chosen such that the full range of the pressure signal is within the ±10 volt capability of the data acquisition system. The value of the scale setting must be large enough to attain a high resolution signal yet caution should be take as to not over scale the signal causing the amplifier to overload. The fact that the transducers are dynamic, drifting of the signal will occur over time, so a scale should be chosen to allow for high resolution and buffer zone for thermal drift. In most cases the scale was set such that the minimum to maximum peaks was approximately 8 volts of the allowable 20 volts. Table 4.2 contains the pressure transducer amplifier scale settings for the test matrix performed.

Transducer Location	Load -15 Nm (closed throttle)	Load 160 Nm (wide open throttle)
Cylinder Pressure	2	10
Port A (14 mm from TDC)	2	10
Port B (22 mm from TDC)	2	5
Port 1 (50 mm from TDC)	2	2
Port 2 (58 mm from TDC)	2	2
Port 3 (66 mm from TDC)	2	2
Port 4 (74 mm from TDC)	2	2

Table 4.2 Pressure Transducer Amplifier Scale Settings.

With Equation (4.3) applied to all data points, Figure 4.6 is re-plotted in Figure 4.7, where the pressure signals are plotted in pressure units of bar absolute.

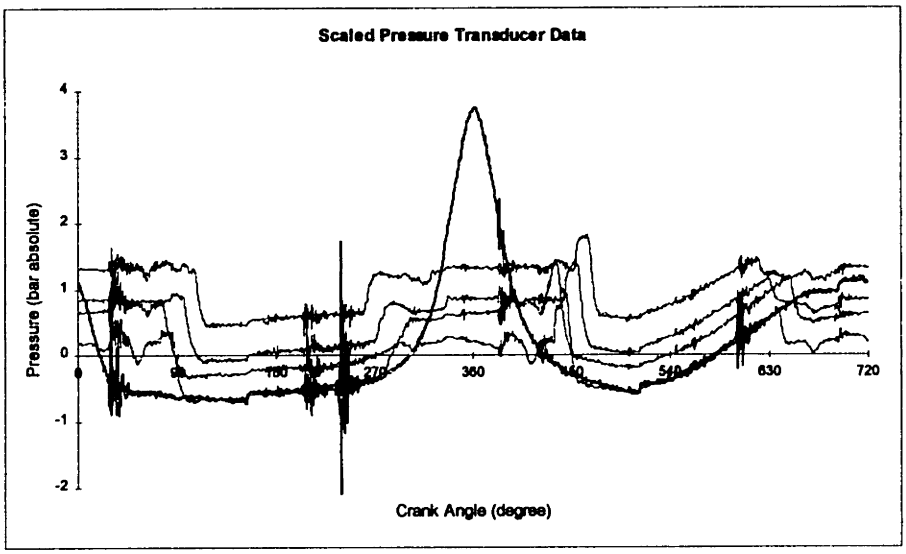

Figure 4.7 Typical Scaled Pressure Transducer Data.

4.2.2 Signal Shifting

Once all the signals are converted to pressure units, each signal must be adjusted to a reference value to align all the signals to the proper off-set. The reference point used for these signal processing was a measured value of the intake manifold pressure which is approximated to be equal to the pressure in the cylinder during the intake stroke. This measurement was obtained

using a static transducer mounted on the intake manifold and visual display value was recorded for each test run. The cylinder pressure is shifted to match the recorded intake manifold pressure during the intake stroke. For the inter-ring pressure ports the signals are shifted to match the cylinder pressure at the crank angles slightly after the pressure port is exposed to the cylinder pressure during the expansion stroke. Examples of the final result of the pressure transducer data processing is shown in Figures 4.8 and 4.9, for phases 1 and 2 and phase 3, respectively.

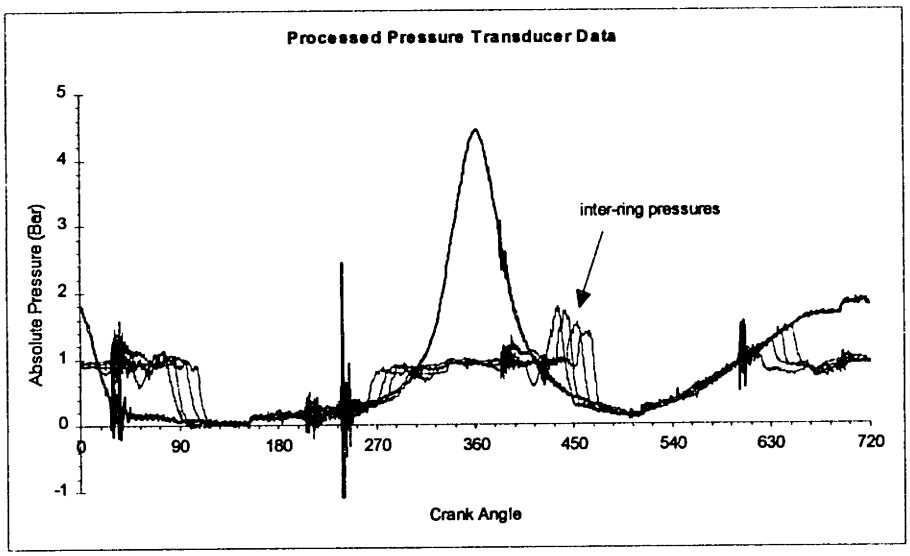

Figure 4.8 Typical Processed Pressure Transducer Data for Phases 1 and 2.

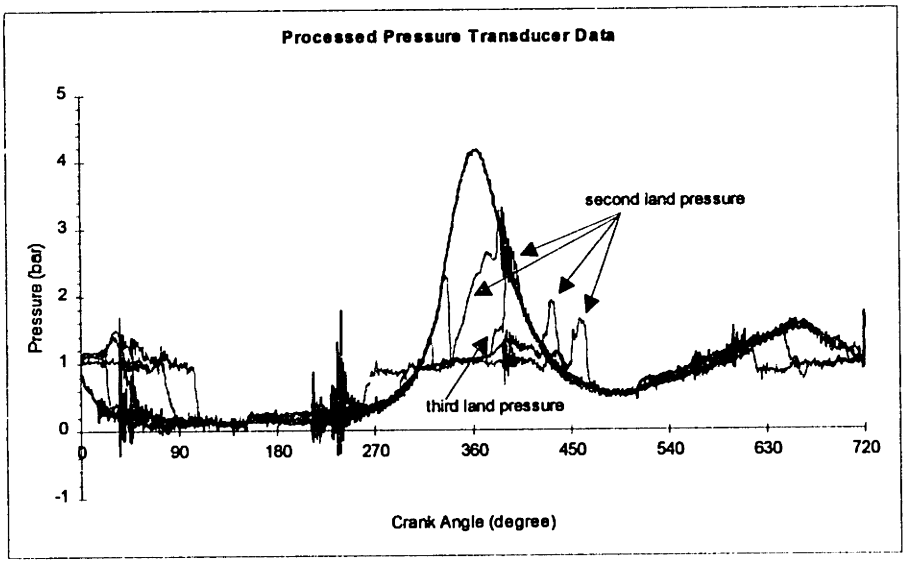

Figure 4.9 Typical Processed Pressure Transducer Data for Phase 3.

An additional point of reference can be used to verify proper shifting of the data, at the region of TDC of the piston from the compression to expansion strokes. During this period all the

pressure ports expect the one located at 14 mm from TDC are exposed to crankcase pressure which is at atmospheric pressure.

Appendix C.1 contains a FORTRAN program that used to process the pressure transducer data using the method of aligning the pressure signals from the inter-ring ports to crank case pressure, atmospheric pressure. The cylinder pressure (and the pressure from port A, for phase 3) would then be matched to the inter-ring pressure during the periods where the piston is below the inter-ring ports, a period when all transducers would be recording the same pressure.

4.3 PROCESSING OF CYLINDER PRESSURE FOR *RINGPACK-OC*

The computer code *RINGPACK-OC* requires input data file of one cycle of cylinder pressure with a one crank angle degree pressure increment, starting at the expansion stroke. The recorded pressure data was sampled at 2000 points per cycle, increments of 0.36 crank angle degree, and by using interpolation the data file was converted to the one crank angle degree increments required by *RINGPACK-OC*. To process this one cycle pressure file, the FORTRAN program, PRESSURE.FOR, was modified to include the necessary lines of code. Refer to Appendix C.1 for the program PRESSURE.FOR, and Appendix C.2 for the additional lines of code used to interpolate the pressure data.

CHAPTER 5 OIL TRANSPORT MODEL

There are two phenomena that will be considered in what drives the oil past the top ring and onto the crown land and combustion chamber where it contributes to the engines oil consumption. These two driving forces are the oil carried through the top ring gap during reverse blow-by and the oil driven through the ring groove.

5.1 REVERSE BLOW-BY

When the pressure of the second land exceeds the cylinder pressure there is gaseous flow through the top ring gap, generally referred to as reverse blow-by. This reverse blow-by has the capacity to carry oil from the second land through the gap and into the combustion chamber, contributing to the engine oil consumption. The values of the mass flow were calculated by a computer model, named *RINGPACK-OC*, using all the engine geometry and the cylinder pressure. The equation used in the code for one-dimensional steady compressible flow through an orifice or flow restriction was [5]

$$\dot{m} = \frac{C_D A_E p_0}{\sqrt{RT_o}} \left\{ \frac{2\gamma}{\gamma - 1} \left[\left(\frac{p}{p_0} \right)^{2/\gamma} - \left(\frac{p}{p_0} \right)^{(\gamma+1)/\gamma} \right] \right\}^{1/2} \tag{5.1}$$

where:
C_D = discharge coefficient
A_E = effective area
p_0 = total pressure
T_0 = temperature upstream of the restriction
p = pressure at the throat of the restriction
R = gas constant
γ = ratio of the specific heats ($c_p/c_v = \gamma$)

The discharge coefficient is a function of orifice dimensions, shape and surface roughness, mass flow rate, and fluid properties (density, surface tension, and viscosity) [5]. If the flow through the orifice is choked, determined by

$$\frac{P}{P_0} = \left(\frac{2}{\gamma + 1} \right)^{\gamma/(\gamma-1)} \tag{5.2}$$

then Equation (5.1) becomes

$$\dot{m} = \frac{C_D A_E p_0}{\sqrt{RT_0}} \gamma^{1/2} \left(\frac{2}{\gamma + 1} \right)^{(\gamma+1)/2(\gamma-1)} \tag{5.3}$$

Equation (5.1) or (5.3) calculates the total mass flow through the ring gap, which includes gas and oil. The difficulty exists in determining the fractional amount of oil in the mass flow through the gap which must be estimated. The author found it reasonable that this fraction of oil

in the mass flow would be affected by significant changes in the oil film thickness found on the second land.

5.2 RING GROOVE OIL TRANSPORT

The ring groove oil transport for the top ring is assumed only when the ring is seated on the top of the piston groove and the pressure behind the ring is greater then the crown land pressure, i.e. the combustion chamber pressure. When this situation arises, a pressure driven flow acts on the oil film between the ring and piston groove, which is assumed to be completely filled, forcing oil to the crown land and there-by contributing to oil consumption, refer to Figure 5.1.

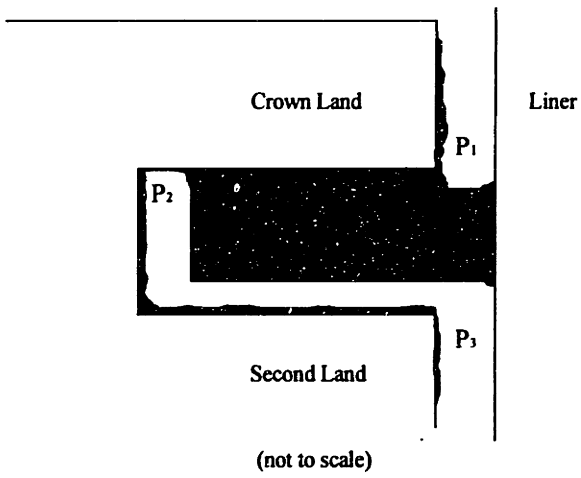

Figure 5.1 Top Ring Groove Oil Transport Model.

Using the equation for pressure driven flow

$$u = \frac{\frac{dP}{dx}}{2\mu} y(y-h) \qquad (5.4)$$

where y is the vertical direction starting from the ring surface and h is the oil film height, refer to Figure 5.2.

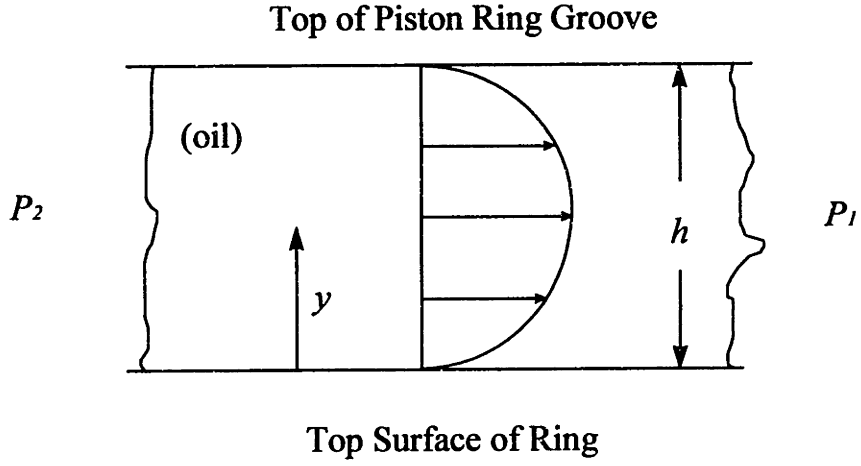

Figure 5.2 Top Ring Groove Oil Transport Model Direction and Height.

Integrating Equation (5.4) gives

$$\int_0^h u dy = \frac{-\frac{dP}{dx}h^3}{12\mu} \tag{5.5}$$

The pressure gradient can be approximated as

$$\frac{dP}{dx} = \frac{-(P_2 - P_1)}{d} \tag{5.6}$$

with d as the top ring depth. Thus the oil mass flow rate through the top ring groove may be expressed as [6]

$$\dot{m}_{oil} = \pi \cdot Bore \cdot \frac{P_2 - P_1}{12vd} \cdot h^3 \tag{5.7}$$

where:
$Bore$ = 0.0827 m
d = top ring depth = 0.00321 m
h = oil film thickness between top of groove and ring (m)
P_1 = cylinder pressure (kg/m s^2)
P_2 = pressure behind top ring (kg/m s^2)

The kinematic viscosity, ν, was calculated using Equation (5.8) for a 10W30 type oil [7].

$$\nu = \kappa \cdot \exp\left[\frac{\theta_1}{\theta_2 + T}\right] \tag{5.8}$$

where: $\kappa = 0.0352$ cSt
$\theta_1 = 1658.88°$ C
$\theta_2 = 163.54°$ C
T = temperature of the oil (°C)

For Equation (5.7) the cylinder pressure was recorded via a transducer and the pressure behind the top ring was calculated by *RINGPACK-OC*. The value for h, the oil film between the top of the groove and the ring must be estimated and since the value is cubed it is the greatest source of uncertainty. For Equation (5.8) the temperature of the oil was estimated to be 200° C for closed throttle operation.

CHAPTER 6 RESULTS AND ANALYSIS

The results of the test matrix performed for this project will be presented with the base line ring pack configuration, being phase 1, the standard design for the test engine. The results from the LIF testing will be presented for three window locations at 50 and 87.5 mm from TDC on the anti-thrust line, designated windows 1 and 3, respectively, and the third window's location at 50 mm from TDC 30° off the anti-thrust line, designated window 1a. The LIF data for windows 1 and 3 will compare the two engine loads for each cycle stroke, concentrating on the oil film thickness on the crown and second lands. Also a comparison for windows 1 and 1a at high load will address the interest of the effect of bore distortion on the oil film thickness. Aside from the LIF data, the inter-ring pressures will be analyzed using a code, named *RINGPACK-OC*, to predict ring positions, flow through the ring crevices and blow-by.

The second part of the analysis of the test matrix will compare the base line condition to the two variations of the ring pack, phases 2 and 3. The LIF comparison will concentrate on windows 1 and 3 for each test load and for the intake and expansion strokes. *RINGPACK-OC* will be used to compare the inter-ring pressure results for the three test cases.

The final analysis of the results will try to correlate the LIF and inter-ring pressures with the oil consumption data measured at the two chosen load conditions.

6.1 PHASE 1

The first test matrix which was designated phase 1, contained the standard ring pack with a top ring gap of 0.35 mm and a second ring gap of 0.56 mm. The LIF and inter-ring pressure data was recorded for two load conditions at 4000 rpm with closed throttle, -15 Nm, and wide open throttle, 160 Nm.

6.1.1 Phase 1 LIF Data

6.1.1.1 Window 1 for -15 and 160 Nm Load

The LIF data is presented for windows 1 and 3 for each stroke in the engine's cycle with the comparison of the two load conditions. Figures 6.1 through 6.4 display the calibrated LIF signals for window 1 at the load conditions of -15 Nm (closed throttle) and 160 Nm (wide open throttle). It should be noted that the LIF signal for the -15 Nm condition has excess noise that was caused by a slight leak in the quartz window glue, leaving a film of oil on the back side of the window. This erroneous oil film measurement was subtracted from the LIF signal, however the effect can clearly be seen on the free liner measurements. This problem for window 1 was improved for the remaining test conditions.

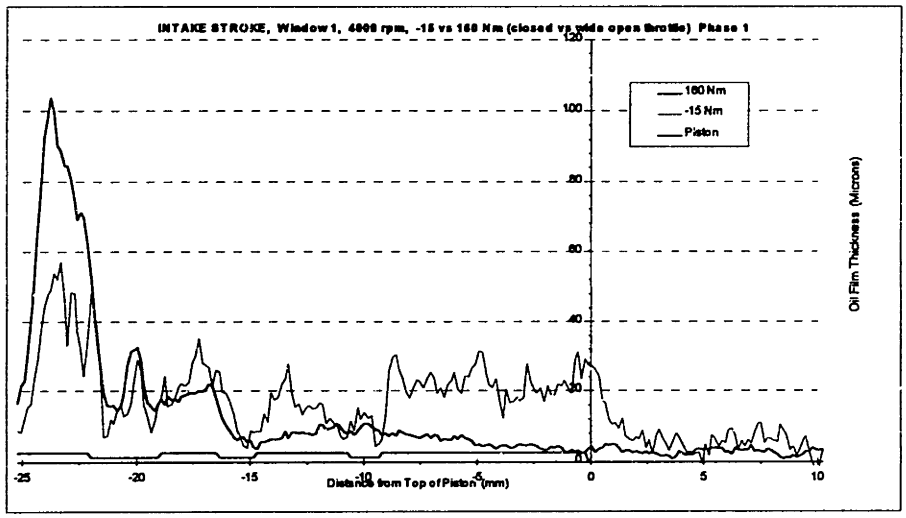

Figure 6.1 LIF Intake Stroke, Window 1, Phase 1.

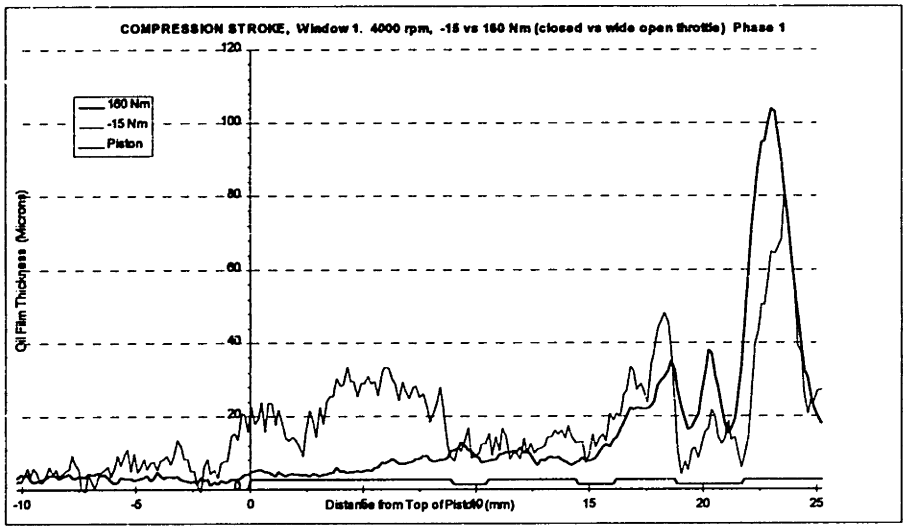

Figure 6.2 LIF Compression Stroke, Window 1, Phase 1.

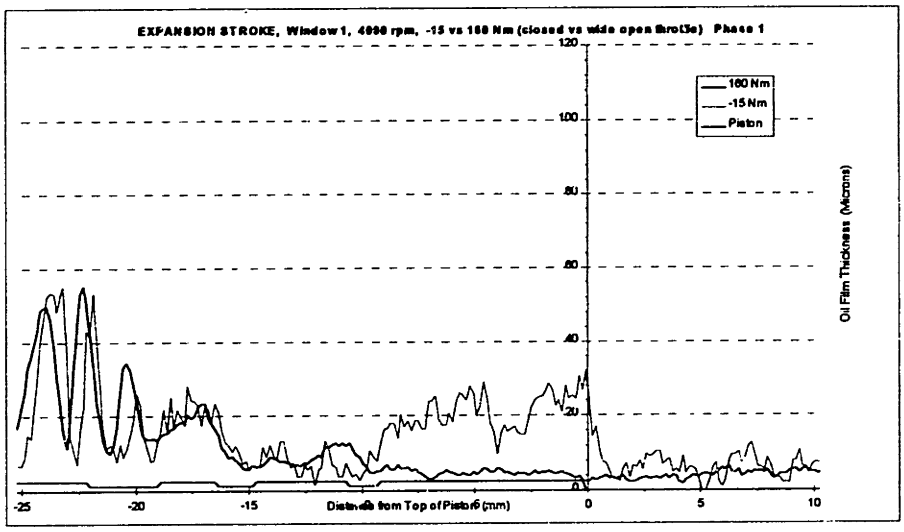

Figure 6.3 LIF Expansion Stroke, Window 1, Phase 1.

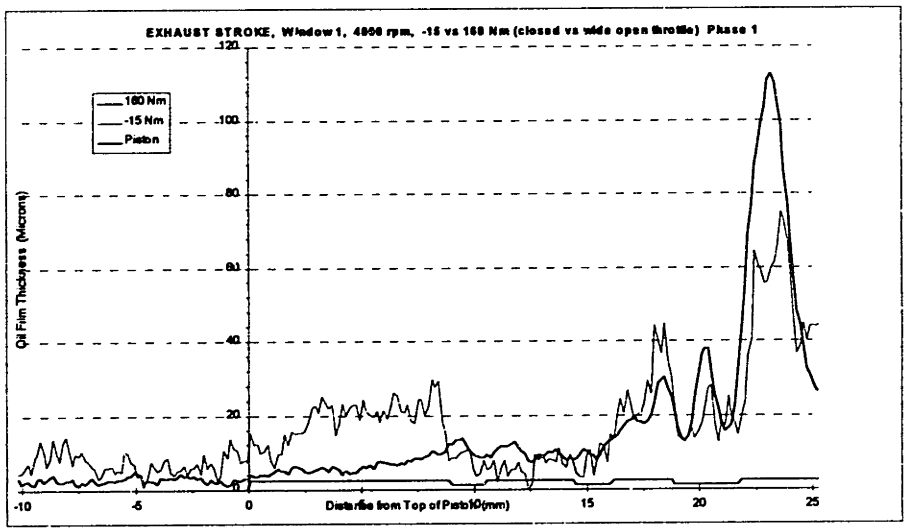

Figure 6.4 LIF Exhaust Stroke, Window 1, Phase 1.

The average oil film thickness on the crown and second lands observed through window 1 are shown in Table 6.1. The LIF signal clearly shows that during the -15 Nm load condition the crown land contains substantially more oil then the 160 Nm load, on the order of four times more oil. This excess oil on the crown land may be explained by the low intake manifold pressure seen during the intake stroke which can draw oil up the piston. The recorded intake manifold pressure at -15 Nm load was 0.25 bar absolute, compared to 1.01 bar absolute during 160 Nm load. Comparing the second land oil film thickness for the two load conditions little change is seen which contradict the crown land oil film thickness. This discrepancy may be explained by the effectiveness of the second ring, also referred to as the oil scrapper ring, which performs more effectively than the top ring such that the second land is less influenced by the low intake manifold pressure.

Stroke	Location	Average Oil Film (microns) -15 Nm Load	Average Oil Film (microns) 160 Nm Load
Intake	**Crown Land**	22.0	5.5
	Second Land	14.5	7.9
Compression	**Crown Land**	23.3	5.7
	Second Land	12.8	8.7
Expansion	**Crown Land**	20.8	4.8
	Second Land	7.6	8.9
Exhaust	**Crown Land**	18.8	6.2
	Second Land	6.3	9.7
Average	**Crown Land**	21.2	5.6
	Second Land	10.3	8.8

Table 6.1 Average Oil Film Thickness on the Crown and Second Lands for Phase 1, Window 1.

6.1.1.2 Window 3 for -15 and 160 Nm Load

The averaged oil film thickness observed through window 3 during the load conditions of -15 Nm (closed throttle) and 160 Nm (wide open throttle) are presented in Figures 6.5 through 6.8, for each engine stoke.

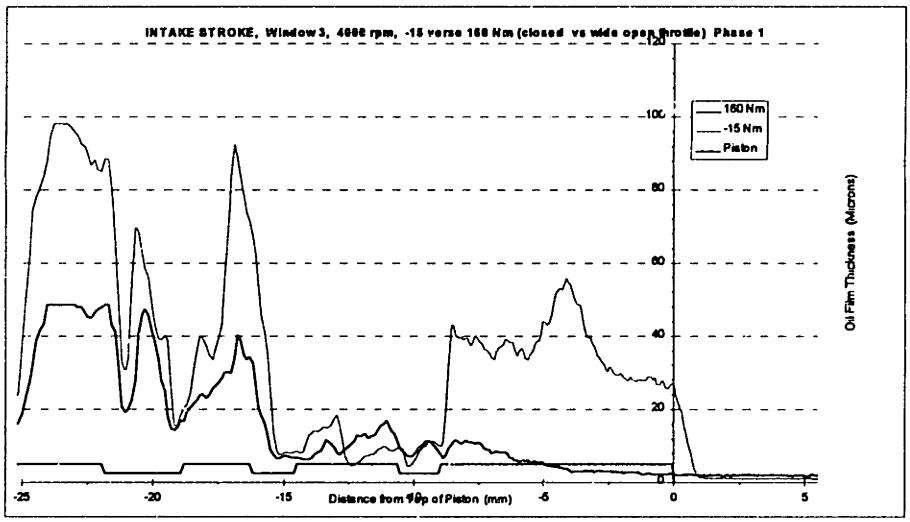

Figure 6.5 LIF Intake Stroke, Window 3, Phase 1.

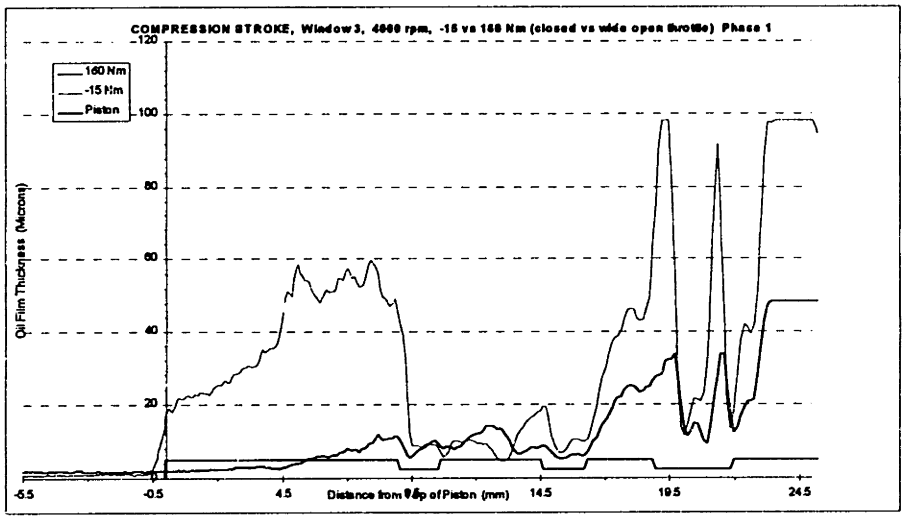

Figure 6.6 LIF Compression Stroke, Window 3, Phase 1.

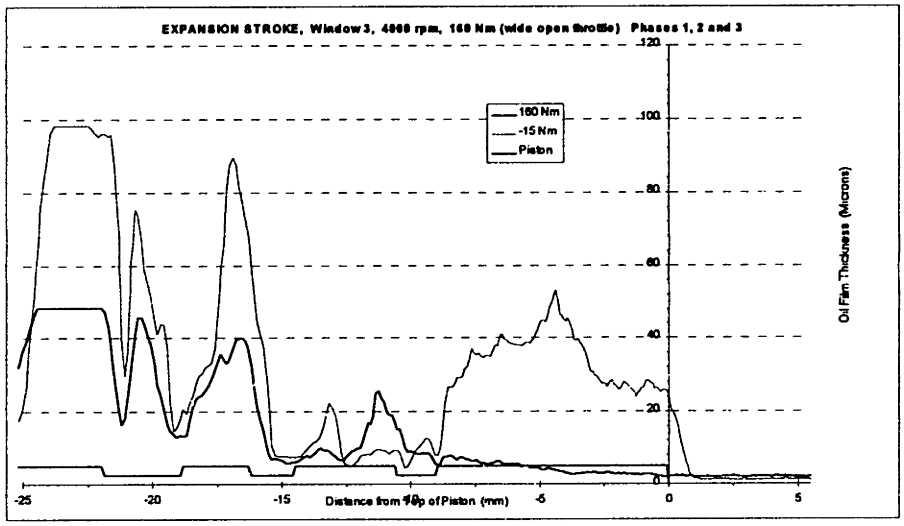

Figure 6.7 LIF Expansion Stroke, Window 3, Phase 1.

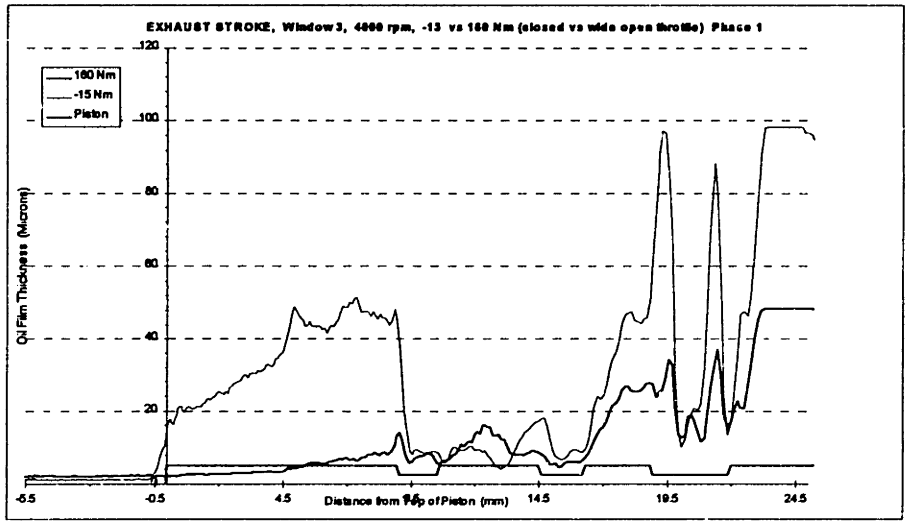

Figure 6.8 LIF Exhaust Stroke, Window 3, Phase 1.

The previous four figures presenting the LIF data observed through window 3 clearly supports the observation seen through window 1, that the crown land holds substantially more oil during the -15 Nm load condition when the intake manifold pressure is extremely low. Table 4.2 lists the average oil film thickness for the crown and second lands for each stroke and the average for all the strokes. The increase in oil film thickness observed on the crown land was of the order of seven times greater for -15 Nm load then 160 Nm load. This increase of order seven is larger then the increase of an order four which was observed for window 1. It can be seen that the signals from window 3 are 'cleaner' on the free liner than that of window 1, which bears weight on whether the difference of order magnitude for the oil film thickness observed on the crown land for windows 1 and 3 should be further investigated. The trend for the two windows are similar and should be noted as such.

		Average Oil Film (microns)	Average Oil Film (microns)
Stroke	**Location**	**-15 Nm Load**	**160 Nm Load**
Intake	**Crown Land**	35.9	5.1
	Second Land	10.3	10.5
Compression	**Crown Land**	38.5	4.5
	Second Land	10.8	10.0
Expansion	**Crown Land**	33.4	4.2
	Second Land	10.3	11.4
Exhaust	**Crown Land**	34.7	4.5
	Second Land	10.3	10.4
Average	**Crown Land**	35.6	4.6
	Second Land	10.4	10.6

Table 6.2 Average Oil Film Thickness on the Crown and Second Lands for Phase 1, Window 3.

6.1.1.3 Windows 1 and 1a for 160Nm Load

The LIF quartz windows located on 30° off the anti-thrust line served the interest of how bore distortion affected the oil film thickness. From Figure 2.4 it is seen that at an engine condition of 4000 rpm, WOT, 50 mm from the top of the cylinder, a -30 micron bore distortion (less than the anti-thrust line radius) on the +30° line was recorded. This difference of the cylinder bore by 30 microns was of interest and the oil film thickness measurements for windows 1 and 1a at WOT are shown in Figures 6.9, 6.10, 6.11 and 6.12.

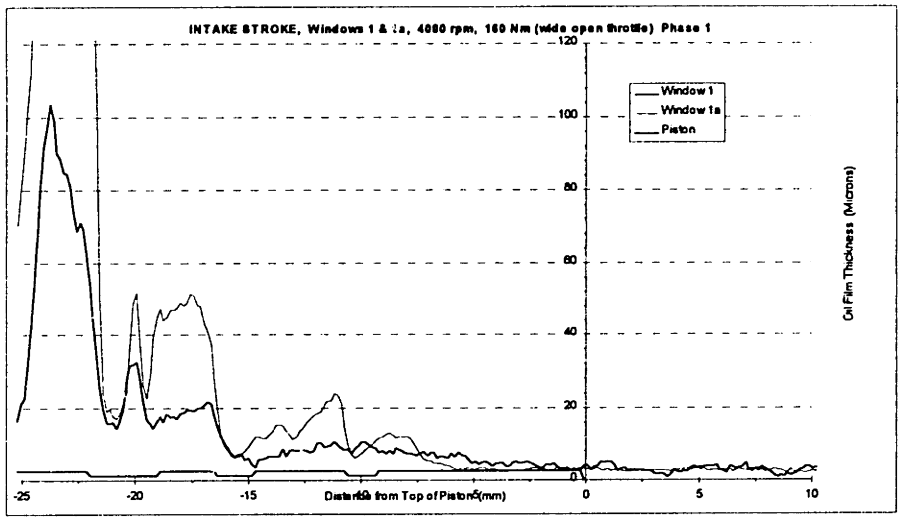

Figure 6.9 LIF Intake Stroke, Windows 1 and 1a, WOT, Phase 1.

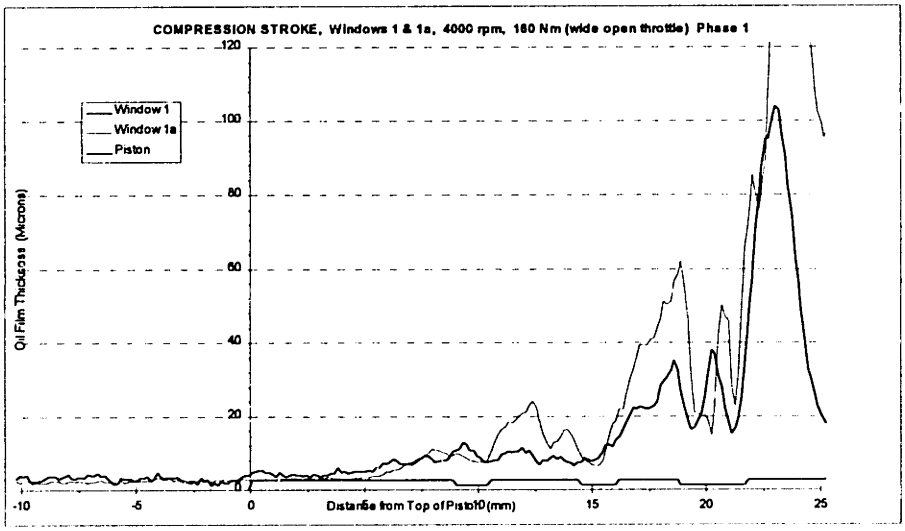

Figure 6.10 LIF Compression Stroke, Windows 1 and 1a, WOT, Phase 1.

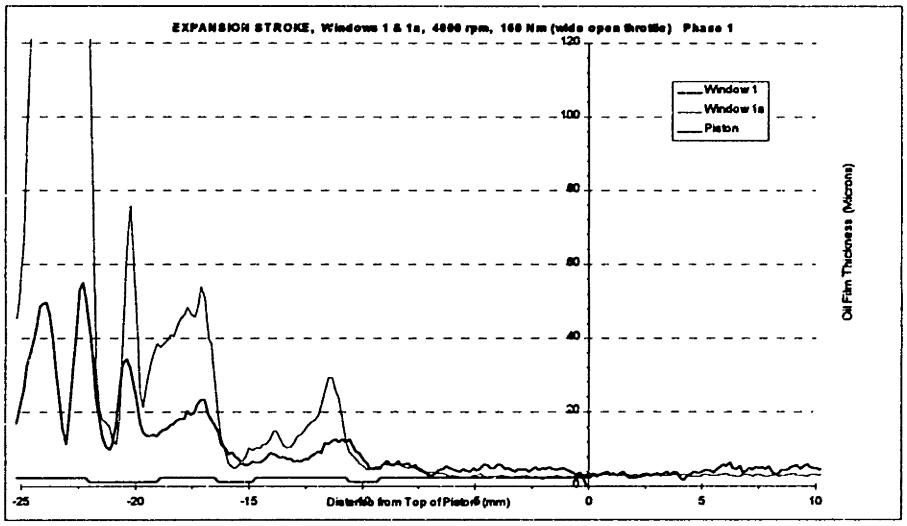

Figure 6.11 LIF Expansion Stroke, Windows 1 and 1a, WOT, Phase 1.

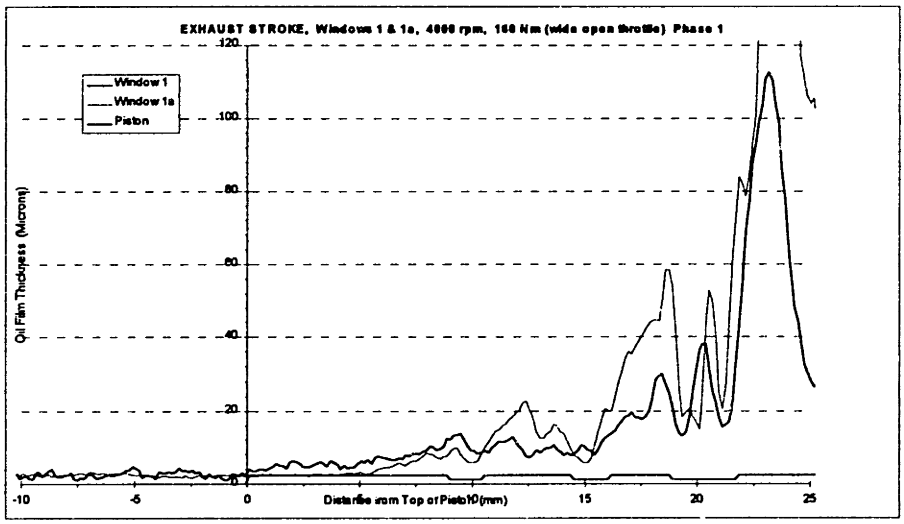

Figure 6.12 LIF Exhaust Stroke, Windows 1 and 1a, WOT, Phase 1.

Table 4.3 lists the average oil film thickness for windows 1 and 1a for each stroke and the average of the full cycle. It is evident from Figures 6.10 through 6.13 and Table 4.3 that the bore distortion located 30° off the anti-thrust line does not affect the oil thickness by 30 microns. This conclusion is not surprising since at the high load of 160 Nm the lands are not carrying excessive oil as seen during the -15 Nm load condition. If the rings do not conform completely to the bore surface , then large bore distortion could cause poor ring contact with the liner, causing high levels of oil on the free liner. However large differences in free liner oil film thickness between the anti-thrust and the 30° off anti-thrust line were not observed; this implies that the rings probably conformed well to the bore. It may be of more interest to measure the bore distortion for the load condition of -15 Nm since for that load the crown land carrying excessive oil and the effects of varying piston-liner clearance could be observed.

Stroke	Location	Average Oil Film (microns) Window 1	Average Oil Film (microns) Window 1a
Intake	**Crown Land**	5.5	5.0
	Second Land	5.7	16.0
Compression	**Crown Land**	4.8	4.6
	Second Land	8.9	16.4
Expansion	**Crown Land**	4.8	3.4
	Second Land	8.9	16.4
Exhaust	**Crown Land**	6.2	3.9
	Second Land	9.7	15.6
Average	**Crown Land**	5.3	4.2
	Second Land	8.3	16.1

Table 6.3 Average Oil Film Thickness on the Crown and Second Lands for Windows 1 and 1a, Phase 1.

6.1.2 Phase 1 Inter-Ring Pressures

The inter-ring pressures measured from the four pressure ports during phase 1 testing, scanned a window of approximately 40 crank angle degrees for each stroke of the engine's cycle. This window is effective during the expansion stroke to understand the general behavior of the land pressures. To further analyze the land pressures a computer model, *RINGPACK-OC*, was run using the measured inter-ring pressures to calibrate the *RINGPACK-OC* program. Once *RINGPACK-OC* is calibrated for the specific cylinder pressure, it can predict blow-by, relative ring positions in the piston grooves, mass flow through the gaps and pressure behind the rings. In this chapter the measured inter-ring pressures will be plotted with the *RINGPACK-OC* results such that proper validation can be observed.

6.1.2.1 Inter-Ring Pressure for -15 Nm Load

Figure 6.13 is the plotted results of the measured inter-ring pressures at the load condition -15 Nm, along with the results obtained from *RINGPACK-OC*. The relative ring positions in the ring grooves, predicted by *RINGPACK-OC*, are plotted in Figure 6.14.

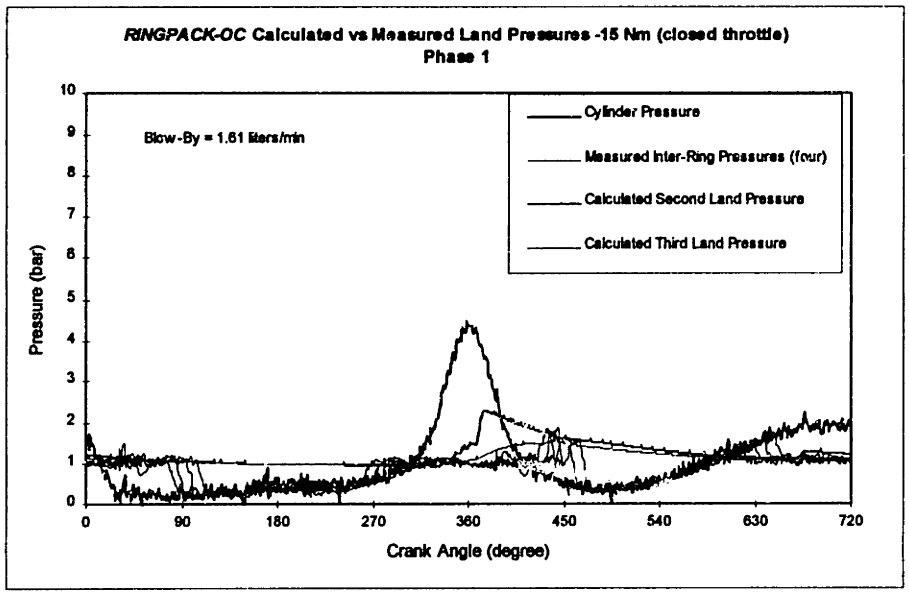

Figure 6.13 Inter-Ring Pressures for -15 Nm, Phase 1.

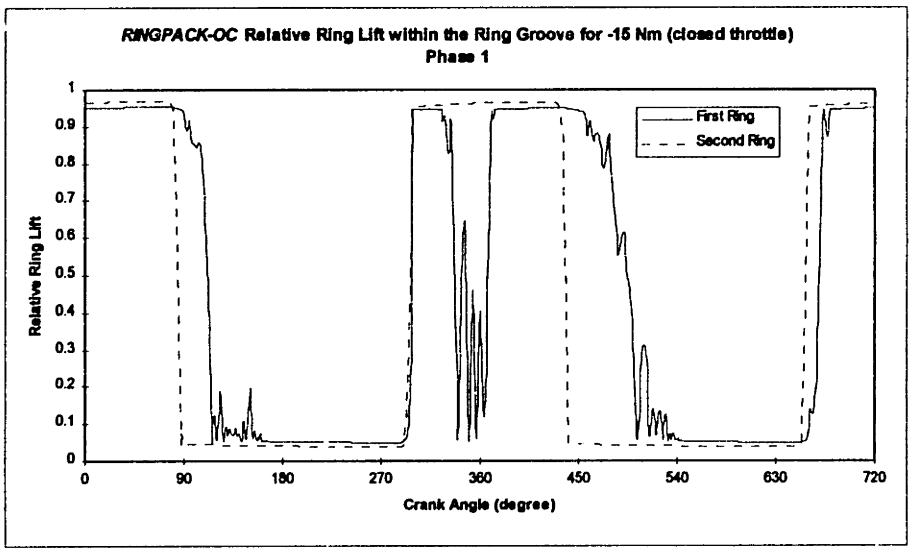

Figure 6.14 Relative Ring Lift within the Ring Groove for -15 Nm, Phase 1.

The results from *RINGPACK-OC* for the second land pressure is of interest because it simulates top ring flutter which is seen in Figure 6.14. Due to the extremely low cylinder pressure the top ring lifts to the top of the groove after mid-stroke during compression, by means of the ring's inertia force. Near TDC the force, due to the pressure gradient between the cylinder and second land pressures, exceeds the inertia force and the ring is forced down to the bottom of the groove. During the ring transition, cylinder gas pressure passes into the second land region, increasing second land pressure. Increasing the second land pressure reduces the force from the pressure gradient and the inertia force can once again drive the ring up to the top of the groove. The ring flutter simulation by *RINGPACK-OC* is strongly supported by the measured inter-ring pressures due to the fact that top ring gap gas flow would not drive the second land pressures to roughly 2

bar at the measuring points while the peak cylinder pressure was only 4.5 bar. The top ring must flutter and lose some of its sealing property to allow for such a rise in second land pressure. This point will be further clarified by observing the wide open condition.

6.1.2.2 Inter-Ring Pressure for 160 Nm Load

Figure 6.15 is the plotted results of the measured inter-ring pressures at the load condition 160 Nm, along with the results obtained from *RINGPACK-OC*. The relative ring positions in the ring grooves, predicted by *RINGPACK-OC*, are plotted in Figure 6.16.

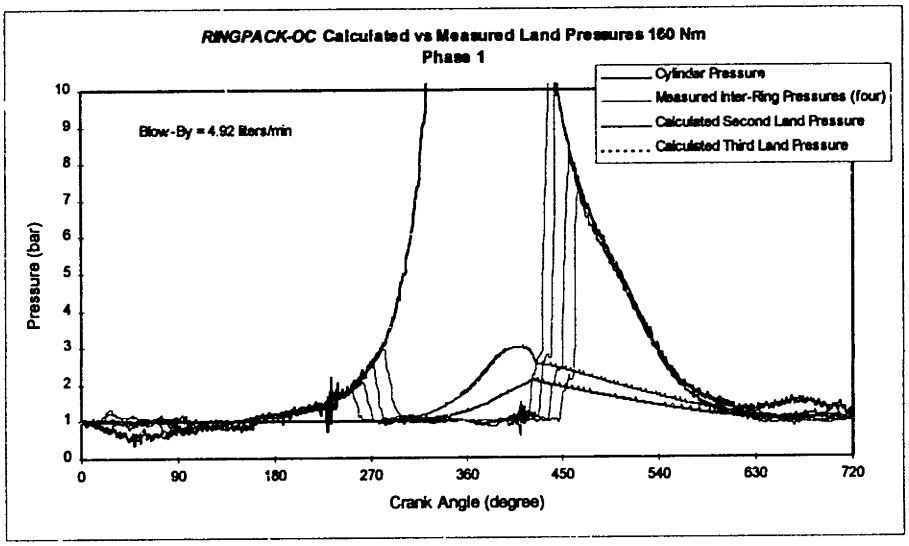

Figure 6.15 Inter-Ring Pressures for 160 Nm, Phase 1.

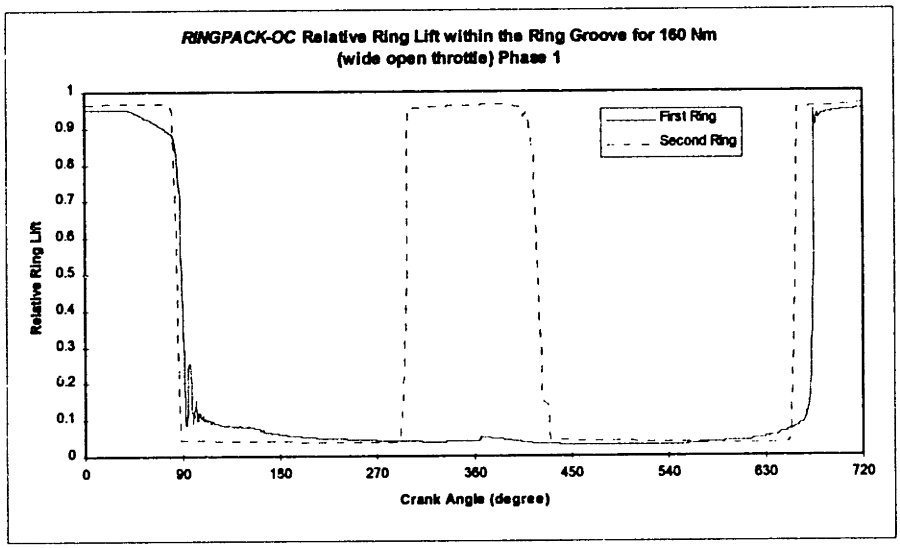

Figure 6.16 Relative Ring Lift within the Ring Groove for 160 Nm, Phase 1.

In Figure 6.15 the maximum measured inter-ring pressure was approximately 2.75 bar absolute, while the cylinder pressure exceeded 40 bar. This ratio of 2.75 to 40 is quiet different then the 2.0 to 4.5 ratio for the inter-ring to cylinder pressure observed for -15 Nm load, which leads to prediction that the top ring is fully seated on the bottom of the ring groove during the wide open throttle condition. *RINGPACK-OC* predicts this stable top ring condition in Figure 6.16.

6.1.2.3 Top Ring Gap Mass Flow

The ring flutter that occurs during the -15 Nm load condition plays a large role in reverse blow-by during the expansion stroke by driving the second land pressure up while the cylinder pressure rises during the compression stroke. When the cylinder pressure drops rapidly during the expansion stroke the rings are seating and sealing properly such that the high second land pressure bleeds off slowly though the top and second ring gaps. The mass flow through the top ring gap was calculated from *RINGPACK-OC* and plotted in Figure 6.18 for -15 and 160 Nm. For the -15 Nm load condition there is a reverse mass flow through the top ring gap during most of the intake and compression stroke, twice as long as for the 160 Nm load condition. Also there is another reverse mass flow for the -15 Nm condition during the expansion and exhaust strokes for a crank angle duration of approximately 200°. Since the condition of -15 Nm has substantially more reverse mass flow through the top ring gap, which has the potential to carry oil to the crown land and combustion chamber, it may be related to the greater oil film thickness observed on the crown land during this condition.

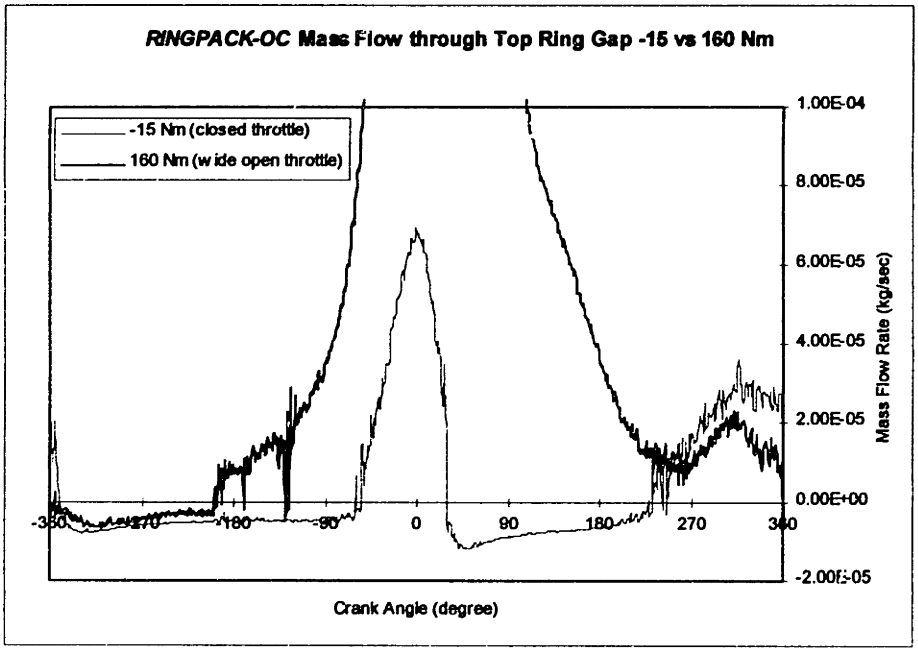

Figure 6.17 Mass Flow through the Top Ring Gap for -15 and 160 Nm, Phase 1.

6.2 PHASES 1, 2 AND 3

The original purpose for the phase 2 testing was to change one parameter, the second ring gap, and observe the changes in oil film thickness and inter-ring pressures. Phase 2 however included two variations from phase1 which was a reduction in ring gap from 0.56 mm to 0.11 mm as well as a different type ring design. The phase 1 second ring was a hooked design while the phase 2 second ring was a negative twist design. This discrepancy was accidental and the results for phase 2 are less valuable since any changes in LIF data can not be strictly attributed to one of the two changes made to the ring pack. Phases 3 had only one variation from the phase 1 ring pack, which was a larger top ring gap of 0.60 mm from the original 0.35 mm.

6.2.1 LIF Oil Film Thickness

The LIF data for phases 1, 2 and 3 will be presented separately for the -15 and 160 Nm load conditions, and only the intake and expansion strokes will be plotted.

6.2.1.1 Window 1 for -15 Nm Load

Figures 6.18 and 6.19 are the plotted LIF data for all phases for -15 Nm load, during the intake and expansion strokes, respectively.

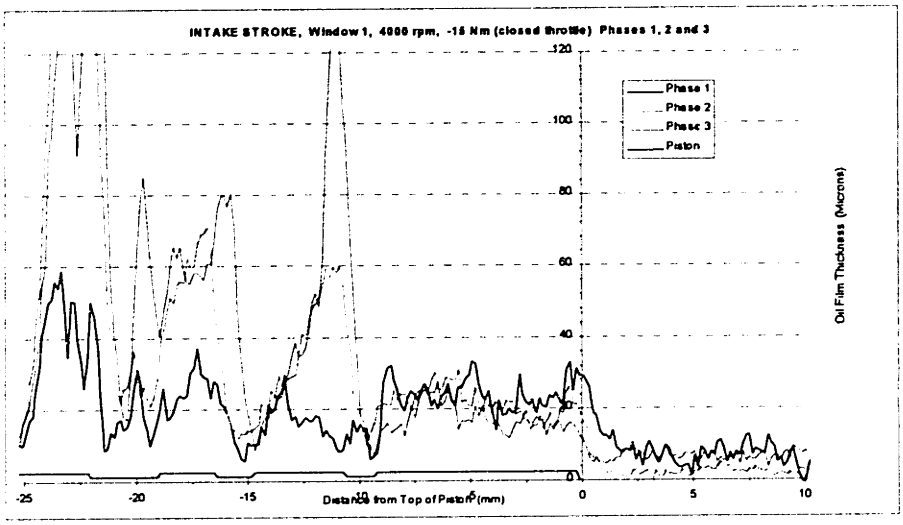

Figure 6.18 LIF Intake Stroke, Window 1, Closed Throttle (-15 Nm), Phases 1, 2 and 3.

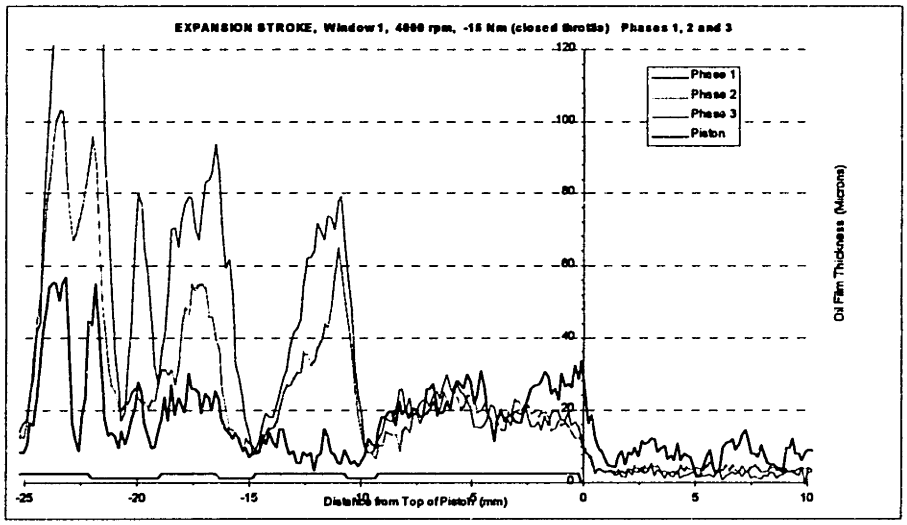

Figure 6.19 LIF Expansion Stroke, Window 1, Closed Throttle (-15 Nm), Phases 1, 2 and 3.

From Figures 6.18 and 6.19, the intake and expansion stroke for phases 1, 2 and 3, respectively, several observations can be made. First the second land oil film thickness for phases 2 and 3 are substantially greater than for phase 1, while the crown land oil film thickness is relatively the same for all phases.

For phase 2 the increase in the second land oil film thickness can be attributed to either the reduction in the second ring gap or the different design for the second ring or a combination of both. For phase 3 the large increase in the oil film thickness on the second land can only be attributed to the increased top ring gap. A simple explanation could be the increased gap area will allow greater reverse blow-by which would draw more oil from the third land and oil control ring. There must also be one other consideration made for the increase in second land oil film thickness for phase 3, the second ring surface wear. There was approximately 90 hours of engine running time between phase 1 and phase 3 testing. This time period includes many hours of high speed, 4000 rpm, testing and the scraper ring may have wore down enough to affect the performance of the ring. Figure 6.20 contains the surface profile for a typical scraper ring after 20, 200 and 600 hours of running time [8].

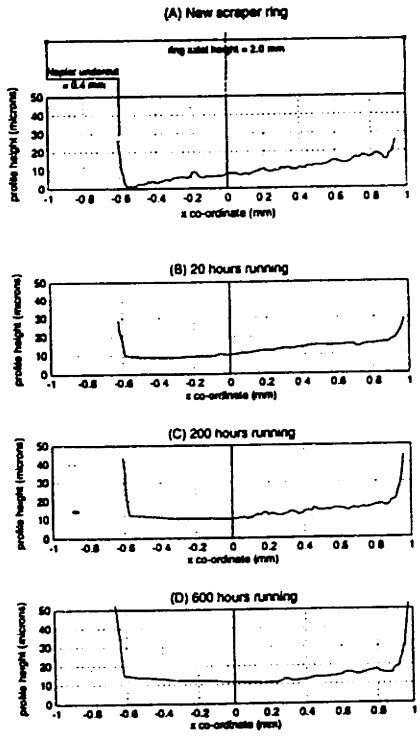

Figure 6.20 Typical Scrapper Ring Wear after 20, 200 and 600 Hours Running.

It would be of interest to perform a surface profile of the test engine's scraper ring after phase 3 and compare it to a new scraper ring. Also it is recommended to reconfigure the ring pack with the phase 1 design and re-test the oil film thickness on the second land.

Closing the second ring gap will increase the bleed off time for the second land pressure, since the path to the lower-pressure third land has been reduced. This slower bleed off will increase reverse blow-by of the second land to the crown land during the expansion and intake strokes. It would there by be reasonable to expect more oil on the crown land for the phase 2 configuration, yet this is not observed. Since the crown land for each of the phases carries similar levels of oil it may be considered that the crown land is at a full carrying capacity with oil, saturated. When there is excessive accumulation of oil on the crown land, mechanical throw-off and gas flow may result in oil being carried into the combustion chamber. In other words , there may be an upper limit to the amount of oil the crown land can carry, which may have been reached by phases 1, 2 and 3 during the load condition of -15 Nm.

6.2.1.2 Window 3 for -15 Nm Load

Figures 6.21 and 6.22 contain the LIF data taken from window 3 at the load condition -15 Nm for phases 1, 2 and 3, during the intake and expansion strokes, respectively. The same trends can be seen for this window as seen by window 1.

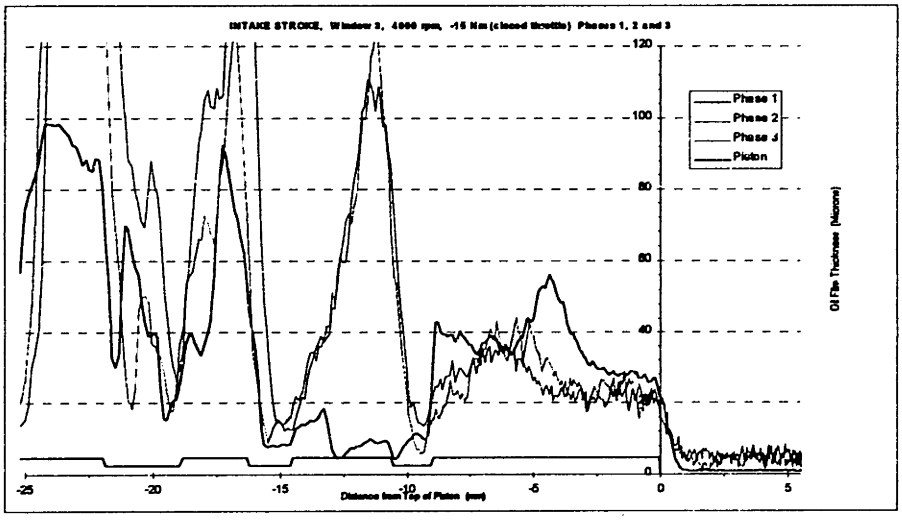

Figure 6.21 LIF Intake Stroke, Window 3, Closed Throttle (-15 Nm), Phases 1, 2 and 3.

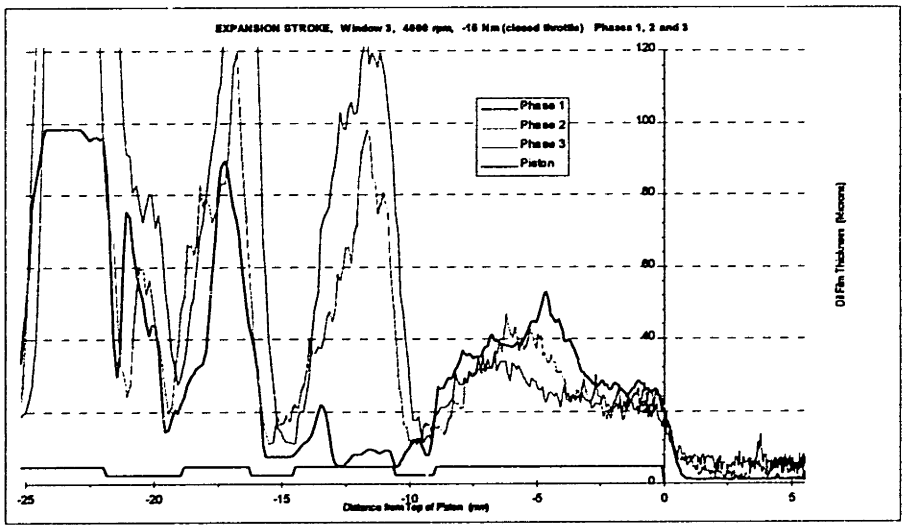

Figure 6.22 LIF Expansion Stroke, Window 3, Closed Throttle (-15 Nm), Phases 1, 2 and 3.

The LIF data recorded through window 3 for all three phases reveals that the second land holds more oil for phases 2 and 3 than for phase 1. This increase in oil was also recorded from window 1. The crown land oil film thickness for window 3 is greater than for window 1, which questions whether the land is actually saturated. However, window 3 is located 37.5 mm below window 1 on the liner and the gas flow and the inertial forces on the crown land at window 3 may be quite different than those at window 1.

6.2.1.3 Window 1 for 160 Nm Load

The load condition of 160 Nm, wide open throttle, was run for all three phases and the LIF data for window 1 is presented for the intake and expansion strokes in Figures 6.23 and 6.24, respectively.

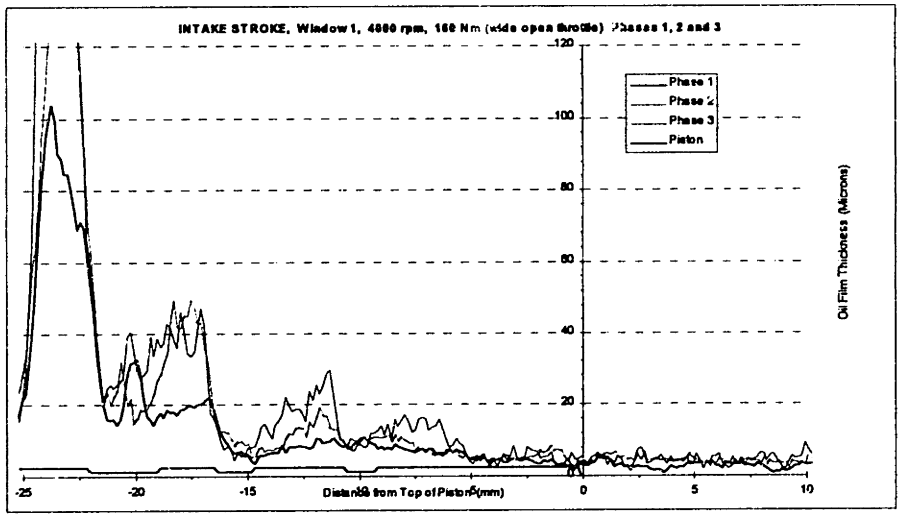

Figure 6.23 LIF Intake Stroke, Window 1, Wide Open Throttle (160 Nm), Phases 1, 2 and 3.

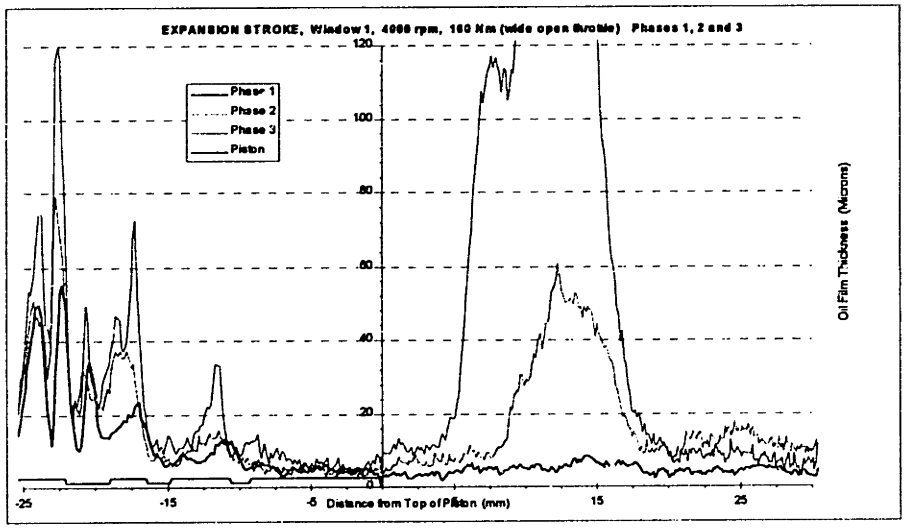

Figure 6.24 LIF Expansion Stroke, Window 1, Wide Open Throttle (160 Nm), Phases 1, 2 & 3.

For Figures 6.23 and 6.24 the crown land appears relatively dry compared with the -15 Nm condition and there is little variation between phases. On the second land the high levels of oil seen at -15 Nm, phases 2 and 3, have dropped considerably to levels similar to those recorded for phase 1.

An interesting observation should be made for Figure 6.24, the expansion stroke for 160 Nm. Both phases 2 and 3 recorded high levels of oil on the free liner after the piston has traveled below the window. It should be stated that LIF 'scans' the piston for oil as it travels by the window, however after the piston travels below the window the LIF records the oil left on the quartz window, i.e. no longer a distance measurement. The horizontal axis for this figure was increased to show the full liner duration time. It appears that oil moves in front of the window on the free liner, remains there for a short duration and then disappears. This may be oil thrown from the piston that is flowing down the liner. This oil puddle is not observed in window 3 and

also is not present in the exhaust stroke, where the piston might have pushed the puddle back into view in window 1. The oil puddle may have disappeared by evaporating as oil vapor, which contributes to oil consumption. Further investigation may isolate this oil puddle to only window 1, which might address some physical problem such as window protrusion or recess as to the cause of the oil puddle.

6.2.1.4 Window 3 for 160 Nm Load

Refer to Figures 6.25 and 6.26 for the LIF data recorded through window 3 at 160 Nm load, for the intake and expansion strokes, respectively.

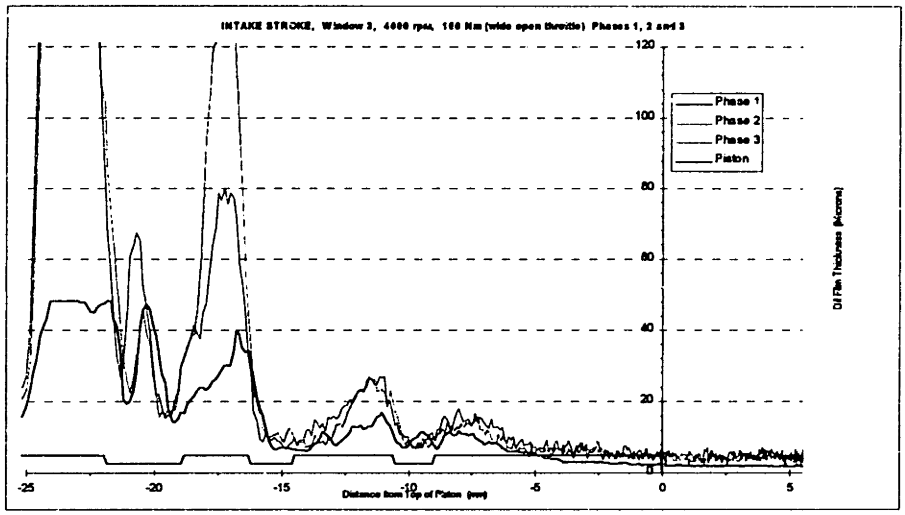

Figure 6.25 LIF Intake Stroke, Window 3, Wide Open Throttle (160 Nm), Phases 1, 2 and 3.

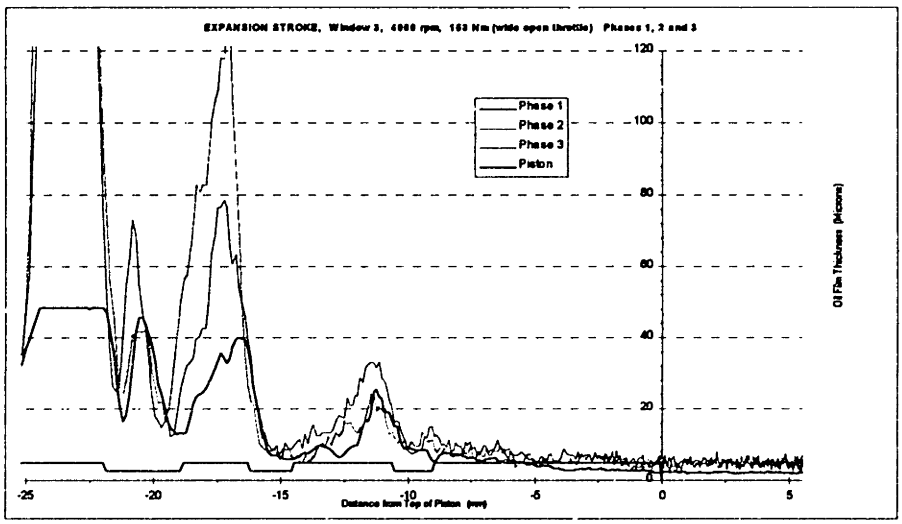

Figure 6.26 LIF Expansion Stroke, Window 3, Wide Open Throttle (160 Nm), Phases 1, 2 & 3.

Figures 6.25 and 6.26 reveal similar trends as seen for window 1, however the oil puddle seen in the expansion stroke in window 1 is not seen in window 3.

The following two tables are a summary of the average oil film thickness recorded on the crown and second lands for ten cycle averages at the loads of -15 and 160 Nm, for windows 1 and 3.

Window 1		Phase 1		Phase 2		Phase 3	
		Oil Film (microns)		Oil Film (microns)		Oil Film (microns)	
Stroke	**Land**	-15 Nm	160 Nm	-15 Nm	160 Nm	-15 Nm	160 Nm
Intake	Crown	22.0	5.5	21.8	6.7	17.5	8.4
	Second	14.5	7.9	37.8	11.4	50.2	17.8
Compression	Crown	23.3	5.7	21.9	5.0	17.7	5.3
	Second	12.8	8.7	35.2	7.3	52.0	15.8
Expansion	Crown	20.8	4.8	18.0	4.6	19.7	7.1
	Second	7.6	8.9	31.7	11.0	46.5	17.5
Exhaust	Crown	18.8	6.2	22.1	5.2	21.4	6.4
	Second	6.3	9.7	34.9	9.0	50.1	15.4
Average	Crown	21.2	5.6	21.0	5.4	19.1	6.8
for Cycle	Second	10.37	8.8	34.9	9.7	49.7	16.6

Table 6.4 Average Oil Film Thickness on the Crown and Second Lands for Window 1, Phases 1, 2 and 3.

Window 3		Phase 1		Phase 2		Phase 3	
		Oil Film (microns)		Oil Film (microns)		Oil Film (microns)	
Stroke	**Land**	-15 Nm	160 Nm	-15 Nm	160 Nm	-15 Nm	160 Nm
Intake	Crown	35.9	5.1	26.9	7.5	25.3	8.6
	Second	10.3	10.5	62.3	15.4	59.7	17.4
Compression	Crown	38.5	4.5	26.5	7.8	25.1	6.2
	Second	10.8	10.0	64.4	15.1	58.2	16.8
Expansion	Crown	33.4	4.2	27.7	6.1	25.0	7.2
	Second	10.3	11.4	56.9	12.8	79.9	19.5
Exhaust	Crown	34.7	4.5	28.1	6.8	24.3	6.1
	Second	10.3	10.4	58.9	15.9	71.8	17.8
Average	Crown	35.6	4.6	27.3	7.1	24.9	7.0
for Cycle	Second	10.4	10.6	60.6	14.8	67.4	17.9

Table 6.5 Average Oil Film Thickness on the Crown and Second Lands for Window 3, Phases 1, 2 and 3.

6.2.2 Inter-Ring Pressures

The inter-ring pressures were recorded for phases 2 and 3 at the load conditions -15 and 160 Nm. Two new pressure ports were installed into the engine for phase 3 and generated new data that can not be directly compared with phase 1. Also direct comparisons may be difficult to make since the cylinder pressure fluctuates from cycle to cycle and matching exact cylinder pressures was found to be difficult. Therefore the trends for each phase will be compared to try to understand the effects of changing the ring gap areas on the inter-ring pressures.

6.2.2.1 Phase 2 Inter-Ring Pressures for -15 Nm

Figure 6.27 plots the measured inter-ring pressures with the results obtained by *RINGPACK-OC* for phase 2 at -15 Nm load. Figure 6.28 presents the relative ring position calculated by *RINGPACK-OC*. Phase 2 ring pack had a reduced gap for the second ring.

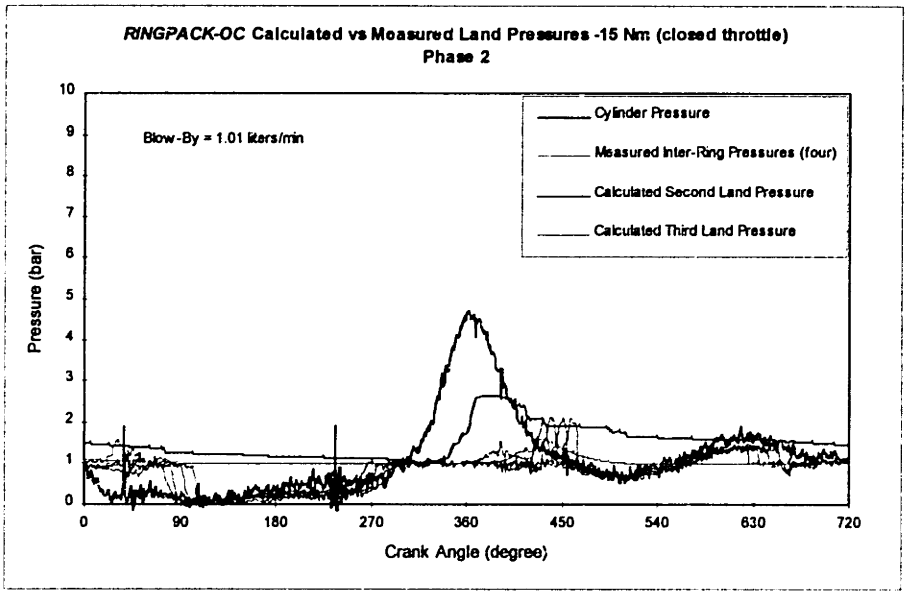

Figure 6.27 Inter-Ring Pressures for -15 Nm, Phase 2.

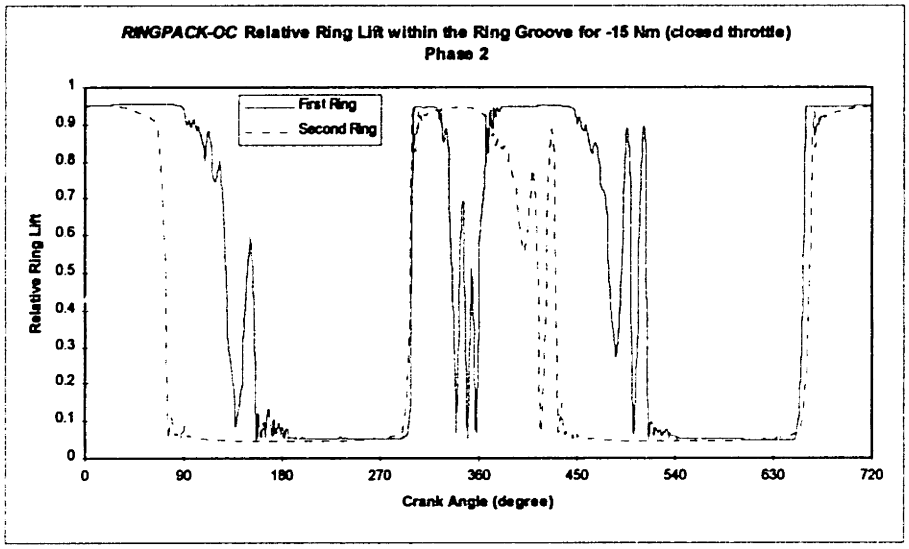

Figure 6.28 Relative Ring Lift within the Ring Groove for -15 Nm, Phase 2.

For the -15 Nm (closed throttle) condition, Figure 6.27 clearly shows a large rise in the second land pressure for a relatively small cylinder pressure, which could indicate top ring flutter. The *RINGPACK-OC* code also predicts this fluttering show in Figure 6.28, as well as some slight second ring flutter. Referring back to Figure 6.15, the relative ring positions for phase 1, the top ring flutter is similar, while the second ring does not flutter for phase 1 as it does for phase2. This can be explained by the negative twist second ring for phase 2, which is prone to fluttering during most conditions due to the fact that the negative twist on the ring exposes most of the top face of the ring to the higher second land pressure, while a zero twist or positive twist ring only exposes the top surface of the ring which extends beyond the piston, refer to Figure 6.29.

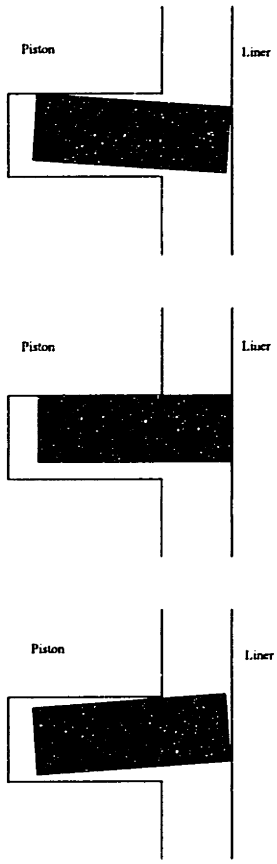

Figure 6.29 Negative, Zero and Positive Twist Rings

The inter-ring pressures for phase 2 were plotted with those of phase 1 in Figure 6.30. Due to cycle-to-cycle fluctuations in peak cylinder pressures, an exact comparison was difficult. For those cycles plotted, the cylinder pressure for phase 1 was greater than that of phase 2, so the phase 1 second land pressure would therefore be higher, which it is for port 1. However in phase 1, the second land pressure drops faster, while third land pressure rises to equal the second land pressure, due to the larger second ring gap. For phase 2 the second land pressure remains visibly constant during the four port measurements, similar to the third land pressures (see four bottom arrows).

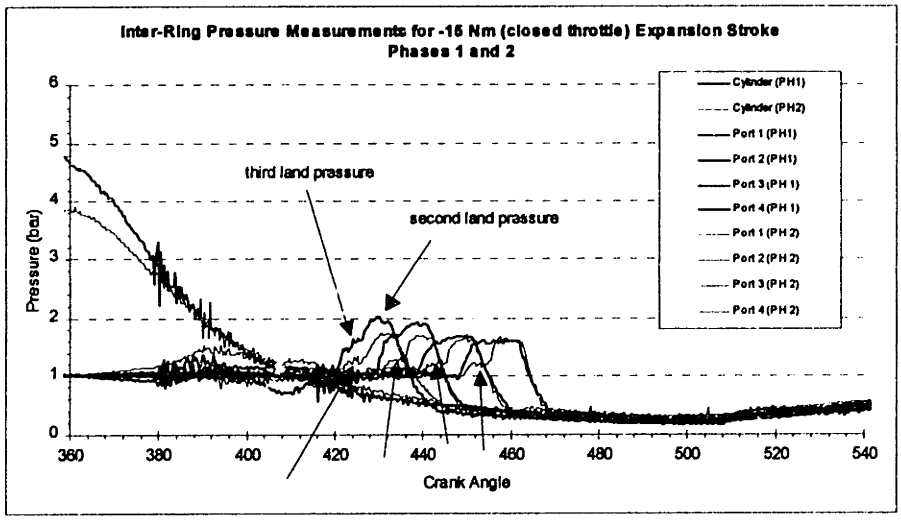

Figure 6.30 Inter-Ring Pressure Measurements for -15 Nm, Expansion Stroke, Phases 1 and 2.

6.2.2.2 Phase 2 Inter-Ring Pressures for 160 Nm

The second and third land pressures were calculated by *RINGPACK-OC* for the 160 Nm load condition for the phase 2 ring pack, refer to Figure 6.31

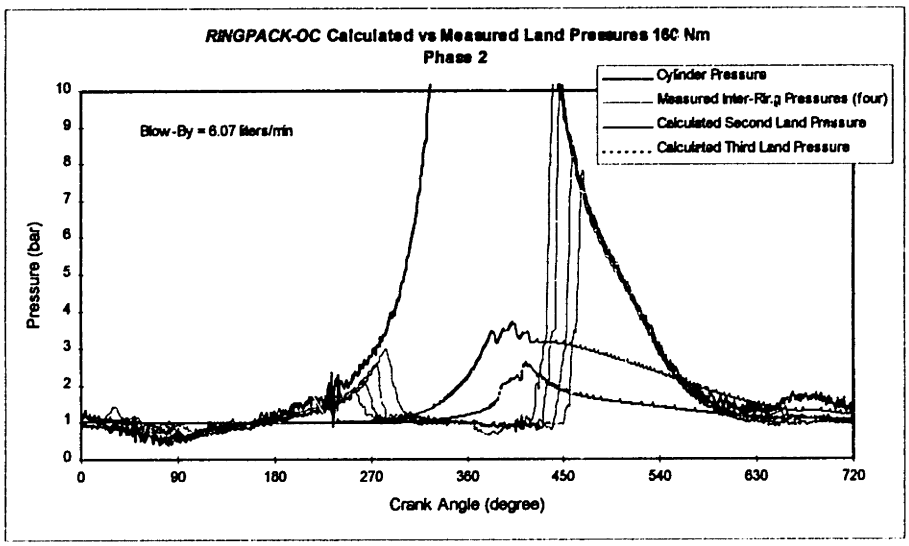

Figure 6.31 Inter-Ring Pressures for 160 Nm, Phase 2.

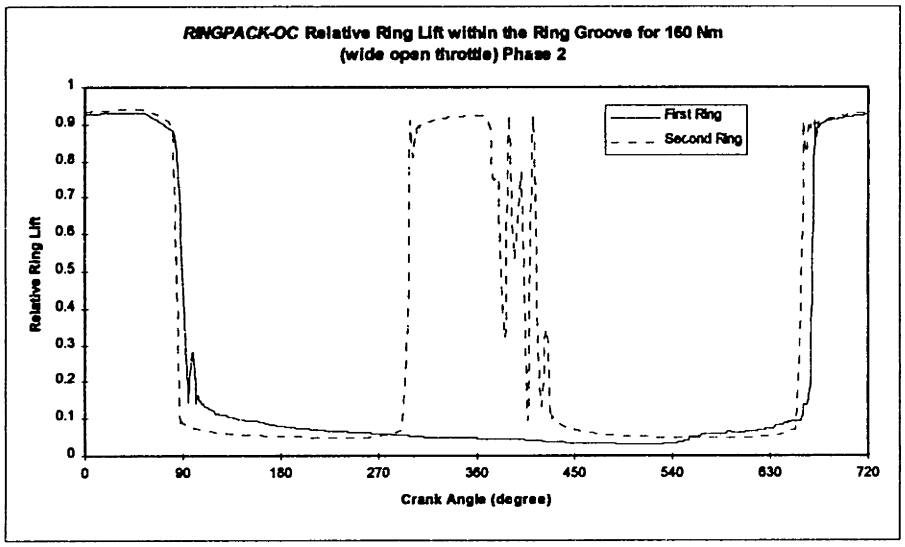

Figure 6.32 Relative Ring Lift within the Ring Groove for 160 Nm, Phase 2.

From Figure 6.31 *RINGPACK-OC* predicts that the second land pressure will rise sharply until a point when the pressure will overcome the second ring inertia force and the ring begins to flutter. The fact that the second land pressure rises faster for phase2 than phase 1, as shown in Figure 6.16, was due to the reduced second ring gap area. Figure 6.32 plots the relative ring positions calculated by *RINGPACK-OC*, which clearly predicts second ring fluttering.

To further understand the effects of the change from phase 1 to phase 2, Figure 6.33 plots both phases for the 160 Nm load condition. The peak cylinder pressures for phases 1 and 2, that are not shown in Figure 6.33, were 41 and 45 bar, respectively.

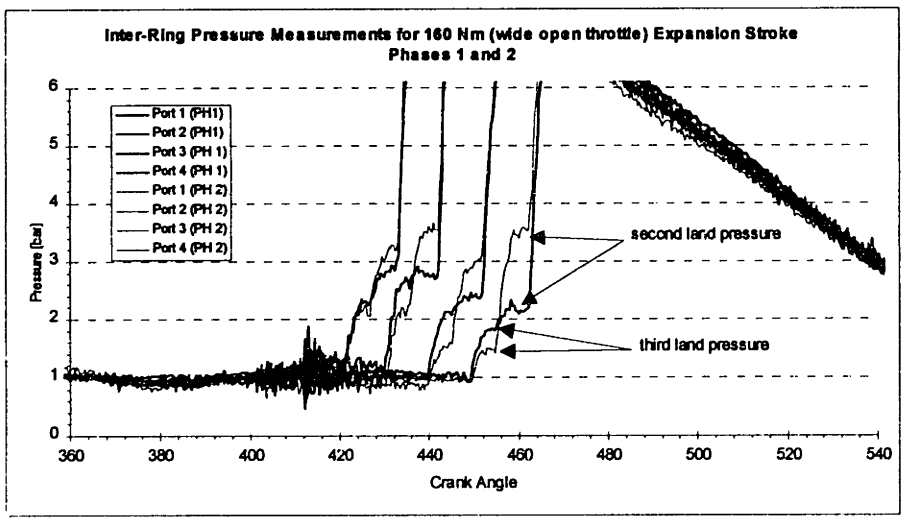

Figure 6.33 Inter-Ring Pressure Measurements for 160 Nm, Expansion Stroke, Phases 1 and 2.

There are two interesting observation taken from Figure 6.33. First, the pressures read from port 4 clearly shows the second land pressure for phase 2 remains higher than phase 1 due to the reduced ring gap. The reduced second ring gap effect is further seen from port 4, by the recorded third land pressure and the pressure difference between the second and third land for each phase. The second observation of interest is the second land pressure fluctuation seen in phase 2 from ports 2, 3 and 4. This fluctuation is most like caused by second ring flutter, which allows the second land to rapidly lose pressure, then increase again due to leakage through the top ring gap. This observation should be related to the negative twist of the second ring as well as the reduced second ring gap area.

6.2.2.3 Phase 3 Inter-Ring Pressures for -15 Nm

The phase 3 ring pack is identical to phase 1, except the increase in the top ring gap. This increased area should allow more gas pressure to leak into the second land, increasing the second and third land pressures. During phase 3, two new pressure port, designated ports A and B, were used to try and capture the second land pressure while top ring flutter occurs. Figure 6.33 plots the measured inter-ring pressures versus the *RINGPACK-OC* calculated land pressures for the -15 Nm load condition using the phase 3 ring pack. Figure 6.35 plots top relative ring positions calculated by *RINGPACK-OC* for -15 Nm.

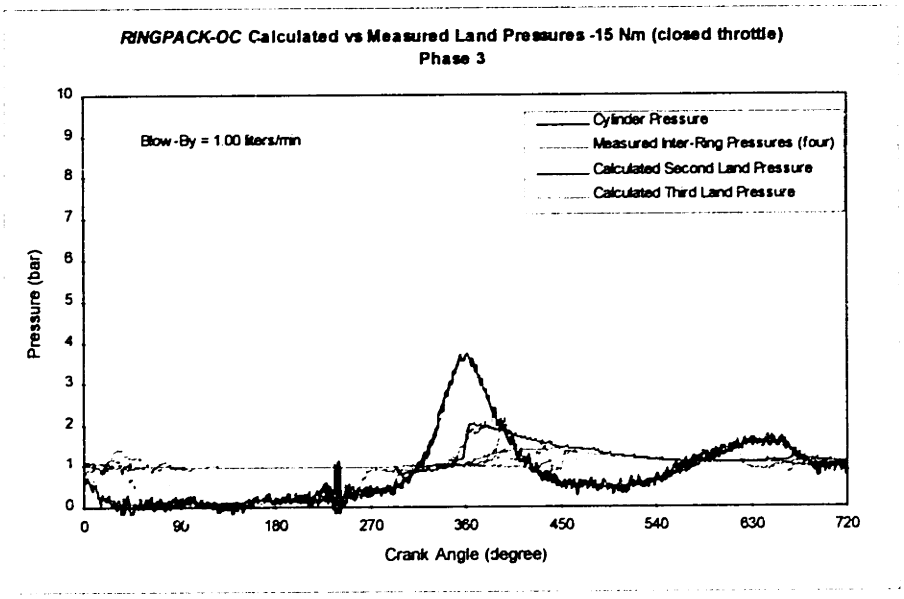

Figure 6.34 Inter-Ring Pressures for -15 Nm, Phase 3.

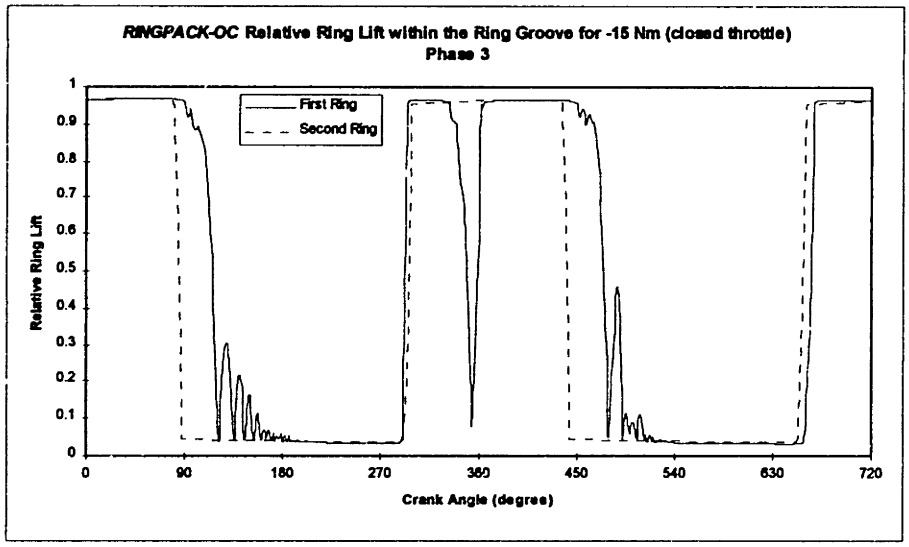

Figure 6.35 Relative Ring Lift within the Ring Groove for -15 Nm, Phase 3.

Figure 6.34 shows close correlation between the actual measured pressure and those calculated by *RINGPACK-OC*. Again top ring flutter was predicted by *RINGPACK-OC* and the highest pressure port records a sharp rise in pressure before TDC on the compression stroke. Figure 6.36 shows the second land pressure rise following the cylinder pressure rise from 340° to after 360° crank angle.

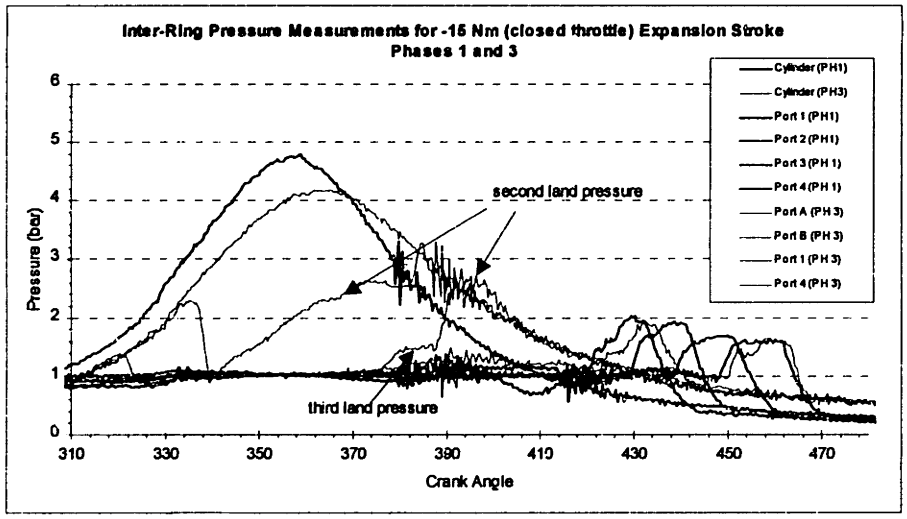

Figure 6.36 Inter-Ring Pressure Measurements for -15 Nm, Expansion Stroke, Phases 1 and 3.

Figure 6.36 compares the inter-ring pressures recorded for phases 1 and 3. The inter-ring pressures measured from ports 1 and 4 are quite similar for both phases even though the top ring gap was nearly doubled for phase 3, which might be explained by the ring fluttering. That is, if the second land pressure rise is due mostly to gas passing through the ring groove during

fluttering condition, and not from gas passing though the top ring gap, then any change in the gap would be less noticeable.

6.2.2.4 Phase 3 Inter-Ring Pressures for 160 Nm

Due to the two additional pressure ports used in phase 3, there were more inter-ring pressure measurements to help calibrate the *RINGPACK-OC* code for the 160 Nm load condition. This additional information however caused the first signs in the limitations of the *RINGPACK-OC* code since the author was unable to match all of the measured inter-ring pressures with the predicted *RINGPACK-OC* pressures. There are a few mechanisms that are not yet written into *RINGPACK-OC*, primarily the ring gap position and piston secondary motion. The ring gap position along with the piston secondary position could influence the gap area, there by effecting land pressures. Also the piston slap that occurs after TDC during the expansion stroke might cause an instant of unstable rings, allow sudden changes in pressures.

The author chose to calibrate *RINGPACK-OC* to the first and fourth pressure port measurements for the 160 Nm, phase 3 condition, there-by remaining consistent with phases 1 and 2. Refer to Figure 6.37 for the gas pressures and Figure 6.38 for relative ring positions.

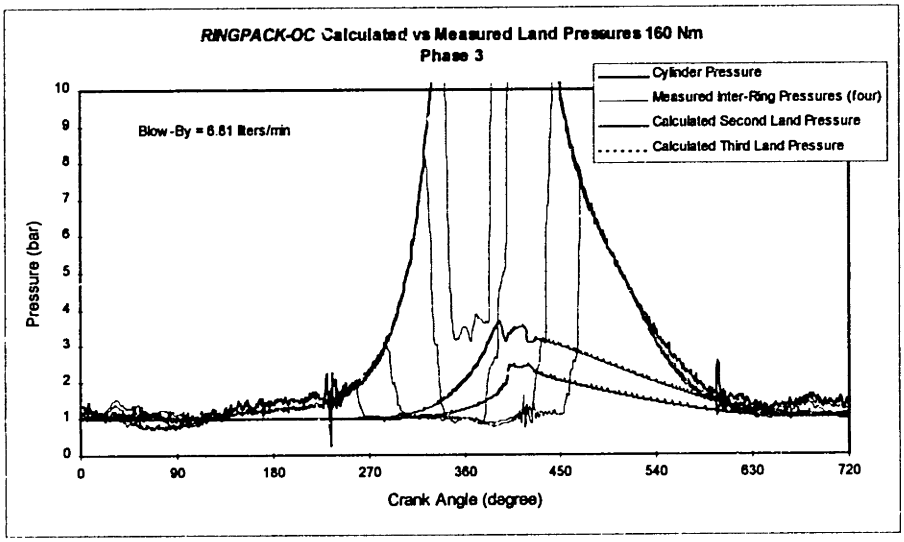

Figure 6.37 Inter-Ring Pressures for 160 Nm, Phase 3.

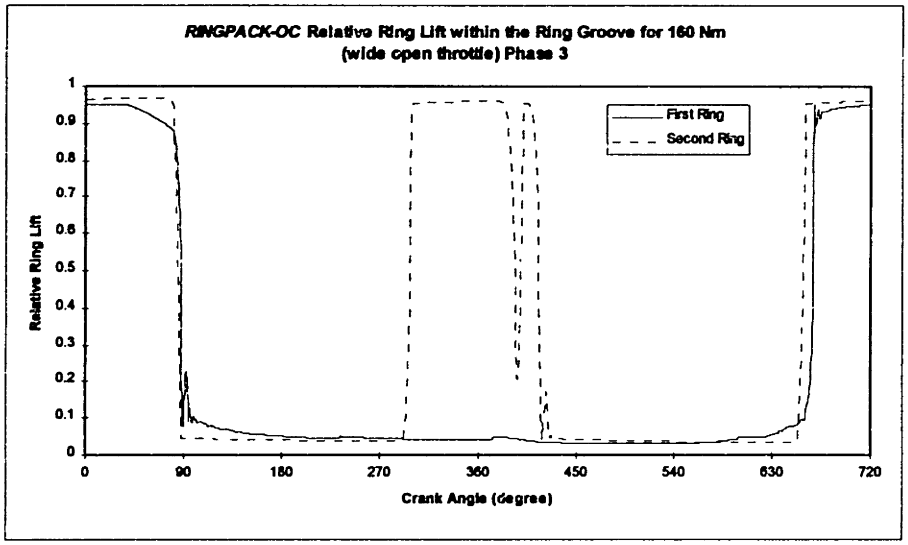

Figure 6.38 Relative Ring Lift within the Ring Groove for 160 Nm, Phase 3.

From Figure 6.38 *RINGPACK-OC* predicts only slight second ring flutter after TDC, however port A clearly shows that the second ring is fluttering to allow for the second land pressure to drop and rise so abruptly.

Figure 6.39 compares the measured inter-ring pressures for phases 1 and 3. The peak cylinder pressure, not shown in Figure 6.39, were 41 and 42 bar for phases 1 and 2, respectively. The increased top ring gap for phase 3 would expect to cause an increase in the second land pressure, which is not the case as seen by ports 1 and 4 in Figure 6.39. It may be that the second land pressure rises faster during the compression stroke for phase 3 but when it reaches a certain point the second ring begins to flutter, there-by releasing pressure to the third land and into the crank case. This same threshold pressure where the second ring begins to flutter might also be reached by the phase 1 rings but only later in the cycle due to the smaller top ring gap. It would be of interest to run the phase 1 cases again and record the inter-ring pressures from ports A and B.

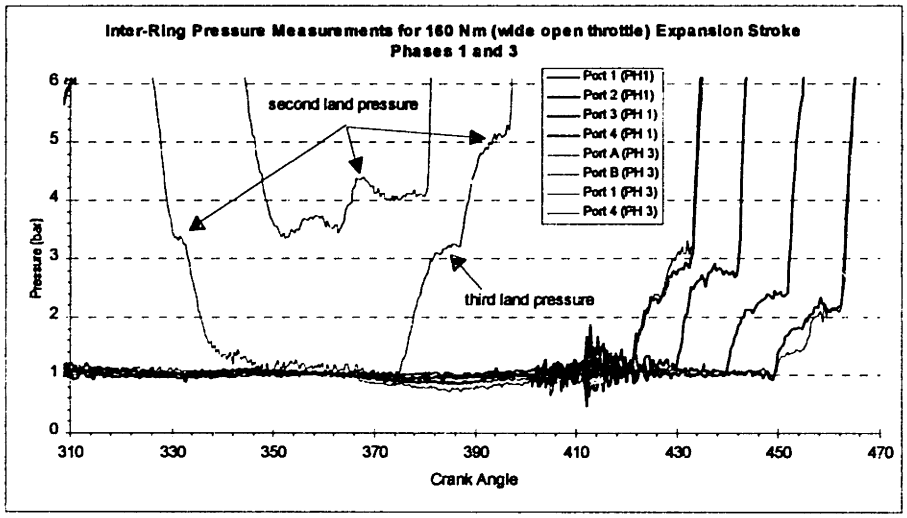

Figure 6.39 Inter-Ring Pressure Measurements for 160 Nm, Expansion Stroke, Phases 1 and 3.

6.3 OIL CONSUMPTION FOR PHASES 1, 2 AND 3

It was of great interest to correlate the oil film thickness data and the inter-ring pressure measurements for each phase to gain an understanding of how ring pack parameters affect oil consumption. Direct comparisons of the oil film thickness and inter-ring data can be made. Using results from *RINGPACK-OC* predictions, further analysis can also explain the behavior of the ring pack.

6.3.1 Drain and Weight Oil Consumption Measurements

The oil consumption data for all three phases was performed using a drain and weight method. This method involves running the engine at the chosen steady state load condition for a standard set time period. The longer the period is the more reliable the results will be, three hours and up is usually recommended [4]. The engine oil is weighed before and after the testing period, allowing the same time for the oil to drain from the engine. The difference in the total weight of the oil before and after testing divided by the test period yields the oil consumption rate.

Table 6.6 lists the measured oil consumption rates for each phase at -15 and 160 Nm load conditions [4].

	Oil Consumption (g/hr)	Oil Consumption (g/hr)
	4000 rpm -15 Nm (closed throttle)	4000 rpm 160 Nm (wide open throttle)
Phase 1	36	13
Phase 2	165	25
Phase 3	105	20

Table 6.6 Measured Drain and Weight Oil Consumption Data.

Form Table 6.6 it is quite clear that the variation in oil consumption for 4000 rpm, the closed throttle, -15 Nm load condition was substantial. Phase 1 oil consumption was far less then phases 2 and 3, which is of interest since the second land oil film thickness was substantially lower for phase 1. The second land oil film thickness for phases 2 and 3 was quite similar yet there was less oil consumption for phase 3.

The degree of variation in oil consumption for 4000 rpm, wide open throttle, was less than for closed throttle operation, however the trend for the three phases was similar. That trend indicates that phase 2 has the highest oil consumption of the three phases, then phase 3, and the lowest values of oil consumption were seen for phase 1.

6.3.2 Oil Transport Model for Phases 1, 2 and 3

An oil transport model was created in hopes of matching the measured values of oil consumption such that a better understanding of what the effects of measured oil film thickness and inter-ring

pressures have on the model. Total engine oil consumption has three contributing factors, oil lost through the ring pack, valve guides and crank case ventilation. This model will neglect the last two of the three listed factors and will focus only on the oil that passes through the ring pack and is lost to the combustion chamber. Because the oil that passes up the piston and through the ring pack must ultimately get by the top ring, this will be the focus point of the oil transport model.

Two contributing factors will be considered for the driving force of the oil to pass by the top ring. When the second land pressure exceeds the cylinder pressure, reverse gas flow will occur through the top ring gap, carrying with it a fraction of oil. Also, when the pressure behind the top ring exceeds the cylinder pressure and the top ring is at the top of the piston ring groove the pressure can force any oil that is between the ring and the groove onto the crown land. Since the major driving force for the model is pressure gradients, only the condition of closed throttle operation will be examined. For the wide open throttle condition the pressure gradients were relatively small and the model was too basic to expect correlation with the measured oil consumption data.

The second land pressure, the pressure behind the top ring, the relative position of the top ring and the mass flow through the top ring gap were all needed for the two oil transport factors, and were obtained from *RINGPACK-OC*. The cylinder pressure needed was obtained from the experimental results.

The results from *RINGPACK-OC* for the relative ring position, pressure behind the top ring and the second land pressure for phase 1, was plotted verse the cylinder pressure in Figure 6.40. The areas where the potential driving force for the oil between the ring and groove is bracketed by the arrows. For this region Equation (4.4) was applied using the cylinder pressure as P1 and the pressure behind the top ring as P2 and the crank angle duration as the time.

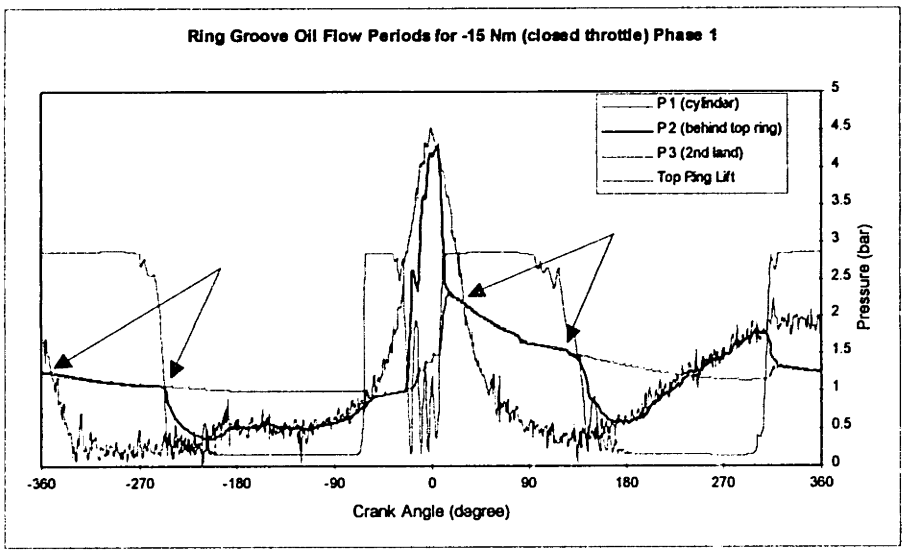

Figure 6.40 Ring Groove Oil Flow Periods at -15 Nm, Phase 1.

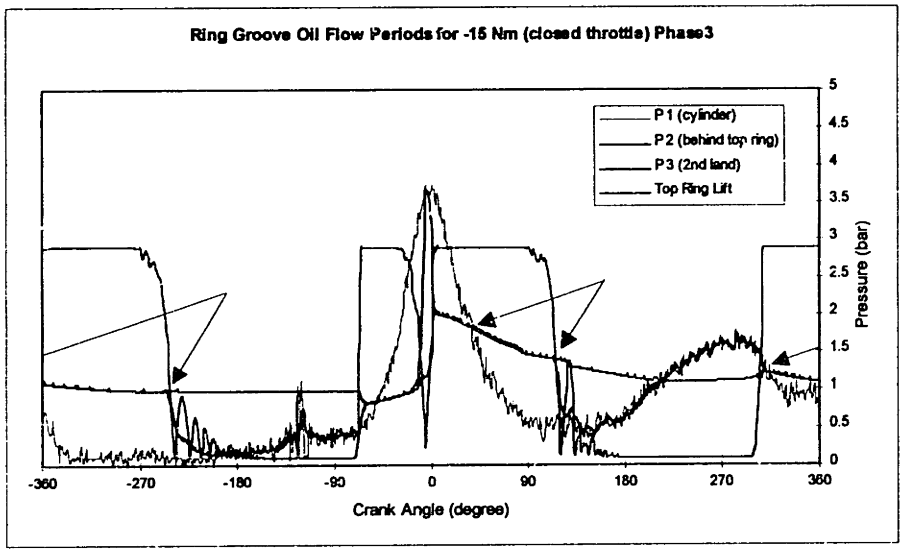

Figure 6.41 Ring Groove Oil Flow Periods at -15 Nm, Phase 2.

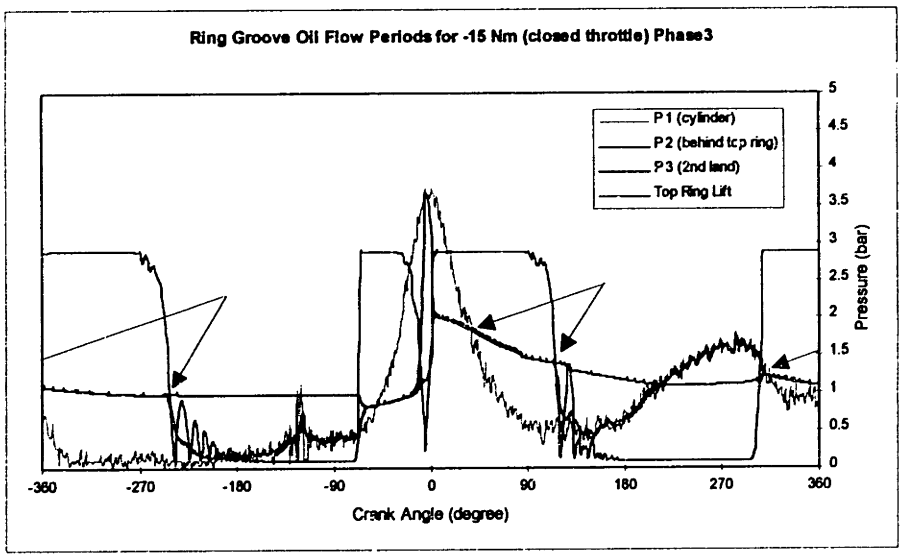

Figure 6.42 Ring Groove Oil Flow Periods at -15 Nm, Phase 3.

Comparing the three phases at -15 Nm, Figures 6.40, 6.41 and 6.42, phases 2 and 3 have a longer period when the ring is at the top of the groove starting in the exhaust stroke and lasting well into the intake stroke. This extended pressure driving time may explain the higher steady state oil consumption measured for phases 2 and 3, as well as the increased second land oil film thickness which may increase the amount of oil in the ring groove.

The gas mass flow through the top ring gap for the three phases, plotted in Figure 6.43, allows direct comparison for the three phases. Since phase 3 increased the top ring gap it can be expected that the mass flow through the gap would increase as seen in Figure 6.43. Also of interest that the phase 1 condition has a positive gas mass flow for most of the exhaust stroke.

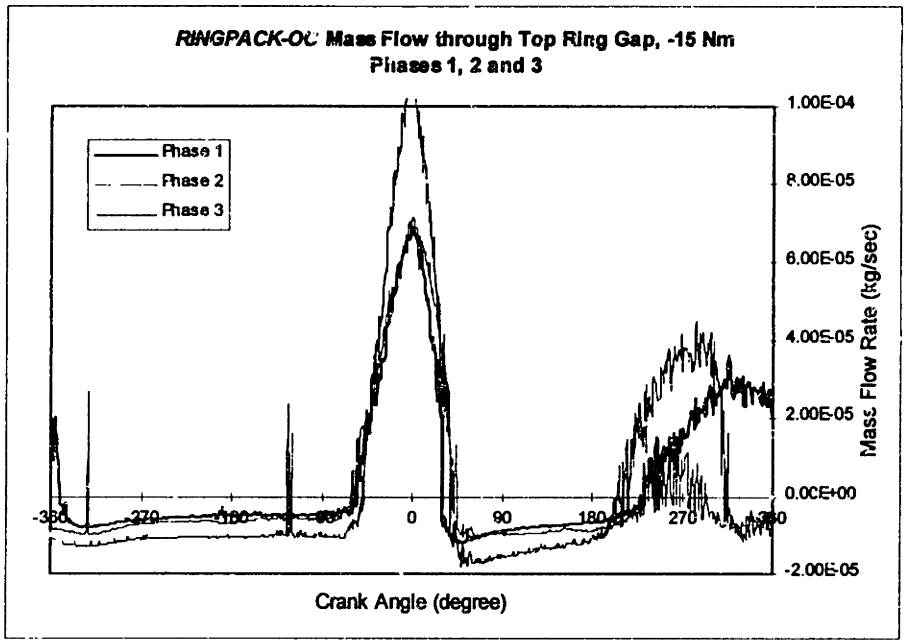

Figure 6.43 Mass Flow through the Top Ring Gap at -15 Nm for Phases 1, 2 and 3.

The assumption was made that the mass flow of gas through the top ring gap and top ring groove carries with it some oil which accumulates on the crown land and enters the combustion chamber, directly contributing to engine oil consumption. Table 6.7 list the values used in the calculated values for oil consumption, assuming certain oil fractions. The value for oil viscosity was held constant for all phases, assuming a constant oil temperature of 200° C in the top ring groove. The values for oil film thickness in the ring groove and the fraction of oil mass in the gap flow were picked to match the measured values of oil consumption. All other values in Table 6.7 were obtained from the *RINGPACK-OC* results for each phase.

The values for the oil mass fraction in the top ring gap flow were picked based on the following reasoning. From other research measurements of the gas to oil ratio in the top ring groove region suggests an oil loading of 0.5 to 1% by weight with a running condition 1200 rpm, 180 Nm [6]. Therefore for phase 1 with a negative load condition, which was observed to have more oil on the lands then at a high load condition, an oil fraction of 5% was used in the oil transport model. Since the oil film on the second land for phases 2 and 3 was substantially higher than for phase 1, the oil fraction was increased to 15%.

There was no way to determine the oil film between the ring and ring groove and these values were found by matching the measured oil consumption values to those calculated by the oil transport model. For phase 1 a film thickness of 2.00 microns provided a good match in oil consumption. Phase 2 required a oil film of 3.45 microns to match oil consumption values, which may be reasonable since the second land oil film thickness for phase 2 was substantially higher then for phase 1. Having more oil on the second land may have an effect on the amount of oil in the ring groove. Finally, phase 3 used a film thickness of 3.00 microns in the top ring groove to match oil consumption values. This value falls between phases 1 and 2, similar to the oil consumption values.

		Phase 1	Phase 2	Phase 3
		-15 Nm	-15 Nm	-15 Nm
Groove Oil Flow	Oil Viscosity [m^2/sec]	2.15E-06	2.15E-06	2.15E-06
	h [microns]	2.00	3.45	3.00
	Cycle Flow [kg]	1.89E-08	1.15E-07	5.99E-08
	Time Duration [s]	0.0085	0.00113	0.0111
	Oil Flow Rate per Cylinder [kg/s]	2.23E-06	1.02E-05	5.41E-06
	Oil Flow Rate per Cylinder [g/hr]	8.0	36.8	19.5
	Oil Flow Rate for Engine [g/hr]	32.0	147.2	78.0
Gap Oil Flow	Total Gas Flow Rate [g/hr]	23.3	25.3	37.0
	Oil Fraction	0.05	0.15	0.15
	Oil Flow Rate per Cylinder [g/hr]	1.17	3.80	5.55
	Oil Flow Rate for Engine [g/hr]	4.7	15.2	22.2
Total Engine	(Gap and Groove Flow Rate) [g/hr]	36.7	162.4	100.2
Measured OC	(Drain and Weight) [g/hr]	36	165	105

Table 6.7 Oil Transport Model Input Values

The oil transport model could not predict the oil consumption values due to the uncertainty of the groove film thickness and oil percent in the gap mass flow, but the results are of interest. The driving force for oil though the ring groove was strong during the closed throttle operation and by increasing the film thickness in the groove the oil consumption rate was substantially increased.

CHAPTER 7 CONCLUSIONS

Operating Condition Differences:

1) The comparison of the LIF data for phase 1 at 4000 rpm, -15 Nm (closed throttle) and 160 Nm (wide open throttle) revealed substantially different amounts of oil accumulation on the piston crown land. For both windows 1 (50 mm from TDC) and window 3 (87.5 mm from TDC) the accumulated oil recorded on the crown land during -15 Nm load condition was on the order of four to six times greater than at 160 Nm. It was also observed that while the crown land oil film varied, the second land oil film remained relatively constant for both test conditions. The measured oil consumption data for -15 Nm was almost three time greater than at 160 Nm, which may be attributed to the increase in crown land oil film thickness observed from the LIF data.

2) The inter-ring pressures were measured for phase 1 at 4000 rpm, at loads of -15 and 160 Nm. At the points of measurement during the expansion stroke, the second land pressure for -15 Nm was 2.0 bar while the cylinder pressure was only 4.0 bar, while for 160 Nm the second land pressure was 2.75 bar and the cylinder pressure was 40 bar. The ratios of second land pressure to cylinder pressure, 1 to 2 and 1 to 14.5, for -15 and 160 Nm, respectively, indicates that the sealing properties of the top ring were failing during the -15 Nm condition. This ring failure was most likely due to top ring fluttering, allowing cylinder gases to pass behind the ring. The computer code, *RINGPACK-OC*, also predicted ring flutter and calculated that the second land pressure for -15 Nm was greater than cylinder pressure for substantially longer periods during the cycle than for 160 Nm. This reverse pressure gradient increases the potential for reverse blow-by and ring groove oil transport, which could directly contribute to increased oil consumption. This increased oil consumption rate was measured for the -15 Nm load condition; it was almost three times greater than the oil consumption rate at 160 Nm.

Piston Ring Configuration Differences:

1) The oil film thickness on the crown land during 4000 rpm, -15 Nm testing condition remained relatively constant for the three phases tested. The second land oil film thickness during the same condition increased substantially for phases 2 and 3 compared to phase 1. For phase 2 this increase may be attributed to the reduction in second ring gap and variation in second ring design. For phase 3 the observed increase in second land oil film thickness may be attributed to the increase in the top ring gap and possibly the effects of wear to the rings and cylinder walls. The measured oil consumption rates for the three phases at -15 Nm load, 4000 rpm, indicated that the increased amount of oil on the second land greatly increased the oil consumption rates for phases 2 and 3.

2) There were only slight variations observed in the oil film thickness data measured for phases 1, 2 and 3 during 4000 rpm, 160 Nm. This wide open throttle running condition had relatively dry crown and second lands and the differences between phases was too subtle to characterize oil consumption rates.

3) The inter-ring pressures for phases 1, 2 and 3 were compared at the running condition of 4000 rpm, -15 Nm load. For all three phases the second land pressure at the common points of measurement were relatively equal. This similarity may be explained by the predicted top ring fluttering which would eliminate any discrepancies in ring gap area since the build up of second land pressure could be attributed mostly to cylinder gas passing around the top ring not through the ring gap. For phase 2 the third land pressure was substantially lower than phase 1 which could be attributed to the reduced second ring gap.

4) The inter-ring pressure for the three phases were compared at the testing condition of 4000 rpm, 160 Nm. The comparison of phases 1 and 2 clearly indicated that the second land pressure for phase 2 does not bleed off as quickly during the expansion stroke, as for phase 1 due to the reduced second ring gap. There was also some erratic behavior for the second land pressure for phase 2 that was not observed in phase 1, which could be explained by second ring flutter. The second land pressure for phase 2 drops and rises between ports which may be caused by ring fluttering. This fluttering could accounted for by either the replacement of the phase 1 hooked second ring with a negative twist ring which tends to enhance fluttering or the reduced second ring gap. No major differences in inter-ring pressure measurements were observed for the common pressure ports of phases 1 and 3.

Bore Distortion Effects:

1) The effects of bore distortion on the piston land oil film thickness was observed by the comparison of windows 1 and 1a. At these window locations a 30 micron bore distortion was measured at a running condition of 4000 rpm, wide open throttle. There was no noticeable variation of the oil film thickness on the order of 30 microns between the two window locations. However there was on average only 5 microns of oil measured on the crown for both windows and on average 8 and 16 microns of oil on the second land for windows 1 and 1a, respectively. If the lands were only carrying minimal amounts of oil then any effect of bore distortion would not be observed.

CHAPTER 8 RECOMMENDATIONS

The following are the author's recommendations of additional testing that could enhance the current work:

1) It would be of interest to re-run the phase 1 ring pack to observe any differences in oil film thickness from the original testing, which might be caused by piston ring and/or cylinder liner wear. An area of particular interest would be the wear of the hooked second ring which may effect the second land oil film thickness, thereby affecting oil consumption. A surface profile could be performed on the second ring after re-running the phase 1 ring pack and compared to a new second ring.

2) Since there were two changes made in phase 2 from the original phase 1 ring pack, it might be of interest to re-run phase 2 ring pack with only the variation of the second ring gap, not including the design change of second rings.

3) If phases 1 and 2 were to be re-tested, as discussed in 1) and 2), it would also be a great interest to record the inter-ring pressures from ports A and B and compare the results with those of phase 3.

REFERENCES

[1] Hiruma, M., Yoshida, H., Furuhama, S. and Shin, K., 1983, "Effect of Piston Ring Movement upon Oil Consumption", JSAE Review, pp.26-33, March 1983.

[2] Tamai, Goro, "Experimental Study of Engine Oil Film Thickness Dependence on Liner Location, Oil Properties and Operating Conditions", MIT Master's Thesis, Dept. of Mechanical Engineering, August, 1995.

[3] Furuhama, S., Hiruma, M. and Tsuzita, M., "Piston Ring Motion and its Influence on Engine Tribology", SAE paper #790860, 1979.

[4] Internal Reporting, Maamouri, M., Desplanches, G., Renault, Paris.

[5] Heywood, J.H., *Internal Combustion Engine Fundamentals*, McGraw-Hill, 1988.

[6] Verbal Correspondence with Tian Tian at MIT.

[7] Taylor, R.I., Kitahara, T., Saito, T. and Coy, R.C., "Piston Assembly Frictionand Wear: The Influence of Lubricant Viscometry", Proceedings of the International Tribology Conference, Yokohama, 1995.

[8] Dowson, D., Taylor, C.M., Childs, T.H.C. and Dalmaz G., *Lubricants and Lubrication*, Elsevier, 1995.

[9] Hoult, D.P. and Takiguchi, M., "Calibration of the Laser Fluorescence Technique Compared with Quantum Theory", Tribology Transactions, Volume 34, pp. 440-444, 1991.

APPENDIX A LIF WINDOW SURFACE PROFILES

Surface profiles were performed on each of the eight installed LIF quartz windows after the cylinder was bored and honed. The recess for each window can be seen in the following figures. For each figure, the surface orientation was if TDC to the right of the window.

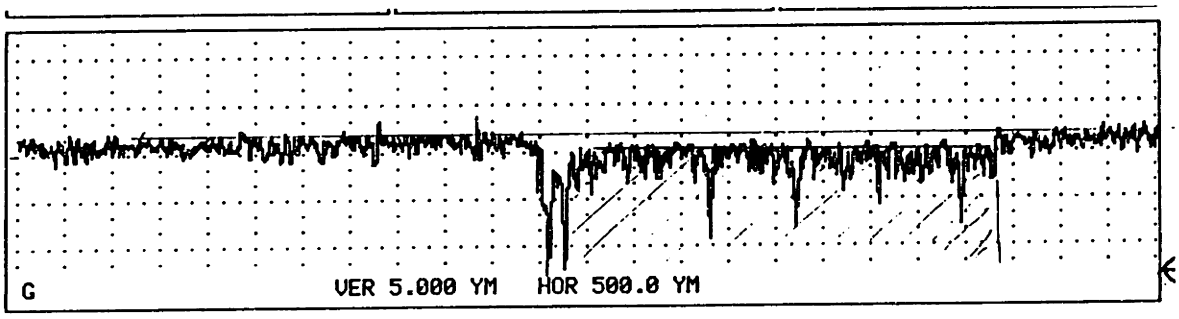

Figure A.1 LIF Window 1 Surface Profile (≈1.5 micron recess).

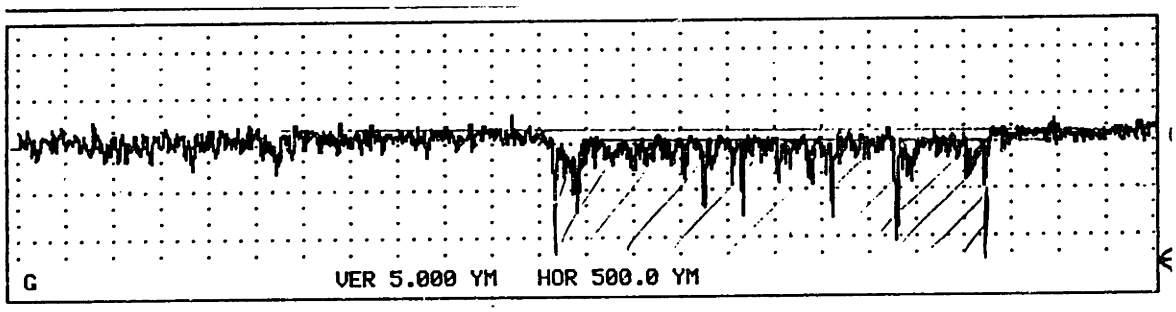

Figure A.2 LIF Window 1a Surface Profile (≈1.0 micron recess).

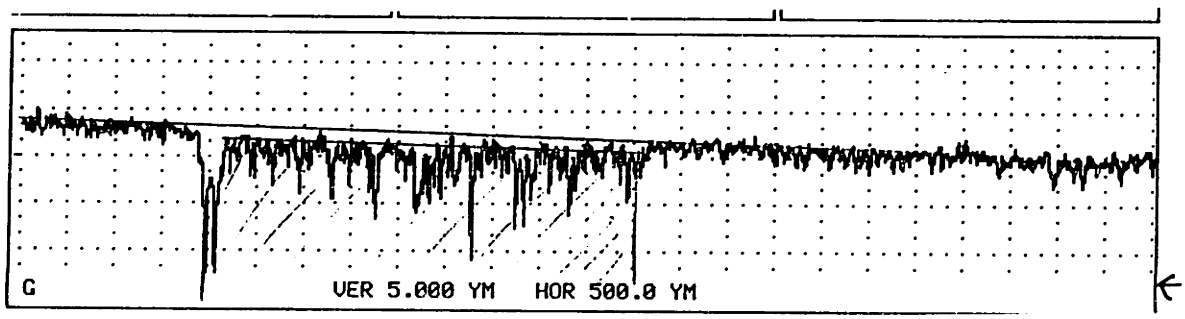

Figure A.3 LIF Window 2 Surface Profile (≈1.5 micron recess).

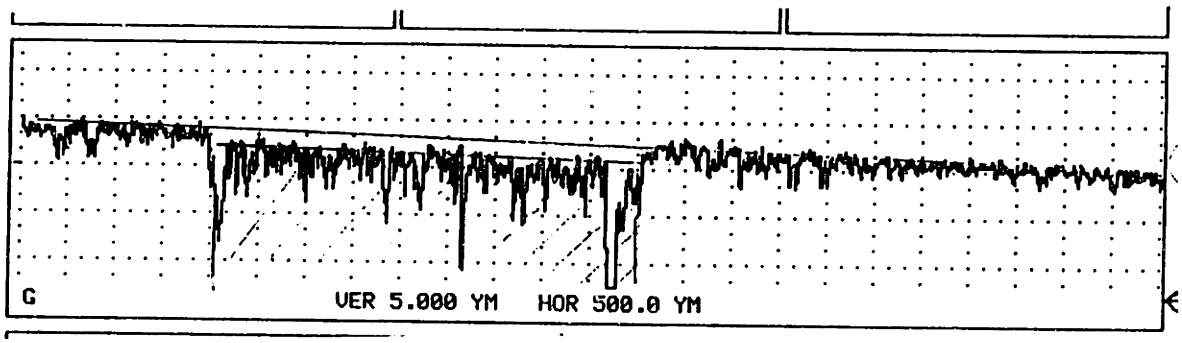

Figure A.4 LIF Window 2a Surface Profile (≈2.0 micron recess).

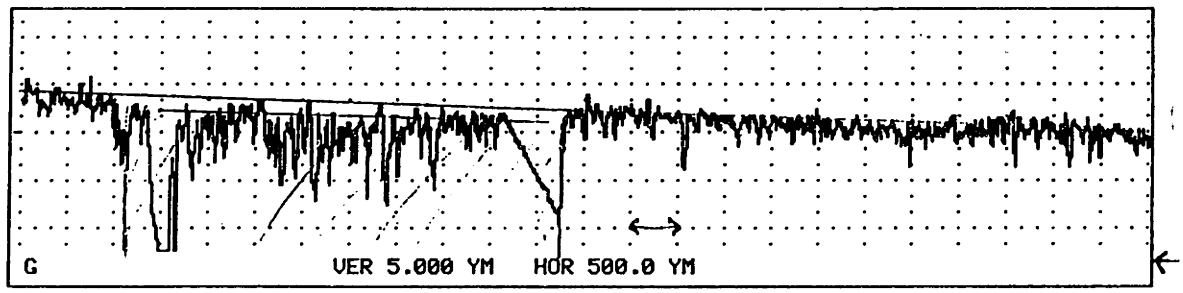

Figure A.5 LIF Window 3 Surface Profile (≈1.5 micron recess).

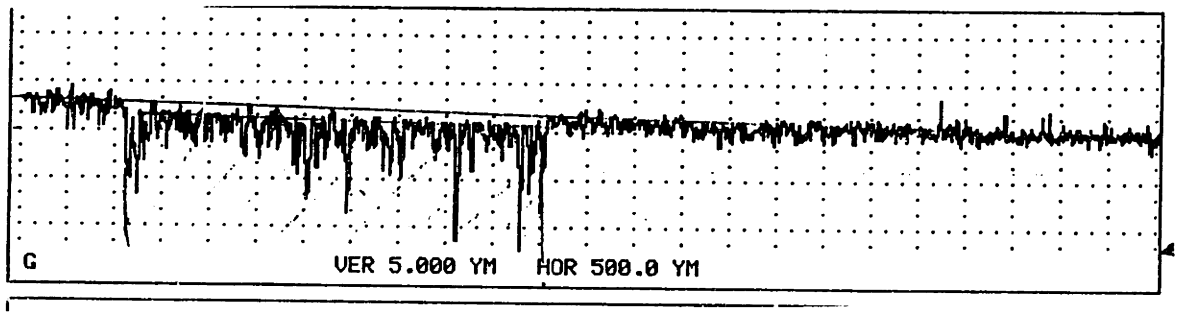

Figure A.6 LIF Window 3a Surface Profile (≈1.0 micron recess).

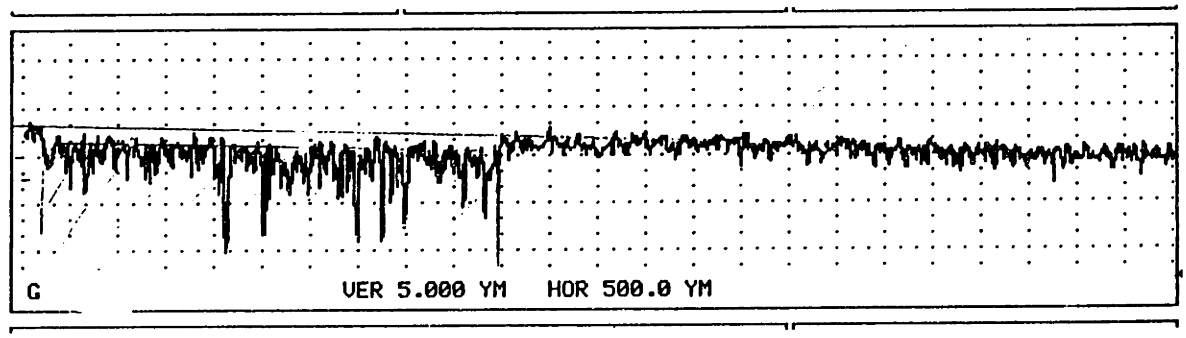

Figure A.7 LIF Window 4 Surface Profile (≈1.5 micron recess).

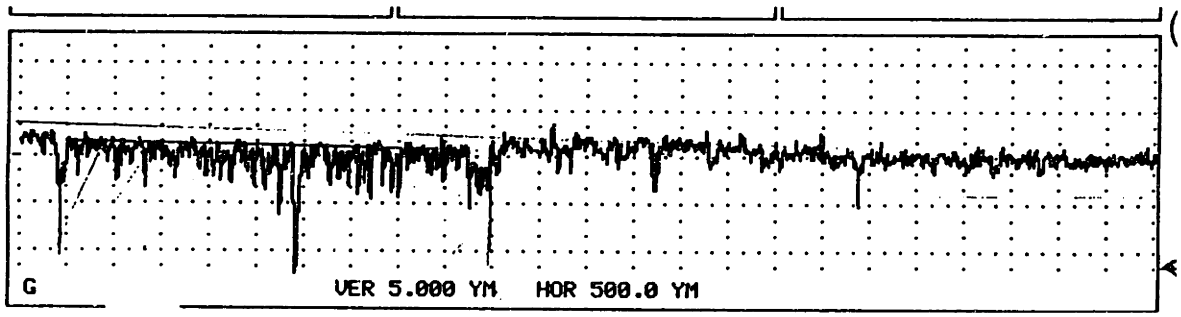

Figure A.8 LIF Window 4a Surface Profile (≈1.5 micron recess).

APPENDIX B LIF PROCESSING PROGRAMS

B.1 LIF DATA AVERAGING

A FORTRAN program was written to average a multi-cycle LIF raw data file into a one cycle averaged LIF data file.

AVERAGE.FOR

```
      integer*2 mc(8000,8)
      real average(8000,8),aver(8000,8)
      character*50 filelist,dt,dtr
      character*50 str

      write(*,*)
      write(*,*)'     ***** LIF Averaging Program *****'
      write(*,*)'{encoder set at start of intake or expansion}'
      write(*,*)
      write(*,*)'Give the number of cycles (<100)'
      read(*,*)ncyc
      write(*,*)'points per cycle...'
      read(*,*)nl
      write(*,*)'give the number of channels'
      read(*,*)nchl
      write(*,*)'which channel contains the cylinder pressure...'
      read(*,*)cylch

C     A FILE CONTAINING MULTIPLE LIF FILE NAMES WITH CORRESPONDING OUTPUT
C     FILE NAMES TO PERFORM MULTIPLE FILE PROCESSING

      write(*,*)'give the file name containing the list of files to be
     &averaged'
      read(*,'(a)')filelist

C     PROCESS FILE NAMES

      open (9,file=filelist,status='old')

2     continue
      read(9,'(a)',end=999)dt
      read(9,'(a)',end=999)dtr

      write(*,*)dt
      write(*,*)dtr

      open (7,file=dt,status='old')
      open (8,file=dtr,status='new')

      n=0
```

```
1   continue

C   REMOVE THE TOP PORTION OF DATA FILE CONTAINING DATA AQUSITION LITERATURE

    read(7,'(a)')str
    if ((str(1:1).ne.'-').and.((str(1:1).ne.' + ').and.
   &  (str(1:1).ne.'0'))) then
      n = n + 1
      goto 1
    end if

C   READ ONE CYCLE OF CYLINDER PRESSURE TO DETERMINE IF SHIFTING IS NEEDED

    do i = 1,nl
     read(7,*)(mc(i,j),j = 1,nchl)
    end do

    fpt = 5
    spt = nl/2 + 5

    if ((mc(fpt,cylch)).gt.(mc(spt,cylch))) then
     shift1 = 1
    endif

C   PERPARE FILE FOR AVERAGING

    rewind 7

    do i = 1,n
     read(7,'(a)')str
    end do

    if (shift1.eq.1) then
     write(*,*)'Shifting data...'
     k = nl/2
     do i = 1,k
      read(7,*)(mc(i,j),j = 1,nchl)
     end do
    end if

C   BEGIN AVERAGING OF LIF DATA FILE

    do i = 1,nl
     do j = 1,nchl
      aver(i,j) = 0
     enddo
    enddo

    do i = 1,ncyc
     do k = 1,nl
      read(7,*)(mc(i,j),j = 1,nchl)
      do j = 1,nchl
       aver(k,j) = aver(k,j) + mc(k,j)
      enddo
```

```
 enddo
end do

do k = 1,nl
 do j = 1,nchl
  average(k,j) = aver(k,j)/ncyc
 enddo
enddo

C   WRITE AVERAGED DATA TO NEW FILE

do k = 1,nl
  write(8,100)(average(k,j),j = 1,nchl)
enddo

100  format (1x,3(f8.1,','),f8.1)

close(7)
close(8)

goto2

999  continue

close(9)

stop
end
```

B.2 LIF DATA SINGLE CYCLE

To calibrate an LIF signal single cycle traces must be viewed to see the tool mark flooding. A averaged LIF file will lose the required resolution. Therefore a raw LIF data file containing multiple cycles must be processes to produce multiple files with single cycle LIF traces.

SINGLE.FOR

```
parameter (nll = 8000)
parameter (nchan = 8)
parameter (nchr = 100)
character*50 dt,dt1(nchr)
character*50 str,su
character*1  cha1,cha2
integer*4 i,n
integer*2 mc(nll,nchan)

C   INPUT DATA

write(*,*)
write(*,*)'*****  This program separates cycles  *****'
write(*,*)
```

```
      write(*,*)'Input the data file to be separated...'
      read(*,'(a)')dt
      write(*,*)'give the output file name...'
      write(*,*)'and 1,2,3,etc.+[.dat] will be added.'
      read(*,'(a)')su
      write(*,*)'give the number of cycles (<100)...'
      read(*,*)ncyc
      write(*,*)'points per cycle...'
      read(*,*)nl
      write(*,*)'give the number of channels'
      read(*,*)nchl
      write(*,*)'which channel contains the cylinder pressure...'
      read(*,*)cylch

C     CREATE MULTIPLE OUTPUT FILES

      ls=len_trim(su)
      do i=1,ncyc
       k=i/10
       k1=i-10*k
       cha1=char(48+k)
       cha2=char(48+k1)
       dt1(i)(1:ls)=su(1:ls)
       dt1(i)(ls+1:ls+1)=cha1
       dt1(i)(ls+2:ls+2)=cha2
       dt1(i)(ls+3:ls+6)='.dat'
      end do

      open (7,file=dt,status='old')

C     REMOVE THE TOP PORTION OF DATA FILE CONTAINING DATA AQUSITION LITERATURE

      n=0
1     continue
      read(7,'(a)')str
      if ((str(1:1).ne.'-').and.((str(1:1).ne.'+').and.
     &  (str(1:1).ne.'0'))) then
        n=n+1
        goto 1
      end if

C     READ ONE CYCLE OF CYLINDER PRESSURE TO DETERMINE IF SHIFTING IS NEEDED

      do i=1,nl
       read(7,*)(mc(i,j),j=1,nchl)
      end do

      fpt=5
      spt=nl/2+5

      if ((mc(fpt,cylch)).gt.(mc(spt,cylch))) then
       shift1=1
      endif
```

```
C    PERPARE FILE FOR SEPERATING CYCLES

     rewind 7

     do i = 1,n
      read(7,'(a)')str
     end do

     if (shift1.eq.1) then
      write(*,*)'Shifting data...'
      k = nl/2
      do i = 1,k
       read(7,*)(mc(i,j),j = 1,nchl)
      end do
     end if

C    BEGIN SEPERATING CYCLES FROM LIF DATA FILE

     do k = 1,ncyc
      do i = 1,nl
         read(7,*)(mc(i,j),j = 1,nchl)
      end do
       open (8,file = dt1(k))
      do i = 1,nl
       write(8,100)(mc(i,j),j = 1,nchl)
      end do
      close(8)
      write(*,*)k
     end do

100   format (1x,i5,7(',',i5))
     stop
     end
```

B.3 PISTON SKIRT SURFACE PROFILE INCREMENT CONVERSION

The FORTRAN program TALLY.FOR was used to covert the original piston skirt surface profile data to data files containing the values for the piston distance increments seen from each LIF window. The parameter level was changed for each vertical window location.

TALLY.FOR

```
C    CHANGE VALUE FOR LEVEL FOR SPECIFIC WINDOW: 1, 2, 3, OR 4

     parameter (level = 4)

     parameter (ptcyc = 4000)
     real incr(226),prof(226),profwin(ptcyc),rad(ptcyc)
     real dist(ptcyc)
     PI = 4.*ATAN(1.)
```

```
c   READ IN ACTUAL TALLY SURFACE DATA

    open(7,file='tally.dat',status='old')

    do i=1,226
      read(7,*)incr(i),prof(i)
    enddo

    close(7)
    open(7, file='tallywn4.dat')

c   SETUP INCREMENTAL PISTON DISTANCE FROM CRANKANGE

    if (level.eq.1) then
      wlevel=50.
    elseif (level.eq.2) then
      wlevel=73.
    elseif (level.eq.3) then
      wlevel=87.5
    elseif (level.eq.4) then
      wlevel=102.
    endif


    pt=ptcyc/2

    xxx=(4.*PI)/ptcyc
    rad(1)=0.
    do i=2,pt+1
      rad(i)=rad(i-1)+xxx
    enddo

    do i=1,pt
      dist(i)=wlevel-196.+(46.5*cos(rad(i))+sqrt(22350.25-2162.25
   &          *(sin(rad(i))**2)))
    enddo

    dists=incr(1)
    diste=incr(226)

    do i=1,pt
      profwin(i)=0
    end do
    do i=1,pt
      dd=dist(i)
      if ((dd.le.diste).and.(dd.gt.dists)) then
        do j=1,226
          if (dd.le.incr(j)) then
            xx=dd-incr(j-1)
            yy=incr(j)-incr(j-1)
            zz=prof(j-1)+(prof(j)-prof(j-1))*xx/yy
            goto 2
          end if
```

```
        end do
2         profwin(i) = zz
        end if
      end do
      do i = 1,pt
        write(7,100)dist(i),profwin(i)
      end do
100   format(1x,f8.2,',',f8.2)
      close(7)
      stop
      end
```

APPENDIX C PRESSURE TRANSDUCER PROCESSING PROGRAM

C.1 CYLINDER AND INTER-RING PRESSURE PROCESSING

The raw pressure transducer data can be processed using a FORTRAN program to perform the tasks as described Chapter 4 Data Processing.

PRESSURE.FOR

```
parameter (nop=721)
real pi(2000,8),po(nop,8),kistler
parameter (nll=8000)
parameter (nchan=8)
parameter (nchr=100)
character*50 dt,dt1(nchr)
character*50 str,su
character*1  cha1,cha2
integer*4 i,n
integer*2 mc(nll,nchan)

C    INPUT DATA

write(*,*)'Input the data file to be "pressure" processed...'
read(*,'(a)')dt
write(*,*)'give the output file name,'
write(*,*)'and 1,2,3,etc.+[.dat] will be added.'
read(*,'(a)')su
write(*,*)'give the number of cycles (<100)'
read(*,*)ncyc
write(*,*)'points per cycle [1]-2000, [2]-4000'
read(*,*)npc
write(*,*)'give the number of channels'
read(*,*)nchl
write(*,*)'enter channel with cylinder #3 pressure data'
read(*,*)cylpr
write(*,*)'enter AVL scale...'
read(*,*)avl
write(*,*)'enter KISTLER scale for first transducer...'
read(*,*)kistler1
write(*,*)'enter KISTLER scale for second transducer...'
read(*,*)kistler2
write(*,*)'enter KISTLER scale for last 2 transducers...'
read(*,*)kistler34


if (npc.eq.1) then
  nl=2000
else
  nl=4000
```

```
      end if

C     CREATE MULTIPLE OUTPUT FILES

      ls=len_trim(su)
      do i=1,ncyc
       k=i/10
       k1=i-10*k
       cha1=char(48+k)
       cha2=char(48+k1)
       dt1(i)(1:ls)=su(1:ls)
       dt1(i)(ls+1:ls+1)=cha1
       dt1(i)(ls+2:ls+2)=cha2
       dt1(i)(ls+3:ls+6)='.dat'
      end do

      open (7,file=dt,status='old')

C     REMOVE THE TOP PORTION OF DATA FILE CONTAINING DATA AQUSITION LITERATURE

      n=0
1     continue
      read(7,'(a)')str
      if ((str(1:1).ne.'-').and.((str(1:1).ne.' ').and.
     &  (str(1:1).ne.'0'))) then
        n=n+1
        goto 1
      end if

C     READ ONE CYCLE OF CYLINDER PRESSURE TO DETERMINE IF SHIFTING IS NEEDED

      do i=1,nl
       read(7,*)(mc(i,j),j=1,nchl)
      end do

      fpt=5
      spt=nl/2+5

      if ((mc(fpt,cylch)).gt.(mc(spt,cylch))) then
       shift1=1
      endif

C     PREPARE FILE FOR SEPERATING CYCLES

      rewind 7

      do i=1,n
       read(7,'(a)')str
      end do

      if (shift.eq.1) then
       write(*,*)'shifting...'
       jp=nl/2
       do i=1,jp
```

```
      read(7,*)(mc(i,j),j=1,nchl)
    end do
  end if

C   SET CONVERTION FACTORS

  xc=10./2048.*avl
  x1=10./2048.*kistler1
  x2=10./2048.*kistler2
  x34=10./2048.*kistler34

C   BEGIN CYCLE TO CYCLE PROCESSING

  do k=1,ncyc
    do i=1,nl
      read(7,*)(mc(i,j),j=1,nchl)
    end do

    up=(nl/2)-4
    dn=(nl/2)+5

    cal3=0
    cal4=0

    do l=up,dn
      cal3=(x34*mc(l,7))+cal3
      cal4=(x34*mc(l,8))+cal4
    end do

    cal_3=1.02-(cal3/10)
    cal_4=1.02-(cal4/10)

    upp=(nl/2)+370
    dnn=(nl/2)+379

    setc=0
    set1=0
    set2=0
    set3=0
    set4=0

    do l=upp,dnn
      setc=(xc*mc(l,4))+setc
      set1=(x1*mc(l,5))+set1
      set2=(x2*mc(l,6))+set2
      set3=(x34*mc(l,7)+cal_3)+set3
      set4=(x34*mc(l,8)+cal_4)+set4
    end do

    set_cp=((set3+set4)/20)-(setc/10)
    set_1=((set3+set4)/20)-(set1/10)
    set_2=((set3+set4)/20)-(set2/10)

    do i=1,nl
```

```
      pi(i,1) = mc(i,4)*xc + set_cp
      pi(i,2) = mc(i,5)*x1 + set_1
      pi(i,3) = mc(i,6)*x2 + set_2
      pi(i,4) = mc(i,7)*x34 + cal_3
      pi(i,5) = mc(i,8)*x34 + cal_4
    end do

    open (8,file = dt1(k))

    do i = 1,nl
     write(8,100)(pi(i,j),j = 1,5)
    end do
    close(8)
100   format(5f11.7)

    write(*,*)k
   end do

   stop
   end
```

C.2 PROCESSING OF CYLINDER PRESSURE FOR *RINGPACK-OC*

The computer code *RINGPACK-OC* require a data file of one cycle of cylinder pressure with a one crank angle degree increment, starting at the expansion stroke. To process this one cycle pressure file, the FORTRAN program, PRESSURE.FOR, was modified at the end of the program to include the follow lines of code:

```
    xn = float(nl)/float(nop-1)
    do i = 1,5
     po(1,i) = pi(1,i)*100000
     po(nop,i) = po(1,i)
    end do
    do i = 2,nop-1
     xj = (i-1)*xn + 1
     j = xj
     do l = 1,5
      po(i,l) = (pi(j,l)*(xj-j) + pi(j + 1,l)*(j + 1-xj))*100000
     end do
    end do

    open (8,file = dt1(k))

    do i = 1,(nop-1)/2
     write(8,100)(i-1),(po(i + 360,j),j = 1,5)
    end do
    do i = 1,(nop + 1)/2
     write(8,100)(360 + i-1),(po(i,j),j = 1,5)
    end do
```